Complexation of actinides and analogues with hydroxamate ligands

Mingjian He

NNT : 2019SACLS413

Complexation d'actinides et d'analogues par des ligands hydroxamates

Thèse de doctorat de l'Université Paris-Saclay
préparée à l'Université Paris-Sud
au sein de l'Institut de Physique Nucléaire d'Orsay

École doctorale n°576 Particules Hadrons Energie et Noyau : Instrumentation, Image, Cosmos et Simulation (PHENIICS)
Spécialité de doctorat : Aval du cycle nucléaire, radioprotection et radiochimie

Thèse présentée et soutenue à Orsay, le 14 novembre 2019, par

Mingjian HE

Composition du Jury :

Pedro DE OLIVEIRA Professeur, Université Paris Sud (LCP)	Président
Christophe DEN AUWER Professeur, Université Nice Sophia Antipolis (ICN)	Rapporteur
Philippe MOISY Directeur de Recherche CEA, CEA (Marcoule)	Rapporteur
Julie CHAMPION Enseignant chercheur, SUBATECH, IMT Atlantique	Examinatrice
Claire LE NAOUR Chargée de recherche, CNRS-IN2P3 (IPNO)	Directrice de thèse

Thèse de doctorat

Acknowledgement

First and foremost, I would like to express my deepest gratitude and appreciation to my supervisor Dr. Claire LE NAOUR. I am very grateful that she accepted me to be her student three years ago. There is no doubt that she is the best supervisor I have ever met. I am very happy and lucky to obtain this opportunity to work with her for the unforgettable three years. Without her help and support, I can never finish this PhD thesis. Her intelligence and attitude to science and research will enlighten and guide my future career forever.

I would like to thank Dr. Vladimir SLADKOV for his helpful guidance. Although I just worked with him for one year, I have still learnt a lot of things from him.

I would like to thank Dr. Melody MALOUBIER and Dr. Jérôme ROQUES for their help in this work. I am very grateful that they helped me a lot to perform the EXAFS data adjustments and the theoretical calculations. Especially I am very thankful to Dr. Melody MALOUBIER who provided me with many valuable suggestions about dissertation writing and thesis presentation.

I would like to thank all the jury members of my defense, Prof. Pedro DE OLIVEIRA, Prof. Christophe DEN AUWER, Prof. Philippe MOISY and Dr. Julie CHAMPION. I am very grateful that they took much time to review my thesis very carefully and gave me many suggestions to improve my dissertation.

I would like to thank all the members in Group PACS and Radiochimie. I am very grateful to enjoy a happy life with them. I would also like to thank all my friends for their concern and help at the hardest time in France. Moreover, I would like to thank and welcome Yang PEI and Meng LUO to join radiochemistry. There is nothing more enjoyable to me than knowing someone continue our work in radiochemistry.

Last but not least, I would like to thank China Scholarship Council which financially supported my life and work at IPNO in Paris-Saclay University. In addition, I would also like to thank Harbin Engineering University for providing me with a faculty position in China.

Contents

List of Abbreviations 1

List of Figures 2

List of Tables 7

I. Introduction 9

II. Bibliographic Study 12

II.1 Actinides 12

II.1.1. General points 12

II.1.2. Actinides in solution 16

II.1.3. Actinides in the environment 25

II.2 Hydroxamate siderophores 28

II.3 Interaction between actinides and hydroxamates 33

II.3.1 Interaction of actinides with monohydroxamates 33

II.3.2 Interaction of actinides with DFB 34

II.4 Summary 36

III. Methodology 37

III.1 Techniques for thermodynamic study 38

III.1.1 Liquid-liquid extraction 38

III.1.2 Ultraviolet-visible absorption spectroscopy 41

III.1.3 Affinity capillary electrophoresis 43

III.2 Techniques for structural study 46

III.2.1 Attenuated total reflectance Fourier-transform infrared spectroscopy 46

III.2.2 X-ray absorption spectroscopy 48

III.3 Stock solution preparations of tetravalent actinides 51

III.3.1 Preparation of ^{227}Th(IV) stock solution 51

III.3.2 Preparation of U(IV) stock solution 53

III.4 Summary 54

IV. Results and Discussion 55

IV.1 Trivalent lanthanides 55

Thermodynamic study with trivalent lanthanides 55

IV.1.1 Complexation of Eu(III) with DFB studied by liquid-liquid extraction 55

IV.1.2 Complexation of Ln(III) with DFB studied by UV-visible spectrophotometry 62

IV.1.3 Complexation of Ln(III) with DFB studied by affinity capillary electrophoresis 67

Structural study with trivalent lanthanides 71

IV.1.4 Structural study of the complexation of Eu(III) with DFB by ATR-FTIR 71

IV.2 Tetravalent actinides 76

Thermodynamic study with tetravalent actinides 76

IV.2.1 Complexation of Th(IV) with DFB studied by liquid-liquid extraction 76

IV.2.2 Complexation of U(IV) with BHA, AHA and DFB studied by UV-visible absorption spectrophotometry 85

Structural study with tetravalent actinides 90

IV.2.3 Structural study of the complexation of Th(IV) with DFB by ATR-FTIR 90

IV.2.4 Structural study of the complexation of An(IV) with DFB by theoretical calculations and EXAFS 93

IV.3 Summary 104

V. Conclusion 106

Appendix 109

Appendix A: Preparation of solutions **109**

Appendix B: Influence of γ-ray energy for counting **111**

Appendix C: Determination of proton concentration **112**

Appendix D: Back and direct extraction of Th(IV) **113**

Appendix E: Study of DFB Stability **115**

Reference **118**

List of Abbreviations

AHA	Acetohydroxamic acid
BHA	Benzohydroxamic acid
DFB	Desferrioxamine B
DFE	Desferrioxamine E
DTPA	Diethylenetriaminepentaacetic acid
EDTA	Ethylenediaminetetraacetic acid
TTA	Thenoyltrifluoroacetone
LLE	Liquid-liquid extraction
SP / sp.	UV-visible Absorption Spectroscopy
ATR-FTIR	Attenuated Total Reflection – Fourier Transform Infrared spectroscopy
DFT	Density Functional Theory
EXAFS	Extended X-ray Absorption Fine Structure
ICP-MS	Inductively Coupled Plasma Mass Spectrometry
XRD	X-ray Diffraction
XANES	X-ray Absorption Near Edge Structure
XAS	X-ray Absorption Spectroscopy
PCA	Principal Component Analysis
HSAB	Hard Soft Acid Base Principle
ACE	Affinity Capillary Electrophoresis
IR	Infrared
em.	Electromigration
pot.	Potentiometry
M	Metal
L	Ligand

List of Figures

Figure I.1 Behavior of actinides in the environment [2018DEN]. 10

Figure II.1 Periodic table of the elements [2019IUP]. 12

Figure II.2 Radial probability, P(R), of 4f and 5f valence electrons from (a) Sm^{3+} and (b) Pu^{3+} [2000CLA]. 14

Figure II.3 Configuration orbital energies (in atomic units) of the lanthanides Sm, Eu, Gd, Tb and the actinides Pu, Am, Cm, Bk (Quantum chemistry calculations based on Dirac-Fock equations) [1978PYY]. 15

Figure II.4 Potential-pH diagram of uranium at 25 °C (U_{tot} 10^{-10} M) using database from OECD/NEA [2005TAK]. 17

Figure II.5 Latimer's diagram of Pu in 1 M $HClO_4$ [1970CLE]. 18

Figure II.6 Possible molecular geometries for the plutonium aquo ions (a) with eight water molecules for Pu(III) and Pu(IV) in three geometric arrangements; (b) Pu(III, IV) with nine water molecules; (c) Pu(V) and Pu(VI), actinyl ions with five water molecules in the equatorial plane and (d) Pu(VII) [2000CLA]. 19

Figure II.7 (a) The color of non-complexed plutonium at various oxidation states in 1 M $HClO_4$ from Pu(III) to Pu(VI) and in strong base for Pu(VII) (b) their corresponding absorption spectra [2000CLA]. 20

Figure II.8 Hydrolysis speciation diagram of mononuclear Th(IV), Cf(III) and Pu(IV) without considering colloid or polymer species. 22

Figure II.9 Common oxidation states of actinides in the environment under different conditions. States mentioned in bracket (−) are unstable; and with a question mark (?) were not confirmed. The oxidation states bolded correspond to the predominant states [2013MAH]. 26

Figure II.10 General structure of hydroxamate functional group. 28

Figure II.11 Desferrioxamine B. 28

Figure II.12 Speciation diagram of desferrioxamine B (I = 0.7 M Na, $HClO_4$, T = 25 °C). ... 30

Figure II.13 Benzohydroxamic acid (BHA) (left) and acetohydroxamic acid (AHA) (right). 30

Figure II.14 Speciation diagrams of benzohydroxamic acid (left) in 0.1 M $NaClO_4$ at 25°C and acetohydroxamic acid (right) in 1.0 M NaCl at 25°C. 31

Figure II.15 Speciation diagram of Eu(III)-DFB ($C_{Eu(III)} = C_{DFB} = 2.5\times10^{-2}$ M) plotted by using the literature data [2011CHR]. 36

Figure II.16 Speciation diagram of Th(IV)-DFB ($C_{Th(IV)} = C_{DFB} = 2.5\times10^{-2}$ M) plotted by using the literature data [1996WHI]. 36

Figure III.1 Schematic diagram of UV-visible spectrophotometer. 42

Figure III.2 Schematic of electroosmotic flow. 43

Figure III.3 Schematic process of affinity capillary electrophoresis 44

Figure III.4 Types of stretching and bending. 46

Figure III.5 Principle of EXAFS. 49

Figure III.6 Percentage of ^{227}Th and ^{231}Pa in each fraction (upper) and the gamma spectra of largest fraction of ^{227}Th and ^{231}Pa (lower) 52

Figure III.7 α liquid scintillation spectrum of an aliquot of the mother solution of U(IV). 53

Figure IV.1 Variations of ^{152}Eu extracted as function of pC_H ($C_{TTA} = 2.5\times10^{-2}$ M in toluene I = 0.7 M (Na, $HClO_4$), T = 25°C). 55

Figure IV.2 Variations of D as function of TTA concentration ($C_{Acetate} = 5\times10^{-3}$ M, I = 0.7 M (Na, $HClO_4$), T = 25 °C, $pC_H = 4.75$) 55

Figure IV.3 Variations of D as function of DFB concentration at different pC_H ($C_{TTA} = 2.5\times10^{-2}$ M, I = 0.7 M (Na, $HClO_4$), T = 25 °C, $C_{Acetate} = 5\times10^{-3}$ M). 56

Figure IV.4 Variations of D_0/D-1 as function of DFB concentration ($C_{Acetate} = 5\times10^{-3}$ M, I = 0.7 M (Na, $HClO_4$), T = 25°C, $pC_H = 4.75$). 56

Figure IV.5 Variations of $\log K'_{cond}$ as function of pC_H. 60

Figure IV.6 Absorption spectra of Eu(III) at different concentrations (pH = 4.0 and I = 0.5 M (Na, $HClO_4$)). 62

Figure IV.7 Absorption spectra of Pr(III) at different concentrations (pH = 4.0 and I = 0.5 M (Na, $HClO_4$)). 62

Figure IV.8 Test of Lambert-Beer Law of Eu(III) at the concentration ranging from 10^{-3} to 4×10^{-2} M at pH = 4.0 and I = 0.5 M (Na, $HClO_4$) at the wavelength of 394 nm. 63

Figure IV.9 Test of Lambert-Beer Law of Pr(III) at the concentration ranging from 6×10^{-4} M to 6×10^{-3} M at pH = 4.0 and I = 0.5 M (H, $NaClO_4$) at the wavelength of 444 nm. 63

Figure IV.10 Absorption spectra of Eu(III) at 10^{-2} M with increasing amount of DFB at pH = 3.7 (left) and 4.5 (right) (I = 0.5 M, $0 \leq CDFB \leq 5.6\times10^{-2}$ M). 63

Figure IV.11 Absorption spectra of Pr(III) at 6×10^{-3} M with increasing amount of DFB at pH = 4.6 (left) and 5.5 (right) (I = 0.5 M $0 \leq C_{DFB} \leq 5.6\times10^{-2}$ M). 64

Figure IV.12 Molar absorbance of Eu^{3+}, EuH_3DFB^{3+} and EuH_2DFB^{2+} 66

Figure IV.13 Molar absorbance of Pr^{3+}, PrH_3DFB^{3+} and PrH_2DFB^{2+}. 66

Figure IV.14 Mobility of 1×10^{-4} M DFB as function of La(III) (black points) and Lu(III) (red points) at I = 0.1 M (left) and 0.5 M (right) pH = 2.5, T = 25 °C. 67

Figure IV.15 IR spectrum of protonated desferrioxamine mesylate at pH=3.1. 71

Figure IV.16 Main functional groups of protonated DFB. 71

Figure IV.17 IR spectra of solutions containing either the mesylate form of DFB (5×10^{-2} M) at pH = 5.5 or methanesulfonate (5×10^{-2} M) at pH = 4.0 [2009BOR]. 72

Figure IV.18 IR spectra of the dried DFB solution at 2.5×10^{-2} M in absence of Eu(III) at pH from 3.1 to 8.9. 73

Figure IV.19 FTIR spectra of air-dried Eu(III)-DFB complexes as a function of pH (from 3.1 to 9.4). $C_{Eu(III)} = C_{DFB} = 2.5\times10^{-2}$ M at room temperature. 74

Figure IV.20 Variations of the percentage of extraction of ^{227}Th as function of pC_H (C_{TTA} = 0.08 M in toluene, I = 0.7 M (Na, $HClO_4$), T = 25 °C). 76

Figure IV.21 Variations of the distribution ratio D of ^{227}Th as function of total TTA concentration in toluene (I = 0.7 M (Na, $HClO_4$), pC_H = 1.0, T = 25 °C). 76

Figure IV.22 Variations of D as a function of DFB concentration at different pC_H (C_{TTA} = 0.08 M, I = 0.7 M (Na, $HClO_4$), T = 25 °C). 79

Figure IV.23 Variations of D_0/D-1 as function of DFB concentration (I = 0.7 M (Na, $HClO_4$), T = 25 °C, pC_H = 1.5) and associated linear fitting. 79

Figure IV.24 Variation of K'_{cond} as function of proton concentration. 82

Figure IV.25 UV-visible absorption spectra of U(IV) at 4.8×10^{-3} M with increasing amount of BHA from 0 to 5×10^{-2} M in 0.5 M HCl at 25 °C. 85

Figure IV.26 UV-visible absorption spectra of U(IV) at 9.6×10^{-3} M with increasing amount of AHA from 0 to 0.8 M in 0.5 M HCl at 25 °C. 85

Figure IV.27 Correlation of stability constants of Pu(IV), Th(IV) and U(IV) with BHA (left) and AHA (right). 87

Figure IV.28 Molar absorbance of U^{4+} and $UBHA^{3+}$. 88

Figure IV.29 Molar absorbance of U^{4+}, $UAHA^{3+}$ and $U(AHA)_2^{2+}$. 88

Figure IV.30 Absorption spectra of U(IV) at 9.6×10^{-3} M with different ratio U:DFB at C_{HCl} = 0.5 M in 0.5 M HCl. 89

Figure IV.31 Variation of U(IV) absorption spectra as a function of pC_H (pC_H from 1.35 to 0.54, $C_U = 9.6\times10^{-3}$ M, $C_{DFB} = 1.1\times10^{-2}$ M). 89

Figure IV.32 FTIR spectra of the air-dried Th(IV)-DFB complexes as a function of pH (from 1.3 to 9.1) $C_{Th(IV)} = C_{DFB} = 2.5\times10^{-2}$ M at room temperature. 90

Figure IV.33 Optimized structure of ligand DFB. 94

Figure IV.34 Optimized structures of ligand DFB with different deprotonation. 94

Figure IV.35 Optimized structures of Th with one hydroxamate group at coordination number = 8 (left) and 9 (right). 95

Figure IV.36 Optimized structures of the complex of Th with one hydroxamate group at Site 1 (first figure), Site 2 (second figure) and Site 3 (third figure). 96

Figure IV.37 Optimized structure of $Th(H_2DFB)$ complex obtained by DFT calculation. 98

Figure IV.38 Optimized structure of Th(HDFB) complex (three bidendate hydroxamates) obtained by DFT calculations. 99

Figure IV.39 Optimized structure of Th(HDFB) complex (one bidentate and two monodentate hydroxamates) obtained by DFT calculations. 100

Figure IV.40 k^3-weighted EXAFS spectra and their corresponding Fourier transform at the Th L_{III} edge of a solution of Th-DFB at pH = 5. Experimental spectrum (circles) and adjustment (red line). 102

Figure IV.41 k^3-weighted EXAFS spectra and their corresponding Fourier transform at the U L_{III} edge of a solution of U(IV)-DFB at pH = 5. Experimental spectrum (circles) and adjustment (red line). 103

Figure V.1 Structure of the complex Th(HDFB). 108

Figure A. 1 Distribution values (D_0) of ^{152}Eu at $pC_H = 4.0$ and 4.2 as function of energy (γ-ray characteristic peak of ^{152}Eu). 111

Figure A. 2 Variation of D as function of contacting time. 113

Figure A. 3 Experimental procedure of back and direct extraction of Th(IV) 114

Figure A. 4 Values of D in the back and direct extraction of Th(IV) at $pC_H = 1$, I = 0.7 M (Na, $HClO_4$) without DFB (left) and at $pC_H = 2$, I = 0.7 M (Na, $HClO_4$) with 0.07 M DFB (right). 114

Figure A. 5 Absorption spectra of DFB at different concentrations (pH = 4.0 and I = 0.5 M (Na, $HClO_4$)). 115

Figure A. 6 Test of Lambert-Beer Law of DFB at the concentration ranging from 10^{-5} to 5×10^{-6} M at pH = 4.0 and I = 0.5 M (Na, $HClO_4$) at the wavelength of 200, 210 and 220 nm. 115

Figure A. 7 Variation of UV absorbance of 1×10^{-5} M DFB solution at 200 nm as function of time. 116

List of Tables

Table II.1 Electron ground-state configurations of lanthanides and actinides [2000CLA]. 13

Table II.2 Oxidation states of actinides in aqueous solution (the most common ones are denoted in bold). 16

Table II.3 Hydrolysis constants of Th(IV), U(IV), Pu(IV), Cf(IV) and Eu(III) at 25 °C. 22

Table II.4 Classification of Bases [1997PEA]. 23

Table II.5 Dissociation constants of H_4DFB^+ at 25 °C. 29

Table II.6 Dissociation Constants of Benzohydroxamic Acid (BHA). 31

Table II.7 Dissociation Constants of Acetohydroxamic Acid (AHA). 32

Table II.8 Stability constants of Th(IV), U(IV) and Pu(IV) with BHA. 33

Table II.9 Stability constants of Eu(III), Th(IV) and Pu(IV) with DFB. 34

Table III.1 Applied techniques and studied systems in this work. 37

Table III.2 ATR-FTIR samples description. 47

Table III.3 Description of EXAFS samples. 49

Table III.4 Applied techniques and experimental conditions of each system in this work. 54

Table IV.1 Conditional stability constants K_{cond} (Equation IV.3) between Eu(III) and DFB at different pC_H. 57

Table IV.2 Corrected conditional stability constants $\log K'_{cond}$ (Equation IV.12) between Eu^{3+} and DFB at different pC_H and comparison with $\log K_{cond}$ (Equation IV.3). 59

Table IV.3 Obtained and published stability constants of $Eu(H_3DFB)^{3+}$ and $Eu(H_2DFB)^{2+}$ 61

Table IV.4 Obtained and published stability constants of $Ln(H_3DFB)^{3+}$ and $Ln(H_2DFB)^{2+}$ for Eu(III) and Pr(III). 65

Table IV.5 Obtained and published stability constants of $Ln(H_3DFB)^{3+}$ for La(III) and Lu(III). 69

Table IV.6 Frequencies and assignments of the major bands in the IR spectra of H_4DFB^+ at pH = 3 and Eu-DFB complex at pH = 9.1. 75

Table IV.7 Estimated values of HTTA and TTA^- concentration and $ThTTA^{3+}$ percentage. 78

Table IV.8 Conditional stability constants K_{cond} relative to the formation of Th-DFB at different pC_H 80

Table IV.9 Obtained conditional stability constants K'_{cond} (Equation IV.47) between Th^{4+} and DFB at different pC_H and comparison with K_{cond} (Equation IV.44). 81

Table IV.10 Obtained and published apparent stability constants of $Th(H_3DFB)^{4+}$ and $Th(H_2DFB)^{3+}$. 83

Table IV.11 Stability constants β_{110} of $An^{IV}L^{3+}$ (EquationIV.63) and β_{120} of $An^{IV}(L)_2^{2+}$ (Equation IV.65). 86

Table IV.12 Frequencies and assignments of the major bands in the IR spectra of H_4DFB^+ at pH = 3 and Th-DFB complex at pH = 9.1 Comparison with Eu-DFB complex at pH = 9.4. 92

Table IV.13 Geometrical parameters associated with Figure IV.36 obtained by DFT calculations. 97

Table IV.14 Geometrical parameters associated with Figure IV.37 obtained by DFT calculations. 98

Table IV.15 Geometrical parameters associated with Figure IV.38 obtained by DFT calculations. 99

Table IV.16 Geometrical parameters associated with Figure IV.39 obtained by DFT calculations. 100

Table IV.17 EXAFS best fit parameters for the Th(IV) and U(IV)-DFB solutions at pH = 5. s_0^2 is the EXAFS global amplitude factor and is fixed to 1; ε is the average noise, $\Delta\chi^2$ is the quality factor and R_f(%) is the agreement factor of the fit. 102

Table IV.18 Formation constants obtained in this work and available in the literatures. 104

Table V.1 Obtained formation constants between trivalent lanthanides and DFB 107

Table A. 1 UV absorbance of 2×10^{-5} M DFB solution (pC_H = 0.7) at 200, 210 and 220 nm as function of time. 117

I. Introduction

The use of actinides for civilian as well as military purposes has led –and still leads- to their environmental release. Atmospheric nuclear tests from 1945 to 1980 are the main source of contamination of the terrestrial and marine environment. It is estimated that about 3.1 PBq of ^{241}Am, 40 PBq of ^{237}Np, 13 PBq of ^{239,240}Pu and 170 PBq of ^{241}Pu have been deposited on Earth [1980PER] [1998BEA]. The contamination from underground nuclear tests is more localized with actinides incorporated in rocks. But plutonium has been detected in groundwater at 1.3 km from the Nevada Test Site where 826 tests were conducted between 1956 and 1992 [1999KER]. Accidental releases, such as the two B52 plane crashes in Palomares in 1966 (Spain) and Thule in 1968 (Greenland), have also contaminated the environment locally. In the context of nuclear energy production, all facilities related to the fuel cycle are likely to face to actinides release in the geosphere and the biosphere, both in normal operation and in the event of an accident. The processing of ore in uranium mines has led to an accumulation of U daughters in mine tailings and pit waters. The fire in a reactor at Winscale in 1957, an explosion of a tank containing radwaste at Kyshtym also in 1957, the explosion and fire of a reactor at Chernobyl in 1986, the cores meltdown at Fukushima in 2011, have also led to actinides spreading but much less than the nuclear weapons testing [1996AIH] [2004LAN] [2010HU] [2015GRA] [2018DEN]. In addition, some naturally occurring actinides with lifetimes comparable to the age of the earth are also present in the environment: ^{232}Th, ^{235}U and ^{238}U are the main primordial radionuclides. By radioactive decay, they produce other actinide isotopes like ^{234}U, ^{231}Pa, ^{230}Th.

Actinides from either natural or anthropogenic sources are of environmental and health concerns due to their high toxicity, long half-life and the exposure risk of internal contamination (accumulation in drinking water or in food). Modeling the behavior of actinides under environmental conditions is therefore essential, but extremely challenging, because of the complexity of the chemistry of actinides on one hand, and the complexity of the environmental medium on the other hand:

- The light actinides ions exist in various oxidation states that exhibit their own reactivity. For example, Pu(IV) is rather insoluble (in the absence of strong complexing agent) whereas Pu(V) is mobile.

- The environmental systems cover surface waters, groundwaters, rocks, clays… with very diverse composition (inorganic and organic ligands, microbes, colloids…).

The chemical interactions of actinides in the environment are summarized in **Figure I.1**. Depending on the pH, the redox potential, the presence of particulates or colloids, the presence of ligands, the actinide ion can undergo a great variety of reactions: sorption, complexation, precipitation, colloid formation…[2010RUN] [2018DEN].

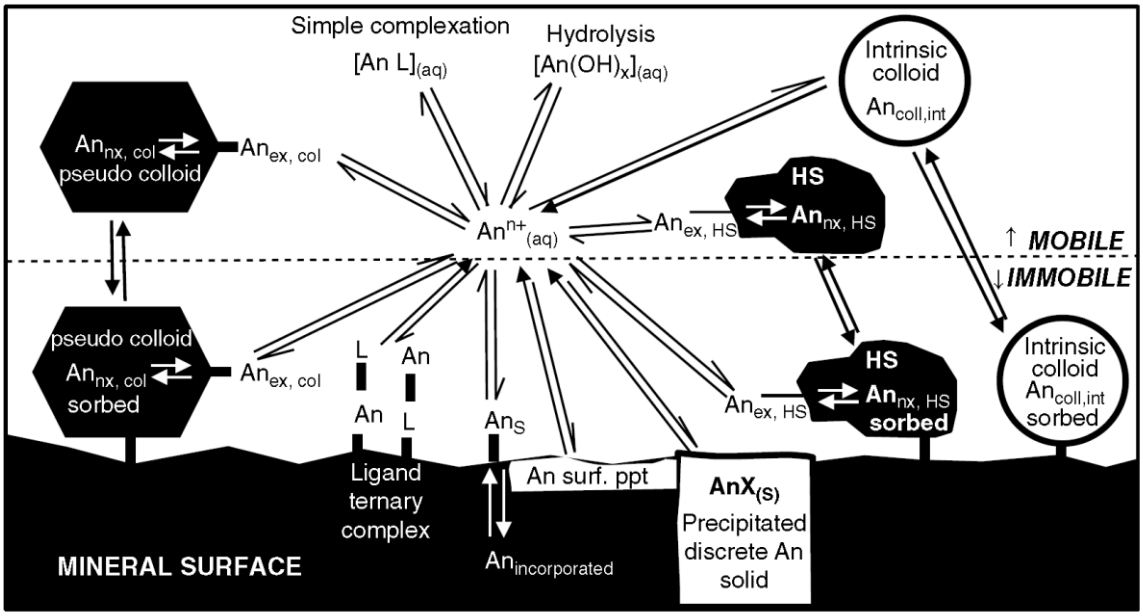

Figure I.1 Behavior of actinides in the environment [2018DEN].

The present work is limited to the study of one type of interaction: the complexation with a naturally occurring organic ligand that belongs to the class of siderophores. Siderophores (Greek: "iron carrier") are small, high-affinity iron-chelating compounds secreted by microorganisms such as bacteria and fungi allowing iron to be transported into the cell [1995NEI]. Since Pu^{4+} and Fe^{3+} have similar charge/radius ratio, Pu^{4+} and other tetravalent actinides are expected to form also strong complexes with siderophores, especially with desferrioxamine B (DFB) [1992BRA]. This ligand possesses three hydroxamate groups (RC(O)N(OH)R') and can therefore acts as a hexadentate ligand (which matches with Fe(III) maximum coordination). Some data relative to the complexation of actinides (IV) with DFB are available in the literature. Formation constants have been proposed by Boukhalfa et al. for Th(IV) [2007BOU] and by Whisenhunt et al. for Pu(IV) [1996WHI]. Additionally, the structure of the complexation of Pu(IV) with desferrioxamine E (similar to DFB) has been characterized by using X-ray diffraction [2000NEU]. A dimer Pu(IV)-DFB has also been recently observed [2014BOG].

The aim of the present work is to develop suitable experimental protocols to collect fundamental data on the complexation between actinides at the oxidation states +III and +IV with desferrioxamine B. For that purpose, trivalent actinides have been simulated by lanthanides and Pu(IV)

by Th(IV) and U(IV). The study was conducting according to a twofold approach: thermodynamic and structural. The thermodynamic study involved different concentrations of metal ions. Liquid-liquid extraction experiments combined with γ-spectrometry were carried out with europium and thorium at ultra-trace scale using the radionuclides ^{152}Eu and ^{227}Th. The complexation of stable lanthanides in macroconcentration and of U(IV) was studied using affinity capillary electrophoresis and/or UV-Vis absorption spectrophotometry. Infrared and X-ray absorption spectroscopies combined with quantum chemistry calculations were the techniques used for the structural study of Eu/Th/U-DFB complexes.

The present PhD thesis is divided in five chapters. The present (first) one is a general introduction in order to explain the context and the aim of the work. The second chapter is a bibliographic study devoted to the chemical properties of actinides and of hydroxamate ligands. In the third chapter, the methodology and the techniques used are described. The results and discussion on the complexation of lanthanides, Th(IV) and U(IV) with some hydroxamates are presented in Chapter IV. Finally, Chapter V presents a general conclusion.

II. Bibliographic Study

II.1 Actinides

II.1.1. General points

Actinides commonly refer to 15 elements from actinium (Z = 89) to lawrencium (Z = 103) as shown in the periodic table presented in **Figure II.1**. However, the placement of Ac (and La) and even Lr (and Lu) has been controversial for many years [1982JEN] [2008LAV]. The elements Ac and La are often placed in d-block below Y in group 3. In the following, actinium is considered as the first member of the actinide series, similarly to lanthanum in the lanthanide series [2010KIR].

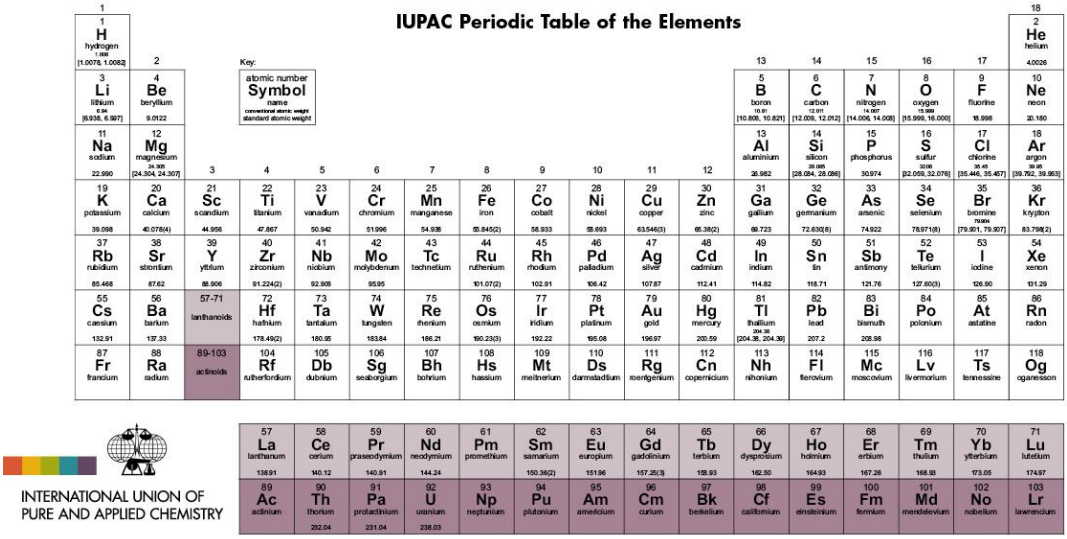

Figure II.1 Periodic table of the elements [2019IUP].

The actinides correspond to the filling of the 5f electron shell as suggested by G.T. Seaborg in 1945 [1945SEA]. Their electron configuration is $[Rn]5f^n6d^m7s^2$, similarly to lanthanides configuration $[Xe]4f^n5d^m6s^2$ [2000CLA] [2011EDE]. The ground–state electron configurations of lanthanide and actinide atoms are reported in **Table II.1**. One could notice that the filling of 5f shell is less homogeneous than the 4f and a special stability of Cm and Gd is observed due to the half-filled 5f and 4f shells respectively. According to the electron configurations listed in **Table II.1**, the 6d orbitals of the actinides appear energetically more accessible than the 5d orbitals of the lanthanides.

Table II.1 Electron ground-state configurations of lanthanides and actinides [2000CLA].

Lanthanide		Configuration			Actinide		Configuration		
La	lanthanum		$5d^1$	$6s^2$	Ac	actinium		$6d^1$	$7s^2$
Ce	cerium	$4f^1$	$5d^1$	$6s^2$	Th	thorium		$6d^2$	$7s^2$
Pr	praseodymium	$4f^3$		$6s^2$	Pa	protactinium	$5f^2$	$6d^1$	$7s^2$
Nd	neodymium	$4f^4$		$6s^2$	U	uranium	$5f^3$	$6d^1$	$7s^2$
Pm	promethium	$4f^5$		$6s^2$	Np	neptunium	$5f^4$	$6d^1$	$7s^2$
Sm	samarium	$4f^6$		$6s^2$	Pu	plutonium	$5f^6$		$7s^2$
Eu	europium	$4f^7$		$6s^2$	Am	americium	$5f^7$		$7s^2$
Gd	gadolinium	$4f^7$	$5d^1$	$6s^2$	Cm	curium	$5f^7$	$6d^1$	$7s^2$
Tb	terbium	$4f^9$		$6s^2$	Bk	berkelium	$5f^9$		$7s^2$
Dy	dysprosium	$4f^{10}$		$6s^2$	Cf	californium	$5f^{10}$		$7s^2$
Ho	holmium	$4f^{11}$		$6s^2$	Es	einsteinium	$5f^{11}$		$7s^2$
Er	erbium	$4f^{12}$		$6s^2$	Fm	fermium	$5f^{12}$		$7s^2$
Tm	thulium	$4f^{13}$		$6s^2$	Md	mendelevium	$5f^{13}$		$7s^2$
Yb	ytterbium	$4f^{14}$		$6s^2$	No	nobelium	$5f^{14}$		$7s^2$
Lu	lutetium	$4f^{14}$	$5d^1$	$6s^2$	Lr	lawrencium	$5f^{14}$	$6d^1$	$7s^2$

Moreover, 4f and 5f orbitals display a relatively small radial extension. They are shielded from interactions with ligands by the $5s^2$, $5p^6$ and $6s^2$, $6p^6$ filled shells for lanthanides and actinides, respectively. This means that the interaction of nf electrons with the electrons from ligands is relatively weak. But the light actinides, from Pa to Am exhibit a more complex behavior since 5f orbitals are more spatially extended whereas 4f orbitals are localized. In addition, the 5f, 6d and 7s orbitals are much closer in energy than the corresponding 4f, 5d and 6s. This is illustrated by the variations of the radial probability of valence electrons (dotted lines) as function of the distance nucleus-electron in **Figure II.2**. The overlap of valence orbitals is less significant in the case of Sm^{3+} as compared to Pu^{3+}. The multiplicity of oxidation states of the light actinides (U, Np, Pu, Am) originates from this feature whereas lanthanide exhibit mainly the trivalent oxidation state.

The electronic structures of lanthanides and especially actinides are also impacted by relativistic effects [1988PYY] [1994BAL]. The increase in Z brings with it an increase in the electric field produced by the bigger number of protons which leads to the increase of the speed of inner electrons that approaches the speed of light. The general idea is that the relativistic increase in the mass of the inner electrons leads to the contraction of s and p shells and to their energetic stabilization. This contraction, in turn, allowing a strong screening of the d and f orbitals from the nucleus charge, leads to relativistic expansion and destabilization of the f and d orbitals [1988PYY] [1994BAL] [1995YAT].

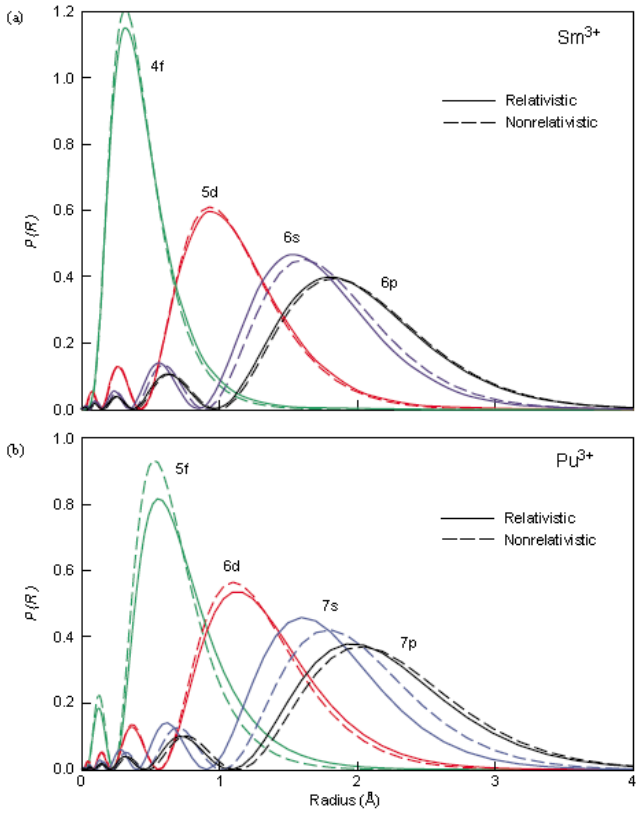

Figure II.2 Radial probability, P(R), of 4f and 5f valence electrons from (a) Sm^{3+} and (b) Pu^{3+} [2000CLA].

The solid lines in **Figure II.2** show that relativistic effects are more pronounced for actinides as compared to lanthanides. And the patterns of orbital energy levels in **Figure II.3** illustrate the higher destabilization of 5f orbitals as compared to the 4f. **Figure II.3** demonstrates also the relativistic effects on spin-orbit splitting of p, d and f orbitals into lower lying $p_{1/2}$, $d_{3/2}$, $f_{5/2}$ and higher lying $p_{3/2}$, $d_{5/2}$, $f_{7/2}$. The outer 6d and 5f electrons of the light actinides are more weakly bound than the 5d and 4f electrons of lanthanides. Thus, these outer electrons are more chemically reactive and can easily be removed leading to multiple oxidation states. From americium, the actinides behave like lanthanides, with the predominance of the +III oxidation state. The increase in Z indeed, leads to the contraction of 5f orbitals, the 5f electrons becoming more and more localized. At the end of the series, +II oxidation state is observed.

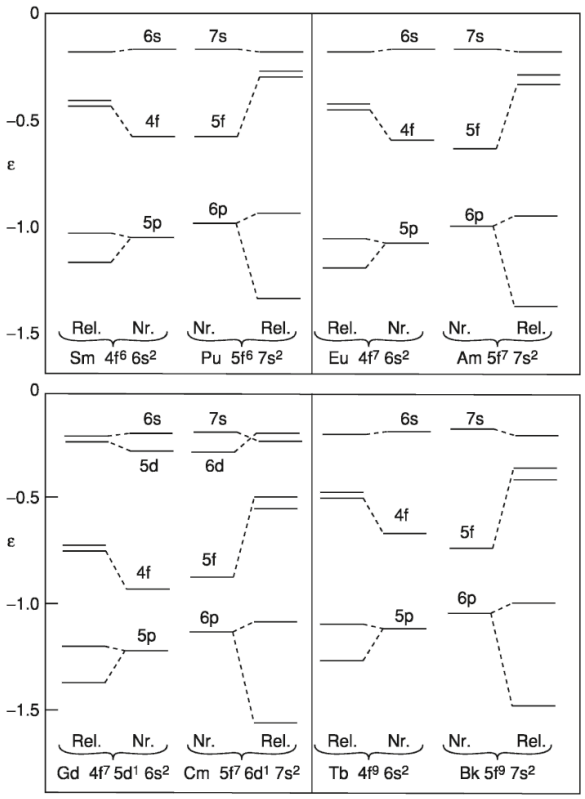

Figure II.3 Configuration orbital energies (in atomic units) of the lanthanides Sm, Eu, Gd, Tb and the actinides Pu, Am, Cm, Bk (Quantum chemistry calculations based on Dirac-Fock equations) [1978PYY].

II.1.2. Actinides in solution

The speciation of actinides in solutions depends on several parameters such as the redox potential, pH, cations and anions concentrations. In this paragraph, essential properties of some actinides in solution, which are necessary for a good understanding of this study, are described.

A) Oxidation states

Depending on the chemical and natural environment, the light actinides may exist in solution under different oxidation states that are presented in **Table II.2**. Americium and curium will be mainly found in the +III oxidation state. The actinides beyond Cm, except No, act as lanthanides and exist in the +III oxidation state.

Table II.2 Oxidation states of actinides in aqueous solution (the most common ones are denoted in bold).

Actinide	Oxidation state					
$_{90}$**Th**			**IV**			
$_{91}$**Pa**			IV	**V**		
$_{92}$**U**		III	**IV**	V	**VI**	
$_{93}$**Np**		III	IV	**V**	VI	VII
$_{94}$**Pu**	II	III	**IV**	V	VI	
$_{95}$**Am**	II	**III**	IV	V	VI	
$_{96}$**Cm**		**III**	IV			
$_{97}$**Bk**		**III**	IV			
$_{98}$**Cf**		**III**				
$_{99}$**Es**		**III**				
$_{100}$**Fm**	II	**III**				
$_{101}$**Md**	II	**III**				
$_{102}$**No**	**II**	III				
$_{103}$**Lr**	II	**III**				

In aqueous solution, thorium has only one stable oxidation state, +IV. Uranium can be found in +III to +VI oxidation states. The most stable is U(VI) as the linear uranyl ion, UO_2^{2+}. The stability area of U(III) lies outside of the stability limits of water: it is quickly oxidized in U(IV). U^{4+} is also stable in solution if no oxidizing agents are present. The kinetics of redox transformations depends if there is a change in the chemical composition between the oxidized and

reduced species. Thus, the reaction between UO_2^{2+} and UO_2^{+} and between U^{4+} and U^{3+} are fast whereas the redox reaction between UO_2^{2+} and U^{4+} is slow [1959NEW] [2010CHO]. U(V) exhibits a strong tendency to disproportionation and exists on a very narrow stability range that cannot be represented in the Pourbaix diagram (**Figure II.4**).

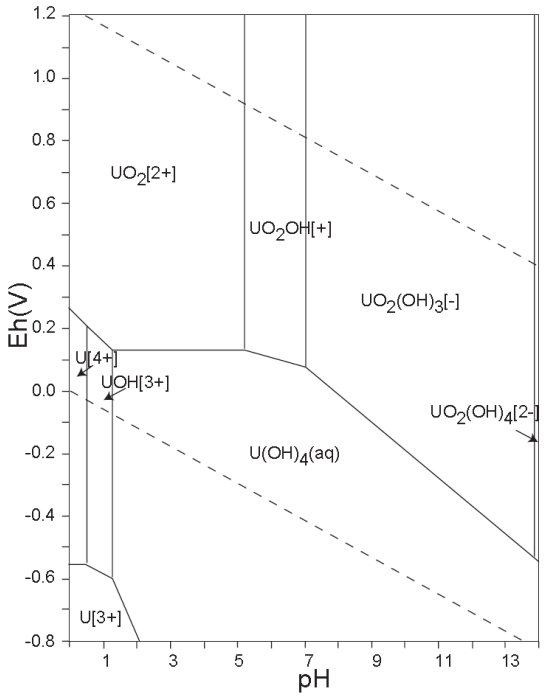

Figure II.4 Potential-pH diagram of uranium at 25 °C (U_{tot} 10^{-10} M) using database from OECD/NEA [2005TAK].

Plutonium has not been used in this work because of handling difficulties (α-emitting isotopes, complicated chemistry), but its redox properties will be briefly described. In solution, plutonium might be present in the +III, +IV, +V and +VI oxidation states as Pu^{3+}, Pu^{4+}, $PuO_2^{+}$and PuO_2^{2+} respectively. Pu(IV) is the most stable species in solution. Usually, Pu(III) and Pu(IV) are more stable in acidic solutions whereas Pu(VI) and Pu(VII) are more stable in alkaline solutions. Pu(V) will be mainly found as the main species in near-neutral solutions at low concentration. The complexity of plutonium chemistry is that all these oxidation states can coexist in the same solution. In acidic media, the redox potentials relative to the couples involving the oxidation states +III, +IV, +V and +VI are all close to 1 V as it can be shown in the Latimer's diagram in **Figure II.5**. It is a unique feature in the periodic table of elements [1970CLE]. This ability to exist under multiple oxidation states in solution is due to the tendency of Pu(IV) and Pu(V) to disproportionate. In acidic solution without complexing ligands, Pu(IV) disproportionate into Pu(III) and Pu(VI). The disproportionation of Pu(V) takes place in moderately acidic solution leading to Pu(IV) and Pu(VI). Generally, those reactions involve two steps with

different kinetics. As uranium, the reactions involving the formation or the breaking of Pu=O bonds are slow, whereas reactions involving a simple electron exchange are fast [1959NEW].

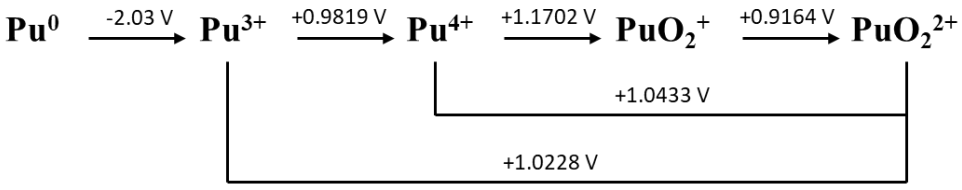

Figure II.5 Latimer's diagram of Pu in 1 M $HClO_4$ [1970CLE].

B) Aqua ions

The hydration structure of actinide ions has been studied mainly by X-ray and neutron scattering, EXAFS and theoretical calculations. However, the exact number of H_2O molecules N_w in the first coordination sphere of An^{3+} and An^{4+} is still under debate: these ions are surrounded by at least 8 water molecules. There is often a difference of 1 molecule between experimental and theoretical values [2006SZA] [2013KNO]. An equilibrium between 8- and 9-coordinated An^{3+}, or between 9- and 10-coordinated An^{4+}, may occur. For instance, the coordination number of Cf(III) with water molecules is determined to be eight by combining EXAFS and Monte Carlo simulation. Moreover, quantum chemistry calculations lead to too small difference in free energy between the corresponding configurations [2010GAL].

The number of water molecules coordinated to Th^{4+} has been found to vary from 9 to 13 [1999MOL] [2002NEC] [2002ROT] [2007HEN] [2009TOR] [2012KNO]. The distance Th-O_w was determined ranging from 2.45 to 2.46 Å at low pH using X-ray absorption spectroscopy. By comparing experimental and theoretical XANES spectra calculated considering different values of N_w and different coordination polyhedra, Chaboy et al. conclude that Th(IV), U(IV) and Np(IV) are surrounded by 9 water molecules that form a tricapped trigonal prism like structure b in **Figure II.6** [2011CHA]. This is consistent with the experimental data of Hennig et al. (U(IV)) [2007HEN] and Antonio et al. (Np(IV)) [2001ANT], but not with Ikeda et al. who found $N_w = 10$ for U(IV) [2009IKE]. The distances An(IV)-O_w were found equal to 2.41, 2.37 and 2.39 Å respectively for U, Np and Pu, the latter being surrounded by 8 or 9 water molecules [1998CON].

At oxidation states +V and +VI, U, Pu, Np and Am exist as molecular ions. They exhibit a linear trans-dioxo bond: the actinyl moiety (An-O_{ax} between 1.75 and 1.82 Å). Due to the steric hindrance produced by this bond, only 5 water molecules coordinate the metal in the equatorial plane with An-O_{eq} distance ranging from 2.36 to 2.52 Å [2006SZA] [2010CHO]. **Figure II.6**

summarizes the possible molecular geometries of aqua ions for plutonium at several oxidation states (+III, +IV, +V, +VI and +VII) [2000CLA].

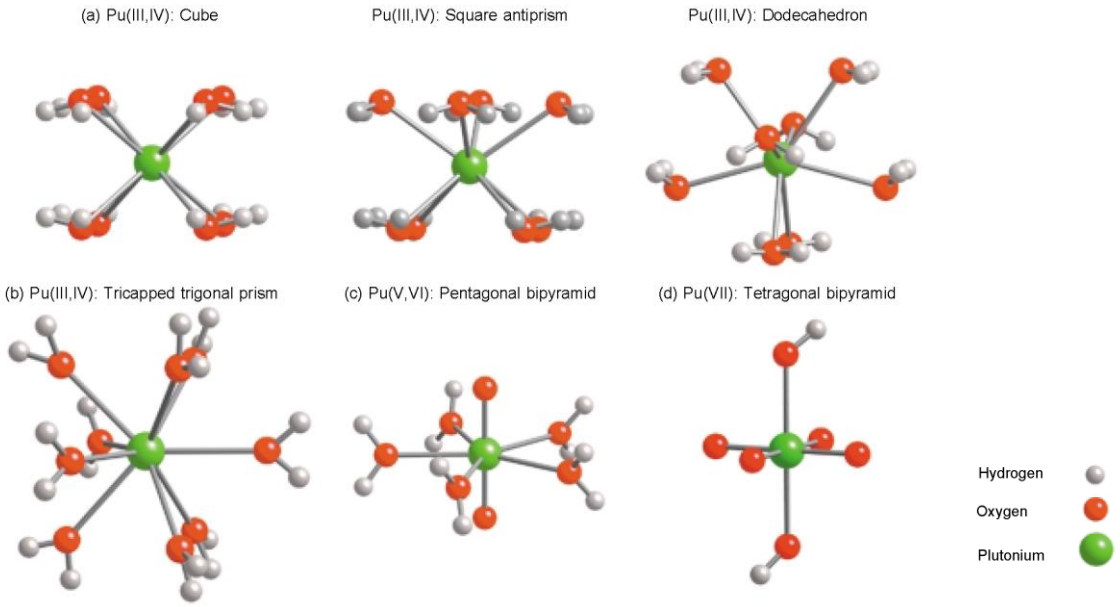

Figure II.6 Possible molecular geometries for the plutonium aquo ions (a) with eight water molecules for Pu(III) and Pu(IV) in three geometric arrangements; (b) Pu(III, IV) with nine water molecules; (c) Pu(V) and Pu(VI), actinyl ions with five water molecules in the equatorial plane and (d) Pu(VII) [2000CLA].

Actinides aqua ions can exhibit a variety of colors depending on their oxidation states. For example, the solutions containing plutonium ions at oxidation states from +III to +VII in non-complexing media are presented in **Figure II.7a**. Each oxidation state exhibits a characteristic absorption spectrum (**Figure II.7b**). The presence of f electrons leads to the presence of sharp absorption bands in the spectrum. Thus, the spectrum of Pu(VII) is the only one without any sharp band. Those sharp bands that can be observed in the visible and near-infrared range reflect the internal 5f transitions [2000CLA].

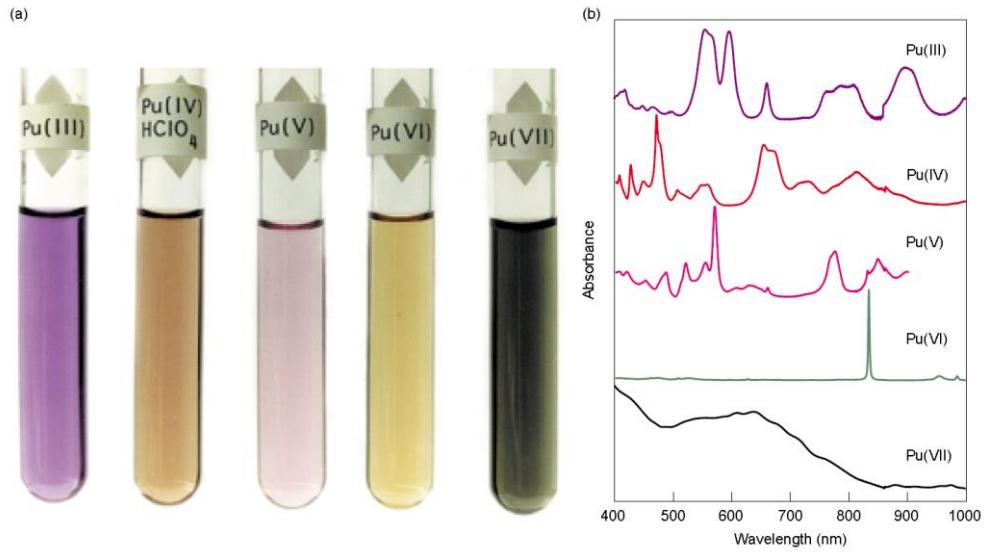

Figure II.7 (a) The color of non-complexed plutonium at various oxidation states in 1 M $HClO_4$ from Pu(III) to Pu(VI) and in strong base for Pu(VII) (b) their corresponding absorption spectra [2000CLA].

C) Hydrolysis

Hydrolysis can be regarded as a complexation with hydroxide in water. For a given actinide, the tendency towards hydrolysis follows the sequence $An^{4+} > AnO_2^{2+} > An^{3+} > AnO_2^{+}$ [1986KAT]. according to the effective charge on the metal ions: in the case of actinyl ions, these charges are indeed 2.3 ± 0.2 and 3.3 ± 0.1 for $An^{V}O_2^{+}$ and $An^{VI}O_2^{2+}$ respectively, because of the covalent bond between actinide and oxygen [1983CHO]. For a given oxidation state (+III or +IV) this tendency increases with Z.

The first step of hydrolysis corresponds to the transfer of a proton from the first coordination sphere to the second. It is followed by the release of proton in the bulk. The hydrolysis equilibria can be described by the following equation:

$$[M(OH_2)_m]^{n+} + hH_2O \rightleftharpoons [M(OH)_h\,(OH_2)_{m-h}]^{(n-h)+} + hH_3O^+ \qquad \text{II.1}$$

Once formed, the hydrolyzed species can undergo condensation reaction according to olation (**Equation II.2**) or oxolation (**Equation II.3**) mechanisms [1992HEN].

$$M-OH + M-OH_2 \rightarrow M-OH-M + H_2O \qquad \text{II.2}$$

$$M-OH + OH-M \rightarrow M-O-M + H_2O \qquad \text{II.3}$$

Hydrolyzed actinide ions tend to undergo mainly condensation by olation, leading to the formation of hydroxo-bridged oligomers [2013KNO]. In the case of An(IV), polymer aging leads

to oxo bridged species [1978JOH]. But a feature of An(IV) chemistry lies in the formation of colloids, for which the first step is the formation of hydrolyzed monomeric species [2009WAL].

The hydrolysis behavior of actinides has been studied for many decades and a large amount of hydrolysis constants (not always consistent) are available in the literature. Some critical reviews devoted to the development of thermodynamic database on equilibria involving actinides in aqueous solution include monomers and oligomers [2001LEM] [2003GUI] [2008RAN]. In the present work, different concentration scales of lanthanides and actinides have been used. Liquid-liquid extraction experiments were performed with metal at ultra-trace and at relative low pH, allowing the condensation of hydrolyzed actinides to be neglected. Higher metal concentrations have been used in spectroscopic measurements, but the use of strongly acidic medium may avoid the formation of colloidal species [2013KER].

In the following, only hydrolysis constants relative to mononuclear species have been considered. The general equilibrium of hydrolysis reaction for mononuclear species can be expressed as:

$$M^{n+} + mH_2O \rightleftharpoons M(OH)_m{}^{(n-m)+} + mH^+ \qquad \text{II.4}$$

Thus, the cumulative hydrolysis constant expressed in concentration is:

$$\beta_m = \frac{[M(OH)_m{}^{(n-m)+}][H^+]^m}{[M^{n+}]} \qquad \text{II.5}$$

Without consideration of colloid and polymer species, the hydrolysis constants of An^{4+} (An = Th, U, Pu), $Cf^{3+}$and Eu^{3+} are presented in **Table II.3**. The speciation diagrams of Th(IV), Cf(III) and Pu(IV) in non-complexing media using the values in **Table II.3** are presented in **Figure II.8**. For Th(IV), hydrolysis starts at pH = 1.0, while the first hydrolysis species of Cf(III) is observed from pH = 5.5. The hydrolysis of Pu(IV) is much stronger than Th(IV): at pH around 0.5, the concentrations of Pu^{4+}, $Pu(OH)^{3+}$ and $Pu(OH)_2{}^{2+}$ are almost the same. The validity of using Th(IV) as model for Pu(IV) can therefore be limited because of the difference in hydrolytic behavior of Th(IV) and Pu(IV).

Table II.3 Hydrolysis constants of Th(IV), U(IV), Pu(IV), Cf(IV) and Eu(III) at 25 °C.

Actinide	β_1	β_2	β_3	β_4	Medium	Method	Reference
Cf(III)	-7.8				0.1 M $NaClO_4$	em.	[1989ROS]
Eu(III)	-7.3				0.7 M NaCl	sol.	[1983CAC]
Th(IV)[a]	-3.35	-8.6	-14.2	-19.4	1.0 M $NaClO_4$	sol.	[2000EKB]
U(IV)[a]	-1.56				0.5 M NH_4Cl	sp.	[1975DAV]
Pu(IV)	-0.45	-1.2	-4.5	-10.8	1.0 M $LiClO_4$	sol.	[1972MET]

a. Values are selected by OECD to estimate the hydrolysis constants at I = 0 [1992GRE] [2008RAN].

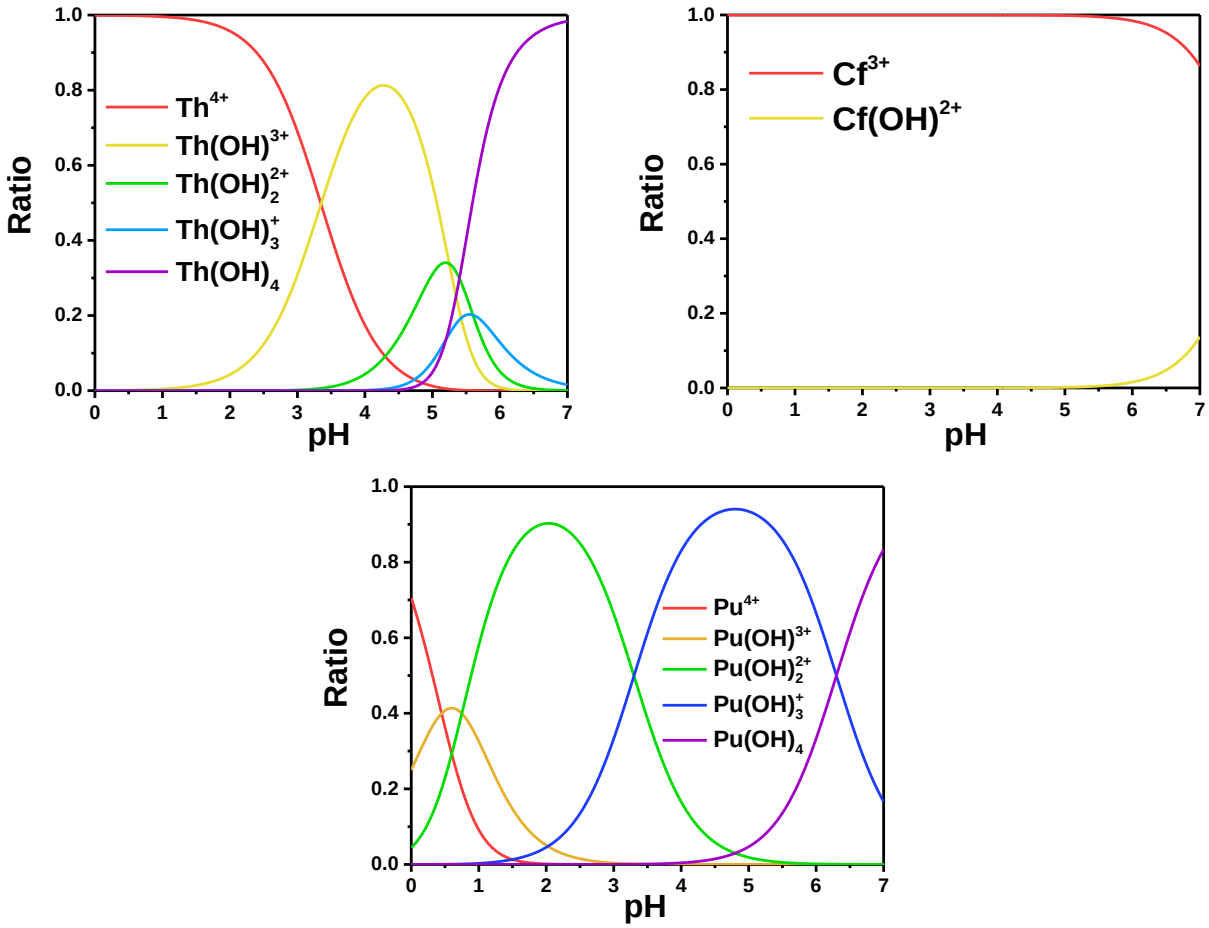

Figure II.8 Hydrolysis speciation diagram of mononuclear Th(IV), Cf(III) and Pu(IV) without considering colloid or polymer species.

D) Actinide complexation

Hard Soft Acid Base (HSAB) principle has been applied to explain qualitatively the interaction between metal ions and inorganic or organic ligands for many years. Hard acids are characterized by small size and high positive charge whereas hard bases exhibit low polarizability and

high electronegativity respectively. On the other hand, soft acids have large size and low positive charge; soft bases have high polarizability and low electronegativity. The general statement of the HSAB principle is that hard acid prefers to coordinate with hard base, and soft acid with soft base [1997PEA].

The common hard, soft and intermediate electron donors are shown in **Table II.4**. According to HSAB principle, actinides ions, with relative high charges and small sizes belong to the class of hard acids. In particular, they interact strongly with oxygen atoms of a great variety of organic compounds.

Table II.4 Classification of Bases [1997PEA].

Hard	Soft
H_2O, OH^-, F^-	R_2S, RSH, RS^-
$CH_3CO_2^-$, PO_4^{3-}, SO_4^{2-}	I^-, SCN^-, $S_2O_3^{2-}$
Cl^-, CO_3^{2-}, ClO_4^-, NO_3^-	R_3P, R_3As, $(RO)_3P$
ROH, RO^-, R_2O	CN^-, RNC, CO
NH_3, RNH_2, N_2H_4	C_2H_4, C_6H_6
	H^-, R^-
Borderline	
$C_6H_5NH_2$, C_5H_5N, N_3^-, Br^-, NO_2^-, SO_3^{2-}, N_2	

Since the strength of the interaction between actinides and a given ligand depends on the effective charge of actinides in the ionic forms, regardless of steric hindrance, the order of the interaction strength should be:

$$AnO_2^+ < An^{3+} < AnO_2^{2+} < An^{4+}$$

This rule can be commonly observed in aqueous solution without ligands or in the presence of inorganic ligands in aqueous solution since the water molecule or inorganic ligand are small enough to ignore the steric hindrance. Thus, the effective charge decides the strength of interaction in this case.

However, with consideration of steric hindrance, the reactivity order of An^{3+} and AnO_2^{2+} may be reversed and the general tendency of actinides to form complexes follows the sequence:

$$AnO_2^+ < AnO_2^{2+} < An^{3+} < An^{4+}$$

Thus, the complex with An(IV) should be most stable in solution due to its highest effective charge. On the contrast, An(V) should normally form the weakest complex with ligands.

At the same oxidation state, the stability of actinide complexes increases with atomic number (decrease of the atomic radii). The effective ionic radii for An(IV) with a coordination number of eight are 1.05, 1.00, 0.96, 0.95, 0.95 and 0.92 Å for thorium, uranium, plutonium, americium, curium and californium, respectively [1976SHA]. Thus, the interaction of Pu^{4+} with ligand is expected to be stronger than that of U^{4+} and Th^{4+}.

II.1.3. Actinides in the environment

Actinides released in the environment have several sources. The sources can be natural or anthropogenic. Most environmental contamination is anthropogenic.

The naturally occurring actinides are composed of primordial nuclides. They were created before our solar system. Among those primordial, ^{238}U, ^{235}U and ^{232}Th can be listed. They were produced from neutron capture reactions during supernova explosions. They are featured by a half-life longer than the age of the Earth. By radioactive decay, primordial actinide nuclides can produce other actinides, called radiogenic nuclides (decay chains). The last kind of naturally occurring actinides are the nucleogenic nuclides. They are issued of natural terrestrial nuclear reaction.

The second sources of actinides in the environment are the anthropogenic actinides. They are mainly due to nuclear weapons fallout, from nuclear power plant activities and incidents. The anthropogenic actinides are mainly composed of the transuranium elements. One of the main sources of actinides in the environment is the weapon tests. From 1945 to 1980, 543 nuclear tests have been conducted in the Northern hemisphere. After 1963, nuclear tests were mainly underground tests to limit the release in the atmosphere. Those tests are equivalent to 0.1 tonne of plutonium released in underground tests and 3.5 tonnes in atmospheric tests. Radionuclides issued from nuclear tests remaining countable possess long half-lives and are mainly ^{241}Am, ^{239,240}Pu, ^{237}Np, but also ^{137}Cs and ^{90}Sr. Accident with nuclear-powered satellites also introduced plutonium in the environment. It was the case in 1964 with the SNAP-9A. Fallouts were mainly located in the Sothern hemisphere and were evaluated to 100 TBq of ^{238}Pu [2013ATW]. Another source is the release of actinides from nuclear plants during plutonium production or reprocessing steps. Some intentional and accidental releases were observed as airborne and/or liquid discharges. Some examples are Sellafield, in the United Kingdom, with the dissemination from 1952 of ^{137}Cs, ^{90}Sr, ^{241}Am, ^{237}Np and ^{239,240}Pu in the North Atlantic Ocean. Other nuclear plants were concerned, such as La Hague in France, Hanford and Rocky Flat in the United States. The last important source of radionuclides in the environment is incidents at nuclear power plants with the most recent examples, Chernobyl in 1986 and Fukushima in 2011. The Chernobyl accident is the most important accident involving a nuclear power plant. The inventory is evaluated to 5.6 kg ^{239}Pu, 48.5 kg of ^{236}U, 0.136 kg of ^{237}Np and 0.52 kg of ^{241}Am (from ^{241}Pu). The composition of the Chernobyl fallout was observed to vary with distance from the accident site [2018DEN].

The mobility and toxicity of actinides in the environment are mainly governed by their speciation and depend on several parameters (pH, I, Eh, inorganic ligands and organic ligands concentrations, etc.). The oxidation state has a strong influence on the mobility of the actinide in the environment. As mentioned previously, some of the light actinides can be present under several oxidation states. Thus, U, Np and Pu can be present under subsurface conditions as An^{3+}, An^{4+}, AnO_2^{+} and AnO_2^{2+}. This feature complicates the prediction of their behavior in the environment. Other actinides of environmental interest are mainly present under one oxidation state, which is the case for Th(IV) and Am(III) for instance (**Figure II.9**). Light actinides in the oxidation states +III and +IV commonly exist in the environment according to the diverse conditions. As regarding the elements used in the present work, Th and Eu (as chemical analog of trivalent actinides) are at the +IV and +III oxidation states respectively. Generally, actinides in the +III and +IV states have a lower solubility and a higher tendency to sorb on mineral surfaces, whereas in the +V and +VI states, a higher solubility is observed enhancing their mobility.

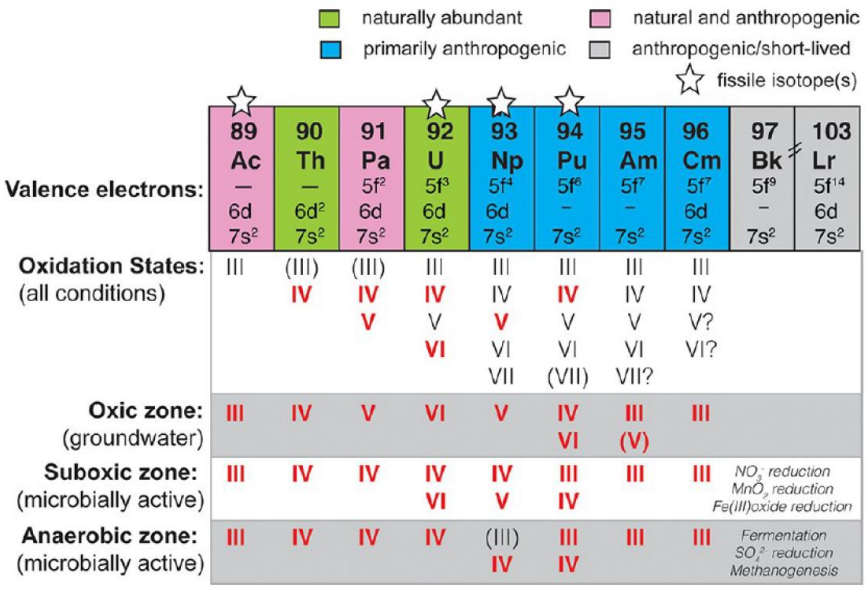

Figure II.9 Common oxidation states of actinides in the environment under different conditions. States mentioned in bracket (−) are unstable; and with a question mark (?) were not confirmed. The oxidation states bolded correspond to the predominant states [2013MAH].

Thus, in reducing environment (anaerobic zone) uranium is mainly present as the low soluble U(IV), whereas in groundwater and in the majority of natural waters, uranium is more soluble in the +VI state. Plutonium speciation in the environment will be strongly dependent on Eh, pH, I, the presence of organic and inorganic ligand, as well as the disproportionation. It may often exist under several oxidation states, from +IV to +VI. Plutonium(III) is only observed in anaerobic environment or in very acidic waters. Pu(V) is the main species in most of natural waters

(aerobic conditions at near-neutral pH) but in very low concentration. The main oxidation states remains Pu(IV) in the environment. Indeed, because of the disproportionation and also because of the low solubility of Pu(IV) the concentration of Pu(V) in natural waters is limited [2007CHO] [2013MAH]. The low solubility of Pu(IV) can reduce its migration by precipitation.

Without complexing ligands, the main species observed in the environment and mainly in natural waters, are hydrolyzed species. In natural waters, the main ligands that can complex with actinides are carbonates and hydroxides. Trivalent actinides form in natural waters mainly $An(OH)^{2+}$, $An(CO_3)_2^-$ and $An(CO_3)^+$ [2007CHO]. However, hydrolysis remains the most important reaction and hydroxyl species have a high tendency to sorb onto colloids, sediments or humic substances. Thorium(IV) species are composed of monomeric and polymeric hydrolysis species according to the pH and the amount of thorium in solution. For instance, at low concentration, $Th(OH)^{3+}$, $Th(OH)_3^+$ and $Th(OH)_4$ will be formed [2007CHO]. For U, Np an Pu, at near neutral pH, the main species are often carbonate species. In natural waters, in presence of carbonate, U(VI) is mainly present as $UO_2(CO_3)_2^{2-}$ and often as $CaUO_2(CO_3)_2$ [1996BER] [2007CHO] [2009PRA] [2013MAH] [2015MAL].

The oxidation state is not the only factor that can influence the migration of actinides in the environment. Another parameter is the sorption of some actinides onto mineral surfaces or colloids. Trivalent and tetravalent actinides are known to sorb readily to surfaces that can reduce their mobility. However, the formation of intrinsic colloids but also the sorption of hydrolyzed species onto colloids leads to further migration of those actinides, especially for plutonium [2007CHO] [2013KER] [2013MAH]. Some studies have shown that Pu migration in the environment could occur by transport on colloidal particles [1999KER] [2002SAN] [2006NOV] [2013ABD] [2013KER].

Their mobility can also be affected by complexation with inorganic and organic ligands, which limits the polymerization. Complexation with organic ligands, from simple carboxylic acids to more complex organic molecules (humic substances) may also strongly influence the actinide behaviors in the environment. The formation of stable complexes with a variety of organic ligands can increase the mobility of the actinide by increasing their solubility. Several organic ligands can be naturally found in the environment, such as humic substances or siderophores.

II.2 Hydroxamate siderophores

The fate of actinides can be strongly affected by the presence of natural organic compounds present in the environment that can modify their speciation and their solubility. Among the relevant organic compounds present in the environment, siderophores are an interesting class of organic complexing ligands. Siderophores are metal-chelating agents secreted by microorganisms and plants [2014AHM]. For the moment, more than 500 different kinds of siderophores are known and are divided into three main classes according to their characteristic functional groups which are hydroxamates (**Figure II.10)**, catecholates and carboxylates. As a member of hydroxamate siderophores, desferrioxamine B (abbreviated name: DFB) was studied in this work in particular because of its commercial availability. Moreover, DFB is estimated to be found in soils at concentrations from 1.7×10^{-7} to 1.3×10^{-8} M [1980POW]. It has a strong ability to bind with actinides owing to its three hydroxamate groups (**Figure II.11**). Collecting fundamental data on actinides-DFB interaction will improve our understanding of their migration behavior in the environment and allow the development of remediation process of contaminated soils and natural waters.

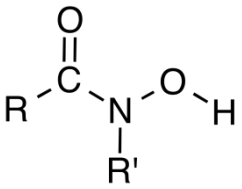

Figure II.10 General structure of hydroxamate functional group.

Desferrioxamine B is a bacterial siderophore containing three hydroxamate functional groups. **Figure II.11** presents the molecule formula of desferrioxamine B. According to HSAB principle, actinides ions are hard acids and hydroxamate group contains O atom donors, i.e hard bases (N is considered as soft in ligands that bear only N atoms) [1983CHO]. Therefore, hydroxamate functional group has a strong ability to coordinate with actinides and stabilize the actinide complex in aqueous solution, and then influence their transport in the environment.

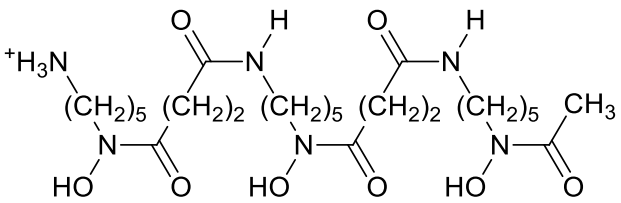

Figure II.11 Desferrioxamine B.

Protonation and deprotonation reactions of organic ligands have a large influence on the formed complexes. The successive dissociation constants available in the literature, starting from totally protonated form of DFB are listed in **Table II.5**. In that case, the four functional groups of DFB (3 hydroxamates and 1 amine) can be involved in protonation-deprotonation process. The constants in **Table II.5** are limited to data available at 25 °C or/and detailed acceptable references.

Table II.5 Dissociation constants of H_4DFB^+ at 25 °C.

$H_nL \rightleftharpoons H_{n-1}L+H$ $Ka_{(5-n)}=[H_{n-1}L][H]/[H_nL]$ $pKa = -\log Ka$

pK_{a4}	pK_{a3}	pK_{a2}	pK_{a1}	I, M	Reference
10.87	**9.57**	**8.97**	**8.35**	**0.1 ($NaClO_4$)**	**[1996HER]**
10.89	**9.55**	**8.98**	**8.32**	**0.1 (KNO_3)**	**[1996HER]**
11.0±0.3	**9.7±0.2**	**9.2±0.1**	**8.4±0.3**	**0.1 (NaCl)**	**[2005DUC]**
10.87	**9.54**	**8.96**	**8.31**	**0.1 (KCl)**	**[1996HER]**
10.79	**9.55**	**8.96**	**8.32**	**0.1 (KCl)**	**[1989EVE]**
10.84±0.01	**9.49±0.02**	**8.96±0.01**	**8.26±0.03**	**0.2 (KCl)**	**[2013TIR]**
10.84±0.03	**9.46±0.01**	**9.00±0.01**	**8.30±0.01**	**0.2 (KCl)**	**[1999FAR]**
10.85±0.01	**9.52±0.01**	**8.96±0.01**	**8.33±0.01**	**0.2 (KCl)**	**[2011SZA]**
10.74±0.09	**9.58±0.02**	**8.93±0.02**	**8.40±0.01**	**0.7 (NaCl)**	**[2011CHR]**
10.89±0.06	**9.70±0.02**	**9.06±0.01**	**8.54±0.01**	**0.7 ($NaClO_4$)**	**[2011CHR]**
10.89±0.02	**9.61±0.01**	**9.05±0.01**	**8.51±0.01**	**1.0 (KCl)**	**[1989BOR]**
10.9±0.1	**9.8±0.2**	**9.2±0.3**	**8.6±0.4**	**1.0 (NaCl)**	**[2010SIM]**

All the values were determined by pot. Except [2010SIM] determined by IR sp.

According to the collected data in the table, it can be seen that the dissociation constants at 0.1 M ionic strength do not depend significantly on the medium composition. A slight increase is observed with increasing ionic strength. Most of the data have been determined by potentiometric titration. The only different technique applied is infrared spectroscopy using a speciation-modeling analysis [2010SIM].

The dissociation constants obtained by Christenson et al. [2011CHR] at I = 0.7 M $NaClO_4$ have been selected in this work since their experimental conditions are the closest to ours. According to the selected dissociation constants [2011CHR], the speciation diagram of DFB is plotted and presented in **Figure II.12**. It can be seen that many different species of DFB exist in a large range of pH. In this work, the thermodynamic study has been conducted at a pH much lower than 6.0. Thus, the predominant species of DFB was always H_4DFB^+ (fully protonated DFB).

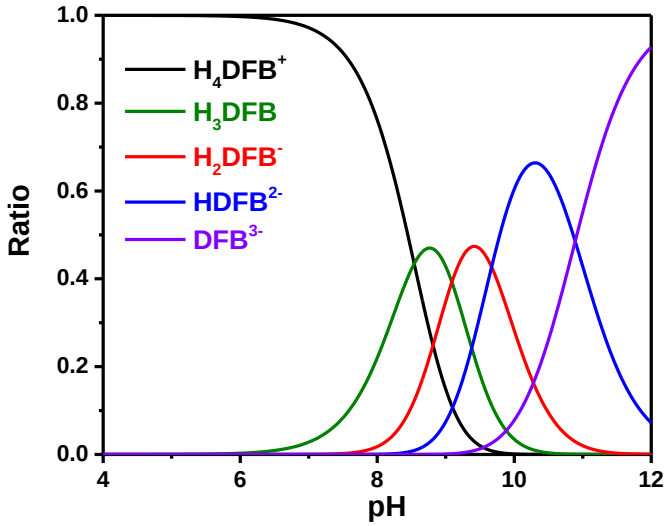

Figure II.12 Speciation diagram of desferrioxamine B (I = 0.7 M Na, $HClO_4$, T = 25 °C).

The available structural information of DFB has been mainly deduced from infra-red spectroscopy measurements [2005EDW] [2005SIE] [2006COZ] [2009BOR]. The detailed discussion and comparison with experimental results are illustrated in **Section IV.1.4**.

Besides desferrioxamine B (DFB), the hydroxamate compounds containing one hydroxamate group such as acetohydroxamic acid (AHA) and benzohydroxamic acid (BHA) were also studied as the analogues of DFB. **Figure II.13** presents the structural formula of BHA and AHA. They can be considered as a model of ligands with multiple hydroxamate groups. In this work, they have been used in the development of an experimental protocol basing on the analysis of UV-Vis absorption spectra.

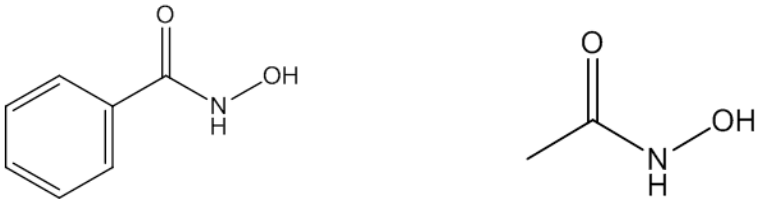

Figure II.13 Benzohydroxamic acid (BHA) (left) and acetohydroxamic acid (AHA) (right).

The dissociation constants of each acid are listed in **Table II.6** and **Table II.7**. Most of the dissociation constants were determined by potentiometric titration and just few dissociation constants were determined by spectrophotometric titration. The used dissociation constants in this study have been chosen according to the determination method and ionic strength. The aim was to select the proper constants at the conditions close to those applied in this work (I = 0.7 M). Thus, for BHA, the constant pK_a = 8.8 was selected. It was determined by Liu et al. at T = 25 °C and I = 0.1 M $NaClO_4$ [1975LIU]. The speciation diagram of BHA obtained from this

constant is depicted in **Figure II.14 (left)**. With the same criteria, for AHA, the dissociation constant pK_a = 9.15 determined by Chung et al. at 25 °C and I = 1.0 M has been selected [2011CHU] and the speciation diagram of AHA obtained from this constant is also depicted in **Figure II.14 (right)**. The pH in this work is controlled to be lower than 6.0. Thus, the species of AHA and BHA should be the non-dissociated one.

Table II.6 Dissociation Constants of Benzohydroxamic Acid (BHA).

HL⇌L+H Ka=[L][H]/[HL] pKa = - logKa

pK_a	T, ℃	I, M	Method	Reference
8.54±0.05	22±1	0 (Davies)	sp.	[2007GLO]
8.79	20	0.1 ($NaClO_4$)	pot.	[1963SCH]
8.76±0.05	22±1	0.1 ($NaClO_4$)	pot.	[2007GLO]
8.8	25	0.1 ($NaClO_4$)	pot.	[1975LIU]
8.757±0.005	25	0.1 (KNO_3)	pot.	[1989KOI]
8.63±0.03	25	0.1 ($NaNO_3$)	pot.	[2007KHA]
8.07±0.06	25	0.1 (KNO_3)	pot.	[2010AKS]
8.10±0.05	25	0.1 (KNO_3)	pot.	[2010AKS]
8.83±0.01	25	0.1 (NaCl)	pot.	[2011TUR]
8.71±0.03	25	0.2 (KCl)	pot.	[2000OBR]
8.65±0.01	25	0.2 (KCl)	pot.	[2005BUG]
8.69±0.02	25	0.2 (KCl)	pot.	[2011SZA]

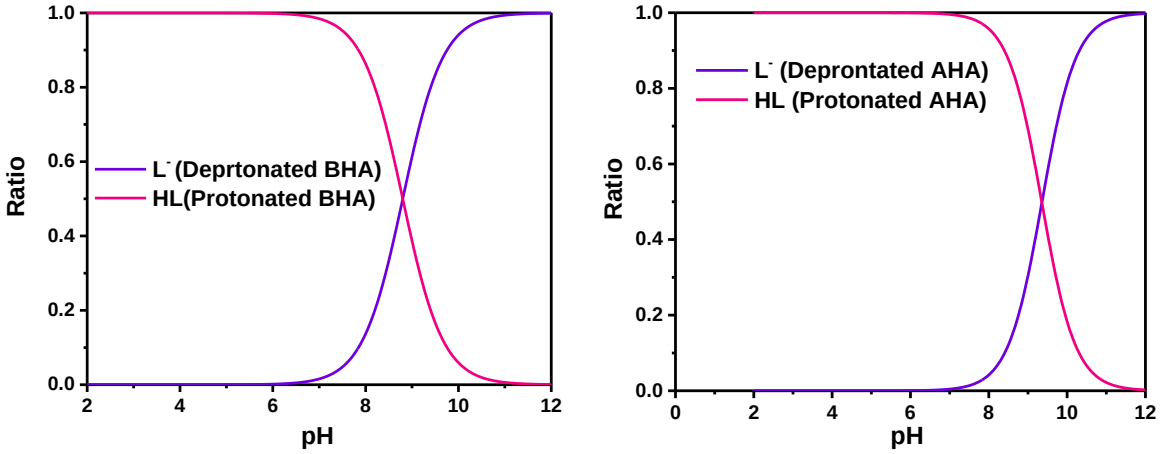

Figure II.14 Speciation diagrams of benzohydroxamic acid (left) in 0.1 M $NaClO_4$ at 25°C and acetohydroxamic acid (right) in 1.0 M NaCl at 25°C.

Table II.7 Dissociation Constants of Acetohydroxamic Acid (AHA).

HL⇌L+H Ka=[L][H]/[HL] pKa = - logKa

pK_a	T, ℃	I, M	Method	Reference
9.35	20	0.1 ($NaNO_3$)	pot.	[1963AND]
9.37	20	0.1 ($NaClO_4$)	pot.	[1963SCH]
9.29±0.06	25	0.1 (KNO3)	pot.	[2010AKS]
9.36±0.01	25	0.1 (NaCl)	pot.	[2011TUR]
9.328±0.006	25	0.1 (KNO_3)	pot.	[1989KOI]
9.40±0.01	25	0.1 ($NaNO_3$)	pot.	[2007KHA]
9.27	25	0.2 (KCl)	pot.	[1999FAR]
9.25±0.01	25	0.2 (KCl)	pot.	[2005BUG]
9.25±0.01	25	0.2 (KCl)	pot.	[2011SZA]
9.15	25	1.0 ($NaClO_4$)	sp.	[2011CHU]
9.018±0.003	22±1	2.0 ($NaClO_4$)	sp.	[2002SIN]
9.12±0.05	25	2.0 ($NaClO_4$)	pot.	[2007SIN]

II.3 Interaction between actinides and hydroxamates

II.3.1 Interaction of actinides with monohydroxamates

The interaction of metal ions with ligands can be described by using the corresponding formation constants. The published stability constants of An(IV) with BHA and AHA are collected and listed in **Table II.8**. The stability constants are normalized to the same equilibrium (**Equation II.6**) in order to compare with each other.

$$iM + nL + mH \rightleftharpoons M_iL_nH_m \qquad \text{II.6}$$

$$\beta_{inm} = [M_iL_nH_m]/[M]^i[L]^n[H]^m \qquad \text{II.7}$$

From the tables, it can be seen that the constants were determined by the techniques such as potentiometric titration, spectrophotometric titration and solvent extraction. The stability constants of Pu(IV) are larger than Th(IV), indicating that the interaction of Pu(IV) is stronger than Th(IV). Barocas et al. determined the stability constants of Th(IV) and U(IV) with BHA by potentiometric titration, but the ionic strength is not clearly indicated [1966BAR].

Table II.8 Stability constants of Th(IV), U(IV) and Pu(IV) with BHA.

$iM+nL+mH \rightleftharpoons M_iL_nH_m$ $\quad \beta_{inm}=[M_iL_nH_m]/[M]^i[L]^n[H]^m$

Actinide	Ligand	logβ_{110}	logβ_{120}	logβ_{130}	logβ_{140}
Th(IV)[a]	BHA	8.97±0.02	17.53		
Th(IV)[b]	BHA	9.6	19.81	28.76	
U(IV)[b]	BHA	9.89	18	26.32	32.94
Pu(IV)[c]	BHA	12.73			
Actinide	**Ligand**	**logβ_{110}**	**logβ_{120}**	**logβ_{130}**	**logβ_{140}**
Th(IV)[a]	AHA	10.50±0.03	19.70±0.05		
Pu(IV)[d]	AHA	14.30±0.03			
Pu(IV)[e]	AHA	14.2±0.2	24.1±0.2	32.2±0.2	

a. The values were determined at T = 25 °C and I = 0.1 M by pot. [2007KHA].
b. The values were determined at T = 25 °C by pot. [1966BAR].
c. The values were determined at T = 25 °C and I = 1.0 M by sol. [1966BAR].
d. The values were determined at T = 25 °C and I = 1.0 M by sol. [2010BRO].
e. The values were determined at T = 22 °C and I = 2.0 M by sp. [2007CAR].

Generally, the complex ability of metal ion increases with atomic number (Z) due to the decrease of ionic radius. Many different models can be used to predict or correct the stability

constants [1999CHA]. Thus, by using the stability constants of Th(IV) and Pu(IV), the stability constants of U(IV) may be estimated in the case of metal in ionic form.

II.3.2 Interaction of actinides with DFB

The complexation of several actinides with DFB has been previously studied. The stability constants of DFB are summarized and listed in **Table II.9**. Because in the literature, equilibrium can be expressed differently, all stability constants listed were normalized to the same equilibrium (**Equation II.6**) in order to compare with each other.

From the table, it can be seen that the interaction of Eu(III) with DFB ($\log\beta_{113}$ = 35.72) is weaker than with Th(IV) ($\log\beta_{113}$ = 41.99). And Pu(IV) exhibit the largest interaction strength with DFB ($\log\beta_{113}$ = 46.37). Eu(III), Th(IV) and Pu(IV) can commonly form the 1:1 complex with DFB and the formation of 1:2 complex was also reported with Pu(IV) [2007NEU] via spectrophotometric titration. For the complex between Th(IV) and DFB, the stability constants with successive deprotonation are determined and the complex involved in hydrolyzed Th(IV) was also studied ($\log\beta_{11-1}$ = 19.49) by Boukhalfa et al. [2007BOU].

Table II.9 Stability constants of Eu(III), Th(IV) and Pu(IV) with DFB.

$iM+nL+mH \rightleftharpoons M_iL_nH_m \quad \beta_{inm}=[M_iL_nH_m]/[M]^i[L]^n[H]^m$

Actinide	$\log\beta_{113}$	$\log\beta_{112}$	$\log\beta_{111}$	$\log\beta_{110}$	$\log\beta_{11-1}$	$\log\beta_{211}$
Eu(III)[a]	**35.72**	**30.91**	**24.56**			
Th(IV)[b]	**41.99**	**40.19**	**37.49**	**29.69**	**19.49**	
Pu(IV)[c]	**46.37±0.5**	**45.76±0.30**	**44.87±0.9**			**84.08**

a. The values were determined at T = 25 °C and I = 0.7 M $NaClO_4$ by pot. [2011CHR].

b. The values were determined at T = 25 °C and I = 0.1 M KCl by sp. [1996WHI].

c. The values were determined at T = 25 °C and I = 0.1 M $NaNO_3$ by sp. [2007BOU].

Besides the thermodynamic studies, many works have also been done to obtain structural information of free DFB and its complex. For example, Siebner-Freibach et al. studied the infrared spectra of free DFB and its complex with Fe as function of pH and temperature [2005SIE]. They reported that the presence of Fe makes C=O (hydroxamate) around 1624 cm^{-1} downshift to lower frequencies around 1586 cm^{-1} according to the curve fitted analysis, which indicates that Fe is complexed with hydroxamate group in DFB. Some other works using FTIR spectroscopy also obtained close conclusions [2005EDW] [2006COZ] [2009BOR]. However, no infrared spectrum was found on actinides-DFB complexes. The work related to the structural study of the complexation between actinides and DFB is also very scarce. In 1999, Neu et al. firstly

characterized the structure of the complex Pu(IV)-DFE by single-crystal X-ray diffraction [2000NEU]. They concluded that Pu(IV) is coordinated with three water molecules and three bidentate hydroxamate groups of one DFE molecule. The ligand DFE (Desferrioxamine E) is very similar to DFB in this work. Both of them have three hydroxamate functional groups and the only difference is that DFE is a cyclic hydroxamate and DFB is a linear one.

Hydroxamates can also act as reducing agents. This property has been considered in nuclear fuel reprocessing for controlling the oxidation states of actinides [1998TAY] [2007CAR]. In the presence of formo- and aceto-hydroxamic acids, reductions of Pu(IV) into Pu(III) and Np(VI) in Np(V) has been observed [1998TAY] [2008CAR]. Under the acidic conditions used in the PUREX process, hydrolysis of hydroxamate moiety in the complex or of free hydroxamic acid, leading to hydroxylamine, has to be taken into account. But in environmental conditions ($5.5 \leq pH \leq 8.2$), where no hydroxylamine is expected to be formed, a rapid reduction of Pu(VI) in Pu(V) was observed upon complexation with AHA and DFB, but Pu(IV) complex and further reduction to Pu(III) were not observed: in environmental conditions hydroxamate groups do not favour the reduction of Pu(V) into Pu(IV) [2018MOR]. Additionally, Boukhalfa et al. also studied the redox properties of Pu(IV)-DFB complex, indicating that the reduction in Pu(III) complex is unlikely to occur [2007BOU].

II.4 Summary

The required knowledge about the complexation between actinides and hydroxamate ligands has been reviewed in this section. The general chemical properties of actinides in aqueous solution and in the environment have been described, including oxidation states, hydration structures, hydrolysis, condensation, complexation, etc. A state-of-the-art knowledge about the properties of desferrioxamine B, benzohydroxamic acid and acetohydroxamic acid, the interaction between tetravalent actinides and trivalent lanthanides with these ligands was presented. The complexation constants available in the literature have been collected, but structural studies are rather scarce.

According to the literature data, speciation diagrams can be plotted using the software HYSS, as illustrated in **Figure II.15** and **Figure II.16**.

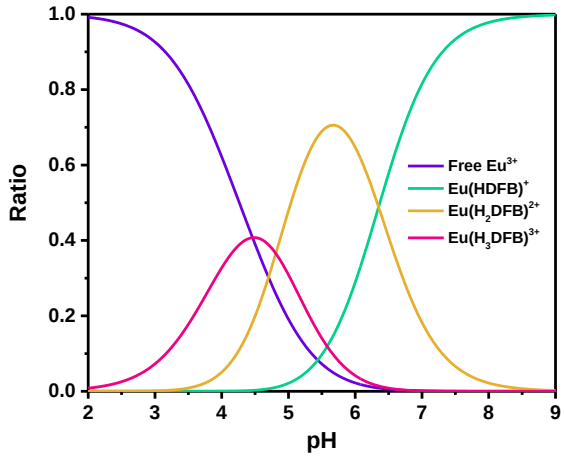

Figure II.15 Speciation diagram of Eu(III)-DFB ($C_{Eu(III)} = C_{DFB} = 2.5\times10^{-2}$ M) plotted by using the literature data [2011CHR].

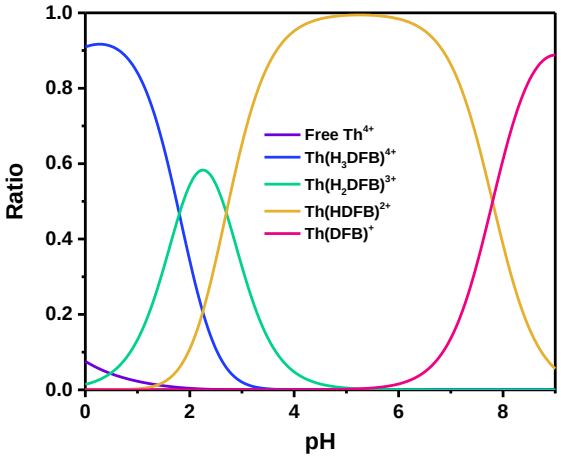

Figure II.16 Speciation diagram of Th(IV)-DFB ($C_{Th(IV)} = C_{DFB} = 2.5\times10^{-2}$ M) plotted by using the literature data [1996WHI].

III. Methodology

This work is focusing on thermodynamic and structural studies of the complexation of trivalent lanthanides (analogues of trivalent actinides) and tetravalent actinides with hydroxamate ligands. The applied techniques, the studied systems and the corresponding experimental conditions are summarized in **Table III.1**.

Table III.1 Applied techniques and studied systems in this work.

Objective	Technique	System	Condition
Stability constant	LLE Combined with γ-spectrometry	^{152}Eu(III)-DFB ^{227}Th(IV)-DFB	T = 25 °C I = 0.7 M (Na, $HClO_4$)
	SP	Pr(III)-DFB Eu(III)-DFB	T ≈ 20 °C (uncontrolled) I = 0.7 M (Na, $HClO_4$)
		U(IV)-AHA U(IV)-BHA U(IV)-DFB	T = 25 °C I = 0.5 M (HCl)
	ACE	La(III)-DFB Lu(III)-DFB	T = 25 °C I = 0.5 M (Na, $HClO_4$)
Structural information	IR	Eu(III)-DFB Th(IV)-DFB	T = 25 °C I ≈ 0.2 M (uncontrolled)
	EXAFS	U(IV)-DFB Th(IV)-DFB	T = 25 °C I ≈ 0.06 M (uncontrolled)

In the perspective of thermodynamic study, the techniques liquid-liquid extraction, UV-visible absorption spectroscopy and affinity capillary electrophoresis were applied to determine the stability constants of the complexes between metal ions and hydroxamate ligands. The tracer scale radioactive metal ions were used in liquid-liquid extraction combined with gamma spectroscopy in order to statistically prevent tetravalent actinides against condensation and develop the protocol for the future study on the scarce actinides. UV-visible absorption spectroscopy was applied to study the metal ions having a good optical absorption property. Affinity capillary electrophoresis was used in this work due to its advantage of homogeneous partition method. In terms of structural study, the techniques ATR-FTIR spectroscopy and EXAFS combined with theoretical calculation were employed to obtain the structural information of the complexation in aqueous solution. The principles of the used techniques, the associated experimental description and preparations of stock solutions of tetravalent actinides are illustrated in the following sections.

III.1 Techniques for thermodynamic study

Radionuclides at tracer scale (10^{-15}-10^{-10} M) are commonly used in radiochemistry, especially with radioactive isotopes having high specific activity of stable elements or of radioelements, (^{95}Zr, ^{239}Np) and with radionuclides not available in macro-amount (At, heavy actinides) [1959ISH] [1969NOR] [1974SIL] [2018GUO].

At such low concentration, in situ species characterization is not feasible [1993ADL]. Partition or transport methods based on radiation or mass detection can be used: for example, liquid-liquid extraction or ion-exchange combined with γ or α spectrometries, capillary electrophoresis combined with ICP-MS are currently used for actinide speciation studies [1996RYD] [2009TOP]. With the radioelements in macro-concentration, conventional techniques of solution chemistry can be used, with caution and technical adaptation allowing handling of radioactive material. In the present work, capillary electrophoresis combined with UV-vis detector and UV-vis spectrophotometry have been used.

III.1.1 Liquid-liquid extraction

A) Principle

In liquid-liquid extraction, a solute is distributed between two immiscible solvents. One generally is an aqueous phase and the other one is an organic phase consisting of an extracting molecule and a diluent. This technique is used in industrial processes, particularly in the reprocessing of nuclear fuel (PUREX, SANEX, DIAMEX, ...) [2002MAD]. In this work, this technique is used as a tool to conduct the speciation study in aqueous phase [1996RYD].

The partition of a metal M is quantified by the distribution ratio *D* according to the following equation:

$$D = \frac{C_{org} \times V_{org}}{C_{aq} \times V_{aq}} \qquad \text{III.1}$$

where *C* refer to the concentration of metal (whatever its chemical form) in both phases.

In the present work, solvent extraction experiments have been performed with the metal at trace scale, using an acidic extractant (β-diketone) that leads to the formation of a neutral chelate in organic phase. In aqueous phase, according to the Rydberg's formalism, the monomer can be written as:

$$M(HpL)_l(HA)_xH_{-y}(H_2O)_z{}^{(n-y)+}$$

Where H_pL and HA are the neutral forms of the ligand and of the extractant, respectively. y stands for the number of group OH^- (y > 0) or H^+ (y < 0). This writing is valid at constant ionic strength and temperature, with non-polar solvents (or low polarity like toluene). In the organic phase, the complex is expected to be neutral. This leads to $N - y = 0$ ($y = N$). So the general form of complex in the organic phase can be written as:

$$\overline{M(HpL)_l(HA)_xH_{-n}(H_2O)_z}^0$$

At constant ionic strength and temperature, thermodynamic activities can be regarded as constant and water molecules do not affect complexation and partition equilibria.

Rydberg's formalism leads to:

$$D = \frac{(\sum_{l=0}^{l_{max}} \sum_{x=0}^{x_{max}} P_{l,x,N} K_{l,x,N} [H_pL]^l [HA]^x [H]^{-N})_{org}}{\sum_{l=0}^{l_{max}} \sum_{x=0}^{x_{max}} \sum_{y=0}^{y_{max}} K_{l,x,y} [H_pL]^l [HA]^x [H]^{-N}}$$

With $P_{l,x,N} = \frac{[M(H_pL)_l(HA)_x H_{-y}]_{org}}{[M(H_pL)_l(HA)_x H_{-y}]}$ the individual distribution ratio of $M(HpL)_l(HA)_xH_{-y}$, otherwise characterized by the formation constant $K_{l,x,y}$, in aqueous phase

$$K_{l,x,y} = \frac{[M(HpL)_l(HA)_xH_y(_z^{(n-y)+}]}{[M][HpL]^l[HA]^x[H]^{-y}} \quad \text{III.2}$$

A mathematical processing of *D* leads to the 3 following relationships that allow the determination of the mean composition and charge of species involved in extraction and complexation equilibria.

$$\frac{\partial logD}{\partial \log [HpL]} = \langle l_{org} \rangle - \langle l_{aq} \rangle \quad \text{III.3}$$

$$\frac{\partial logD}{\partial \log [HA]} = \langle x_{org} \rangle - \langle x_{aq} \rangle \quad \text{III.4}$$

$$\frac{\partial logD}{\partial \log [H]} = -n - (-y) \quad \text{III.5}$$

B) Experimental

Organic phase was prepared by dissolving TTA (thenoyltrifluoroacetone) in toluene. Aqueous phase consists of DFB, $NaClO_4$, $HClO_4$ and radionuclides (^{152}Eu or ^{227}Th). The preparations of both phases are described in **Appendix A**.

1. System ^{152}Eu-DFB

Direct extractions (Eu introduced in aqueous phase) were performed away from light in a temperature-controlled water bath (25 °C) at 50 rpm stirring speed during 26 hours. This contact time has been proven to be sufficient to reach equilibrium, the limiting step being partition of the extractant [2003JAU]. Both phases were carefully separated and their activity wer determined by gamma spectrometry. The *D* values were determined according to the counts of each phase at 121 keV. Additionally, it is verified that the values of D_0 in absence of ligands were not significantly influenced by the energy for counting (**Appendix B**). The determination method of proton concentration is described in **Appendix C**.

2. System ^{227}Th(IV)-DFB

Because of insufficient reproducibility in direct extraction experiments with Th, a new protocol based on Sasaki's work, has been developed [2008SAS]. ^{227}Th(IV) was first quantitatively extracted into the organic phase, a TTA solution prepared by dissolution of TTA-hydrate in toluene pre-equilibrated with an aqueous phase of a given pC_H. Then aqueous phases with DFB concentration ranging from 0 to 0.08 M at a given pC_H were contacted during 3 hours with the ^{227}Th-loaded TTA solution at 25 °C. This time was proved to be sufficient to reach equilibrium (**Appendix D**). Then aliquots parts of same volume of each phase were withdrawn and their activity determined by γ-spectrometry at 236 keV, allowing the distribution ratio to be calculated.

Experiments with ^{227}Th have been performed in glass vials with walls protected by galxyl parylene (Comelec) in order to prevent the adsorption of Th(IV) on glasses walls. Sorption of Th as well as of the complex $Th(TTA)_4$ from perchlorate solutions on glasses has namely already been observed [1969EDR].

III.1.2 Ultraviolet-visible absorption spectroscopy

A) Principle

Ultraviolet–visible spectroscopy refers to absorption spectroscopy in the spectral region with wavelength ranging from 200 to 800 nm. An atom or ion can absorb ultraviolet and visible light (electromagnetic radiation), which can lead to excitation of electrons promoted to higher energy levels [2017SKO].

Most of lanthanides and actinides (whatever their oxidation states) exhibit sharp characteristic absorption bands in the ultraviolet-visible region due to f-f transition. For example, plutonium at different oxidation states forms color ions as shown in **Figure II.7**. The color of substance species depends on the wavelength of absorbed energy. Beer–Lambert law states that the absorbance of a solution is directly proportional to the concentration of the absorbing species in the solution and the path length [2016WOR].

$$A = log_{10}\left(\frac{I_0}{I_t}\right) = \varepsilon cL \qquad \text{III.6}$$

where A is the measured absorbance, I_0 is the intensity of the incident light at a given wavelength, I_t is the transmitted intensity, L is the path length, and c is the concentration of the absorbing species. For each species and wavelength, ε is a constant known as the molar absorptivity or extinction coefficient. This constant is a fundamental molecular property in a given solvent, at a particular temperature and pressure, and has units of L/M·cm.

In the case of a mixture of absorbing species, the total absorbance is the sum of the absorbance of each individual species as shown in **Equation III.7**.

$$A_{tot} = \sum A_i = \sum \varepsilon_i c_i L \qquad \text{III.7}$$

where ε_i is the absorbance extinction coefficient of each species and c_i is the concentration of each species. A_{tot} is the total absorbance of all species. L is the light path length through the sample.

According to **Equation III.7**, the stability constant can be deduced from the experimental variation of the total absorbance as a function of ligand or metal concentration using non-linear fitting programs [1993CLA].

Experimentally, absorbance was measured using an UV-visible spectrophotometer. Its schematic diagram is shown in **Figure III.1**.

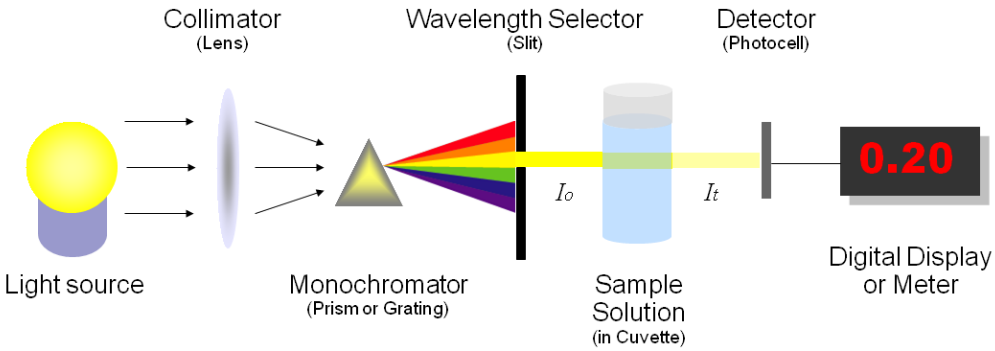

Figure III.1 Schematic diagram of UV-visible spectrophotometer.

B) Experimental

The studied organic ligands AHA BHA and DFB possess broad and intense absorption bands around 200 nm. Variation of the absorption of organic ligands in ultraviolet-visible spectral region is therefore difficult to analyze. Alternatively, the spectral signal of lanthanide or actinide metal ions is followed by UV-visible spectrophotometer. It is expected that the obtained spectra can show the successive variation of the absorption spectra as the increase of the concentration of organic ligands.

The experiments of lanthanides were performed with Agilent Technologies Cary 60 UV-visible spectrophotometer. The baseline was defined by deionized water (MilliQ). The same 1 cm path length cuvette (QS) was used throughout the whole experiment. Before the measurement, the cuvette was washed at least twice by the sample solution which was going to be measured. The scan speed was 3 nm/s and the interval was 0.5 nm. The temperature was roughly estimated to be 20 °C. The software HypSpec was used for spectral data processing [1996GAN].

The experiments of tetravalent with U(IV) were performed with SHIMADZU, UV-2501-PC UV-visible spectrophotometer. The baseline was defined by deionized water (Millipore directQ3). The same cuvette was used throughout the whole experiment. Before the measurement, the cuvette was washed at least twice by the sample solution which was going to be measured. The scan speed was 3 nm/s and the interval was 1 nm. The measurements were conducted at 25 °C using a Peltier temperature controller.

III.1.3 Affinity capillary electrophoresis

A) Principle

Electrophoresis refers to the migration of charged species under the influence of an electric field. In capillary electrophoresis, a potential gap is applied between the ends of a capillary dipping into a conductive solution called electrolyte allowing ions to be separated according to their migration rate v. The electrophoretic mobility μ of the charged species represents the proportionality factor between v and E. It depends on two opposite forces, electrostatic and friction, and it is constant in a given medium [1993GUZ]. The electrophoretic mobility is expressed as:

$$\mu_{ep} = \frac{q}{6\pi r\eta} \qquad \text{III.8}$$

where μ_{ep} is the electrophoretic mobility of a species in a given media. q is the charge of ions and r represents the hydrodynamic radius of ions. η is the dynamic viscosity of the electrolyte.

Due to the differences in charge/size ratio of ions in solution, the ions migrate through the capillary at different speed. Smaller size and higher charge can facilitate the migration. In addition, electrolyte, ionic strength and temperature have an influence on viscosity η and further influence on migration μ [1993GUZ]. Electroosmotic mobility μ_{eof} is an important phenomenon in capillary electrophoresis, indicating the flow of electrolyte under an electric field. **Figure III.2** presents the schematic of electroosmotic flow. The deprotonation of SiOH groups on the silica capillary leads to the formation of a double layer. The outer layer free ions can be moving towards electrode, leading to the electroosmotic flow in an electrolyte-filled capillary under high-voltage [2017SKO].

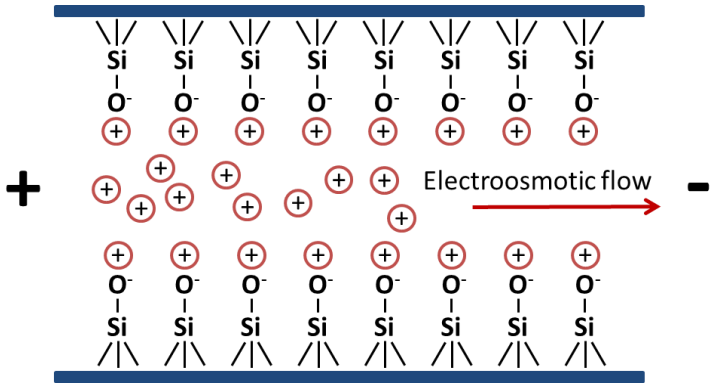

Figure III.2 Schematic of electroosmotic flow.

Thus, in the existence of electroosmotic flow, the migration velocity and time can be expressed as:

$$v = \frac{(\mu_{ep} + \mu_{eof})V}{L} \quad \text{III.9}$$

and

$$t = \frac{lL}{(\mu_{ep} + \mu_{eof})V} \quad \text{III.10}$$

where L is the length of the capillary, V is the voltage applied across the capillary and l is the distance between the point of injection and the detector.

The schematic process of affinity capillary electrophoresis is shown in **Figure III.3**. The injected sample travels through the capillary and interacts with ligands in the electrolyte to form complex. The migration time of sample is varied as the variation of ligand concentration in the electrolyte.

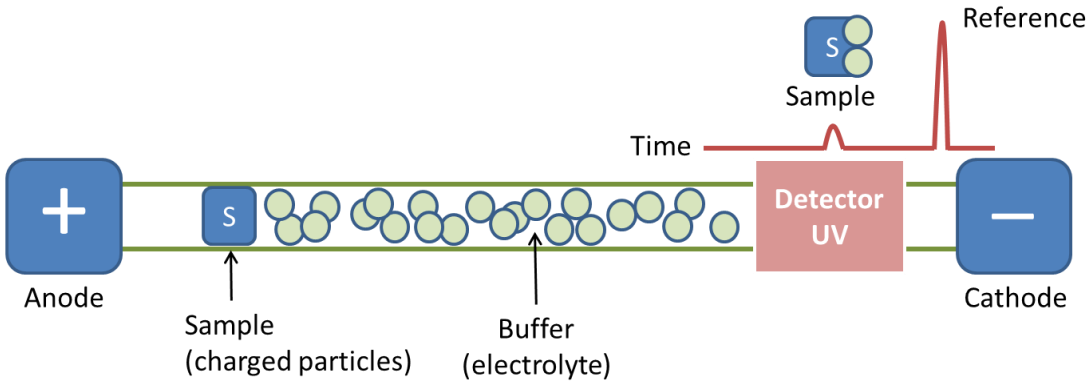

Figure III.3 Schematic process of affinity capillary electrophoresis.

If the kinetic of equilibrium is much faster than the separation time, the apparent electrophoretic mobility is the integration of individual mobility of each species in the sample. In other words, the individual mobility of all the species in the sample makes the contribution to the total electrophoretic mobility [2008CHE]. Thus, the electrophoretic mobility can be described as:

$$\mu_{ep} = \frac{\sum \mu_i C_i}{C_{tot}} = \sum \mu_i \alpha_i \quad \text{III.11}$$

where μ_i is the migration mobility of each species and C_i is the concentration of each species. C_{tot} is the total concentration of all species. α_i is the molar fraction of each species.

Thus, according to **Equation III.11**, the stability constant can be deduced from the experimental variation of the global electrophoretic mobility as a function of ligand or metal concentration using non-linear fitting programs [2016SLA].

B) Experimental

The experiments were performed with the instrument P/ACE system MDQ capillary electrophoresis (Beckman Coulter, France). The system was equipped with a power supply at 0 - 30 kV high voltage and a UV-vis spectrophotometric diode array detector. UV direct detection at 200 nm was applied to record the mobility of analyst. A capillary (50 μm inner diameter and 363 μm outer diameter) made from fused silica was purchased from Beckman Instruments and was used with a total length (Lt) of 31.2 cm and an effective separation length (Ld) of 21 cm. The capillary was set up in an interchangeable cartridge with circulating liquid coolant. The ambient temperature was maintained at 25 °C. Every single measurement was repeated at least three times. Data acquisition and processing were carried out with Karat 32 software (Beckman Coulter, France). Prior to using, the capillary was conditioned by successive washes with 0.1 M sodium hydroxide, deionized water and the prepared buffer solution, respectively. It was rinsed for 2 minutes (at a pressure of 103.4 kPa) with the background electrolyte for study before beginning the electrophoresis.

III.2 Techniques for structural study

III.2.1 Attenuated total reflectance Fourier-transform infrared spectroscopy

A) Principle

Infrared spectroscopy refers to absorption spectroscopy in infrared spectral region. The analysis of the interaction of infrared light with molecules allows to determine functional groups in molecules (organic or inorganic) and to determine the structure of a complex. This is a vibrational spectroscopy. Infrared spectra are from the different vibrational and rotational modes of a molecule. Thus, the absorption of infrared radiation leads to the excitation of those vibrations and rotations. To observe a vibrational mode, it is necessary that the dipole moment change during the vibration. For polyatomic molecules, there are many different modes of vibrations in which bending and stretching are the simplest ones [2000STU]. **Figure III.4** presents the possible vibration types. From the figure, it can be seen that stretching vibrations are characterized by a change of bond lengths and bending vibrations is featured by a modification of bond angles [1989HAR].

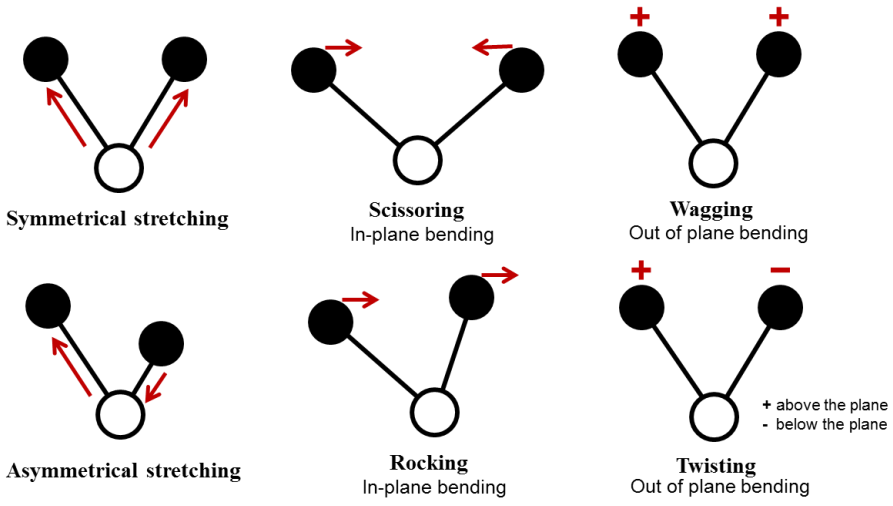

Figure III.4 Types of stretching and bending.

The vibration frequency depends on the masses of the two bound atoms and on the bond strength. The other atoms connected can also slightly influence the frequency. Generally, the wavenumber cm^{-1} is used to indicate the absorption energy of bonds. The larger the wavenumber of the infrared energy absorbed to make resonance, the higher the frequency of vibration in the bonds of molecules. The infrared absorption spectrum can reflect the characteristic

of molecule structure since the absorption wavenumbers are affected by the mode of vibration, the mass of atom, and the strength of bonds [2000STU].

Infrared spectrometer is the instrument to measure the absorption of infrared radiation passing through a sample. There are many types of infrared spectrometers with different advantages. In this work, the used technique was ATR-FTIR short for Attenuated Total Reflectance Fourier Transform Infrared Spectroscopy. The main advantage of ATR-FTIR is that the sample in solid or liquid form can be directly measured without any preparation [1993MIR]. Because the penetration depth is so thin, the infrared absorption of water molecules can be minimized and even be neglected. Since there are usually many bonds with diverse vibrations in molecules, the infrared spectrum can contain many similar wavenumbers of absorptions, which result in the difficulties to analyze the spectrum. Thus, this technique is often applied to study the structure of molecules qualitatively.

B) Experimental

An aliquot of 10µL of each solution was deposited on the surface of the ATR diamond and let dry during half an hour at room temperature. The air-dried samples were analyzed on an IR affinity 1 spectrometer (Shimadzu) with a single reflection ATR (Miracle10, Shimadzu) module and a DLATGS detector. The infra-red spectra were recorded in the range 4000-700 cm^{-1} (resolution 2 cm^{-1}, 64 scans per spectrum). The samples studied by ATR-FTIR in this work are summarized in **Table III.2**.

Table III.2 ATR-FTIR samples description.

Sample	Concentration	pH
free DFB	**[DFB] = 25 mM**	**3.3**
Eu-DFB	**[Eu] = [DFB] = 25 mM**	**1.3 to 9.1**
Th-DFB	**[Th] = [DFB] = 25 mM**	**3.1 to 9.4**

III.2.2 X-ray absorption spectroscopy

A) Principle

X-ray absorption spectroscopy (XAS) refers to absorption spectroscopy in X-ray spectral region with energies ranging approximately from 500 eV to 500 keV (wavelength from 0.25 Å to 25 Å).

This is a powerful technique using synchrotron radiation and based on photoelectric effect. XAS analysis provides information on the electronic properties (oxidation states) of an absorbing atom, as well as, its local structural information (bond distances, neighboring atoms, coordination number).

An incident X-ray photon is absorbed by an atom leading to the excitation or ejection of a core electron. The photoelectron ejected can be considered as a wave emitted in all directions. This wave can then be scattered by nearby atoms, returning to the absorbing atom. It can influence the density of electrons and affect the absorption coefficient μ. Thus, as shown in **Figure III.5**, if we suppose there would be no neighboring atom, the absorption spectrum should be the blue ones. However, in fact, with the existence of neighboring atoms, the scattered photoelectrons can modulate the amplitude of new-created photoelectron wave-function at the absorbing X-ray atom and the actual absorption spectrum should be the red ones.

Electronic and structural information are obtained from the absorption spectrum (**Figure III.5**). This spectrum can be divided in two parts: the XANES and the EXAFS oscillations. The pre-edge and edge correspond to the XANES spectrum (X-ray Absorption Near Edge Structure). This part of the spectrum allows to access to the charge of the absorbing atom. The oscillations correspond to the EXAFS part of the spectrum (Extended X-ray absorption fine structure). Those oscillations are from interferences that can be constructive or destructive between the original wave and the scattered waves from the nearby atoms. The study of the EXAFS spectrum is essential to obtain information on the local structure around the absorbing atom.

XAS is often used to study the speciation of actinides. This is an element specific technique that can be performed at large concentration range (down to 10^{-5} M). Generally, analyses are performed at mM range. Moreover, XAS analyses may be carried out on different sample type such as gas, solutions, amorphous solid, crystalline solid.

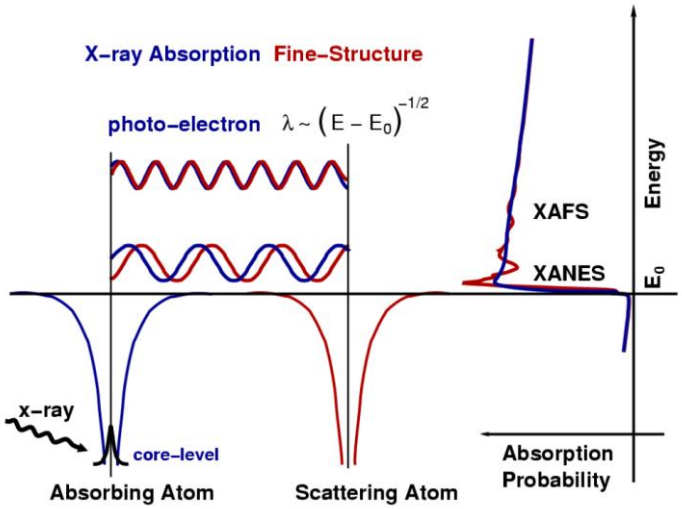

Figure III.5 Principle of EXAFS.

XAS analysis has been used to study the local structure of thorium(IV) and uranium(IV) in the Th(IV)-DFB and U(IV)-DFB complexes. Measurements were performed at the thorium and uranium L_{III} edge corresponding to the excitation of $2p_{3/2}$ electrons to unfilled d orbitals.

B) Experimental

The samples studied by EXAFS are summarized in **Table III.3**.

Table III.3 Description of EXAFS samples.

Sample	Concentration	pH	Edge
Th(IV)-DFB	**[Th] = 5 mM** **[DFB] = 6 mM**	**5**	**L_{III} (16 300 eV)**
U(IV)-DFB	**[U] = 5 mM** **[DFB] = 6 mM**	**5**	**L_{III} (17 166 eV)**

XAS at the thorium L_{III} edge (16300 eV) and uranium L_{III} edge (17 166 eV) were conducted on the MARS beamline of the SOLEIL synchrotron facility. The monochromator was set with the Si(220) crystal and the mirrors with the Pt strips. The optics of the beamline consist of a water-cooled double-crystal monochromator (FMB Oxford), used to select the incident energy of the X-ray beam and for horizontal focalization, and two large water-cooled reflecting mirrors (IRE-LEC/SESO) that are used for rejecting the harmonics at high energy and vertical collimation and focalization. Energy calibrations were conducted at the Y K edge at 17038 eV. EXAFS measurements were conducted in fluorescence mode using a 13-element high purity germanium detector (ORTEC). Due to the possibility of redox reactions under large photon flux, XANES

of the uranium(IV) solutions were monitoring over time to verify the oxidation states (+IV and +VI). The multiple scattering around 15 eV above the edge, featuring the presence of the trans-dioxo from U(VI) was not observed during the acquisition.

Data processing was carried out using the Athena code [2005RAV]. The E_o energy was identified at the first inflection point. Fourier transformation (FT) in k^3 was performed between 2.8 and 14 $Å^{-1}$ with Hanning windows using the ARTEMIS code [2005RAV]. Spectral noise was calculated using the CHEROKEE code [2009MIC] [2013MIC] by using the Fourier back transform filter above 6 Å corresponding to the noise spectrum. The r factor (%) and the quality factor (QF, reduced χ^2) of the fits were provided from ARTEMIS. Phases and amplitudes were calculated using the FEFF9 simulation code [2010REH] using the model structures obtained by the DFT computational method as described in the dedicated section. Three simple scattering paths were included in the fit. The first two simple paths corresponded to oxygen atom scattering, differentiating oxygen atoms from the hydroxamate groups, Th-$O_{N/C}$, and oxygen atoms from water molecules, Th-O_{wat}. The last path corresponds to carbon and nitrogen (Th···C/N) atoms scattering from the hydroxamate groups.

III.3 Stock solution preparations of tetravalent actinides

III.3.1 Preparation of ^{227}Th(IV) stock solution

The isotope ^{227}Th is one of the decay products of ^{231}Pa. During the purification of ^{231}Pa from its daughters, performed by anion exchange chromatography in HCl medium, the isotopes that were not fixed on the resin (^{227}Ac, ^{227}Th, ^{223}Ra) have been stored for several years [1956KRA] [2005LEN]. Since the solution of daughters still contains a small amount of ^{231}Pa, an additional purification was carried out in order to completely remove protactinium. This solution in 10 M HCl was transferred to a column filled with the macroporous anion exchanger Bio-Rad AG-MP1 (100-200 mesh). Then fresh solution of 10 M HCl was percolated on the column until ^{227}Th was no longer detected by γ-spectrometry. Finally, the residual ^{231}Pa was eluted with 10 M HCl / 1 M HF.

The progress of the purification was monitored by analysis each fraction (500 µL) by γ-spectrometry as illustrated in **Figure III.6**. The elution histogram (**Figure III.6 upper**) shows that purified ^{227}Th is obtained in the first 4 mL of 10 M HCl. Gamma spectra of the ^{227}Th and ^{231}Pa fractions are illustrated in **Figure III.6 lower**. Obviously, the ^{227}Th fraction does not contain ^{231}Pa: the three characteristic peaks of ^{231}Pa located at 284.4, 300.8 and 303.5 keV are not observed. But the ^{227}Th fractions still contains ^{231}Pa daughters: ^{223}Ra at 155.2 and 270.4 keV, ^{211}Bi at 351.9 keV and probably ^{227}Ac. The isotope ^{227}Ac cannot be observed (no γ emission).

The hydrochloric solution of ^{227}Th was evaporated to dryness for medium change. The mother solution was prepared in 4 M $HClO_4$; at the time of its use, the ^{227}Th concentration was 4.5 10^{-8} M.

Just prior to liquid-liquid extraction experiments, an aliquot of ^{227}Th mother solution (10 to 50 µL) was evaporated to dryness in a PTFE crucible and the residue taken up in 0.1 M $HClO_4$. Depending on the pC_H value used in experiments, an additional dilution was carried out. The amount of Bi and Ra isotopes was too low to be detected by γ-spectrometry after distribution between organic and aqueous phases.

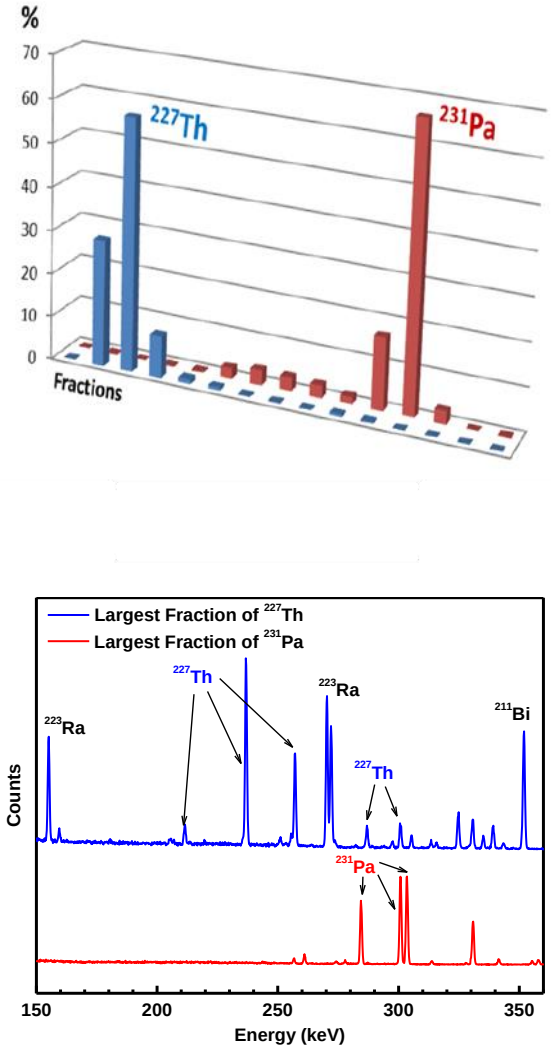

Figure III.6 Percentage of ^{227}Th and ^{231}Pa in each fraction (upper) and the gamma spectra of largest fraction of ^{227}Th and ^{231}Pa (lower).

III.3.2 Preparation of U(IV) stock solution

A piece of the uranium metal was washed successively with acetone, concentrated nitric acid and water, allowing the color of U piece to change from black to silver. Then it was quickly contacted with ~12 M HCl to initialize the reaction and transfer to a beaker containing HCl at about 2 M. The dissolution solution was centrifuged in order to eliminate the black solid residue. The obtained U(IV) solution was characterized using PERALS (for determination of U concentration) and acid-base titration (for determination of HCl concentration. The (IV) stock solution is stored in a freezer compartment.

PERALS analysis has been performed by using ALPHAEX scintillation cocktail. An aliquot of U(IV) solution was first oxidized in U(VI) by H_2O_2 and diluted in 0.5 M HNO_3 in order to get quantitative extraction of U(VI) [1997DAC]. The spectrum presented in **Figure III.7** exhibits two peaks: one associated to ^{238}U, and the other to ^{234}U, isotope in secular equilibrium with ^{238}U. A deconvolution was carried out to determine the activity due to ^{238}U. The analysis, carried out four times, has led to:

$C_U = 0.190 \pm 0.007\ M$

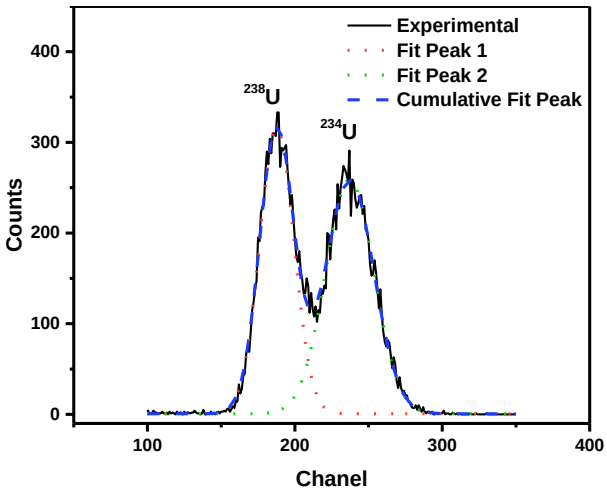

Figure III.7 α liquid scintillation spectrum of an aliquot of the mother solution of U(IV).

The determination of the proton concentration was conducted by titration with NaOH, after addition of DTPA in order to avoid hydrolysis and precipitation of U(IV) [1968CAR]. The titration, performed 3 times, led to:

$C_{HCl} = 1.6 \pm 0.1\ M$

III.4 Summary

This chapter was devoted to the presentation of the methodology used for the investigation of the complexation of tri- and tetra-valent actinides with hydroxamates. The techniques used for the thermodynamic study are liquid-liquid extraction with element at tracer scale, UV-visible absorption spectrophotometry and affinity capillary electrophoresis. For the structural study, ATR-FTIR and X-ray absorption spectroscopies combined with DFT calculations are going to be used. The principle of each technique and its implementation have been described in this part, as well as the preparation of stock solution of ^{227}Th and U(IV). The applied techniques and experimental conditions of each system in this work are summarized in **Table III.4**.

Table III.4 Applied techniques and experimental conditions of each system in this work.

Technique	C_M, Molar	Metal	C_L, Molar	Ligand	Condition
LLE	10^{-8}	^{152}Eu(III)	0 to 0.07	DFB	T = 25 °C I = 0.7 M (Na, $HClO_4$)
	10^{-12}	^{227}Th(IV)	0 to 0.07	DFB	
SP	6×10^{-3}	Pr(III)	0 to 5.6×10^{-2}	DFB	T ≈ 20 °C (uncontrolled) I = 0.7 M (Na, $HClO_4$)
	10^{-2}	Eu(III)	0 to 5.6×10^{-2}	DFB	
	4.8×10^{-3}	U(IV)	0 to 5×10^{-2}	BHA	T = 25 °C I = 0.5 M (HCl)
	9.6×10^{-3}	U(IV)	0 to 0.8	AHA	
	9.6×10^{-3}	U(IV)	0 to 2×10^{-2}	DFB	
ACE	0 to 4.5×10^{-2}	La(III)	10^{-4}	DFB	T = 25 °C I = 0.5 M (Na, $HClO_4$)
	0 to 4.5×10^{-2}	Lu(III)	10^{-4}	DFB	
IR	2.5×10^{-2}	Eu(III)	0 to 2.5×10^{-2}	DFB	T = 25 °C I ≈ 0.2 M (uncontrolled)
	2.5×10^{-2}	Th(IV)	0 to 2.5×10^{-2}	DFB	
EXAFS	5×10^{-3}	U(IV)	0 to 6×10^{-3}	DFB	T = 25 °C I ≈ 0.06 M (uncontrolled)
	5×10^{-3}	Th(IV)	0 to 6×10^{-3}	DFB	

IV. Results and Discussion

IV.1 Trivalent lanthanides

Thermodynamic study with trivalent lanthanides

IV.1.1 Complexation of Eu(III) with DFB studied by liquid-liquid extraction

A) Preliminary study in the absence of DFB

It is known that TTA exhibits good ability to extract a wide range of metallic cations from acidic media [1961POS]. In order to determine the formation constants of Eu-DFB complex in aqueous solution, the competition between the formation of Eu-TTA chelate in organic phase and Eu complexation in aqueous phase must be established in the proper experimental conditions. **Figure IV.1** presents the percentage of Eu(III) extracted in organic phase as function of pC_H. It can be seen that when pC_H is higher than 3.5, Eu(III) is quantitatively extracted into the organic phase in the absence of DFB.

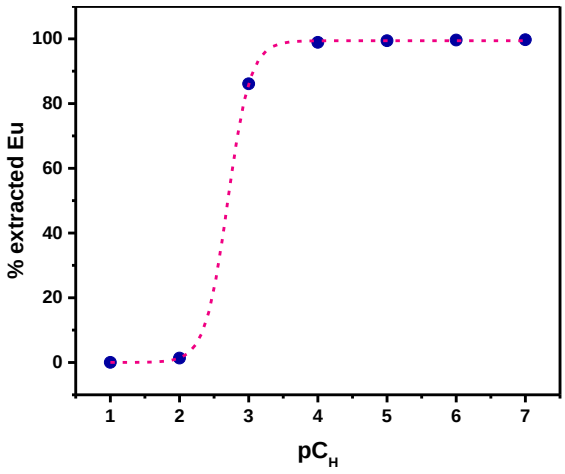

Figure IV.1 Variations of ^{152}Eu extracted as function of pC_H (C_{TTA} = 2.5×10^{-2} M in toluene I = 0.7 M (Na, $HClO_4$), T = 25°C).

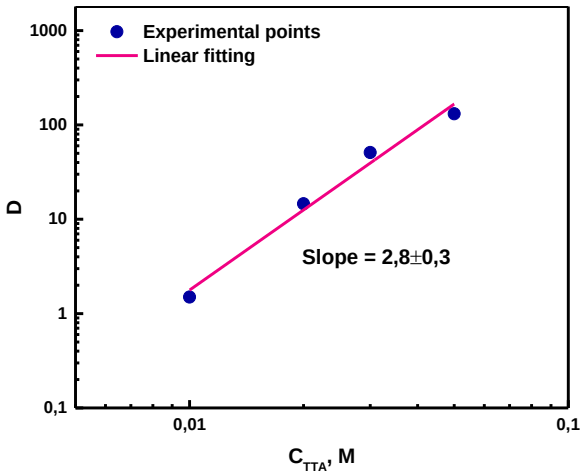

Figure IV.2 Variations of D as function of TTA concentration ($C_{Acetate}$ = 5×10^{-3} M, I = 0.7 M (Na, $HClO_4$), T = 25 °C, pC_H = 4.75).

The variation of the distribution ratio D of ^{152}Eu has been determined as function of the total TTA concentration at pC_H = 4.75. The hydrolysis of Eu(III) can be neglected in this condition [2003RAM]. Working at constant ionic strength and temperature allows correlating the slope of the logarithmic variations of D to the difference in the mean number of TTA molecules per

Eu atom between species in organic and aqueous phase. The variations in **Figure IV.2** lead to a slope equal to 2.8 ± 0.3. As mentioned in the literature [1970IKE] [1989MOH], the slope decreases with increasing pH due to the formation of TTA complex in aqueous phase. The extraction equilibrium in the system can be described as:

$$Eu^{3+} + 3\overline{HTTA} \overset{K_{ex}}{\leftrightarrow} \overline{Eu(TTA)_3} + 3H^+ \qquad \text{IV.1}$$

B) Determination of conditional stability constants K_{cond}

Figure IV.3 presents the variation of distribution ratio (D) of ^{152}Eu as function of DFB concentration for different values of pC_H. Error bars do not appear in **Figure IV.3** since they have the same size of the experimental points.

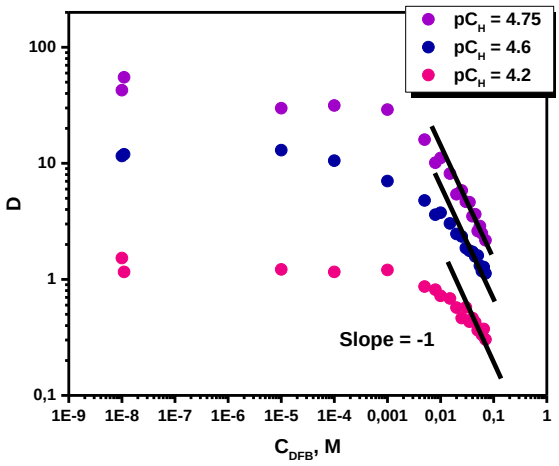

Figure IV.3 Variations of D as function of DFB concentration at different pC_H (C_{TTA} = 2.5×10^{-2} M, I = 0.7 M (Na, $HClO_4$), T = 25 °C, $C_{Acetate}$ = 5×10^{-3} M).

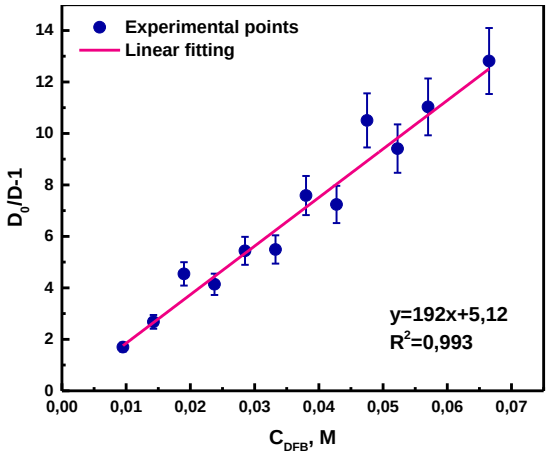

Figure IV.4 Variations of D_0/D-1 as function of DFB concentration ($C_{Acetate}$ = 5×10^{-3} M, I = 0.7 M (Na, $HClO_4$), T = 25°C, pC_H = 4.75).

The values corresponding to C_{DFB} = 0 (D_0) have been arbitrarily drawn at C_{DFB} = 10^{-8} M. Whatever the acidity, the extraction curves display the same general shape: a plateau is first observed at low DFB concentration. Then the D values decrease with the increase in DFB concentration, reflecting the formation of complex in aqueous phase. The slope of the logarithmic variations of D indicates that the maximum stoichiometry of the complex is one according to **Equation III.3**. Thus, the equilibrium in the system can be described as:

$$Eu(III) + DFB \overset{K_{cond}}{\longleftrightarrow} Eu - DFB \qquad \text{IV.2}$$

$$K_{cond} = \frac{[Eu - DFB]}{[Eu(III)][DFB]} \qquad \text{IV.3}$$

The conditional stability constants can be determined according to **Equation IV.4**.

$$\frac{D_0}{D} - 1 = K_{cond}[DFB] \qquad \text{IV.4}$$

Figure IV.4 shows an example to calculate K_{cond} at pC_H = 4.75. Theoretically, D_0/D-1 is proportional to DFB concentration. According to the linear fitting, the obtained value of slope is equal to the value of the conditional stability constant. The obtained stability constants at pC_H = 4.75, 4.60 and 4.20 are summarized in **Table IV.1**. It can be seen that the values of K_{cond} increase with increasing pC_H.

Table IV.1 Conditional stability constants K_{cond} (Equation IV.3) between Eu(III) and DFB at different pC_H.

pC_H	K_{cond}	$\log K_{cond}$
4.75	**192±12**	**2.28±0.03**
4.60	**123±7**	**2.09±0.03**
4.20	**40±3**	**1.60±0.03**

The conditional stability constants for the equilibrium (**Equation IV.2**) has been determined without considering the possible formation of Eu(III) species in aqueous phase, like $Eu(OH)^{2+}$, $Eu(CH_3COO)^{2+}$ or $Eu(TTA)^{2+}$. The determination of the corresponding corrected values of K_{cond} is described below.

C) Determination of corrected conditional stability constant K'_{cond}

Here is to calculate the conditional stability constants taking Eu^{3+} as the chemical form of Eu(III). In aqueous phase, apart from DFB, the molecules possibly interacting with Eu^{3+} are H_2O, TTA and acetate. The corresponding equilibria and associated constants are written from **Equation IV.5** to **Equation IV.14**.

Hydrolysis:

$$Eu^{3+} + nH_2O \overset{\beta_{OH,n}}{\longleftrightarrow} Eu(OH)_n{}^{(3-n)+} + nH^+ \qquad \text{IV.5}$$

$$\beta_{OH,n} = \frac{[Eu(OH)_n{}^{(3-n)+}][H^+]^n}{[Eu^{3+}]} \qquad \text{IV.6}$$

Complexation with TTA in aqueous phase:

$$Eu^{3+} + mHTTA \overset{\beta_{TTA,m}}{\longleftrightarrow} Eu(TTA)_m{}^{(3-m)+} + mH^+ \qquad \text{IV.7}$$

$$\beta_{TTA,m} = \frac{[Eu(TTA)_m{}^{(3-m)+}][H^+]^m}{[Eu^{3+}][HTTA]^m} \quad \text{IV.8}$$

Complexation with acetate:

$$Eu^{3+} + iCH_3COOH \overset{\beta_{acetate,i}}{\longleftrightarrow} Eu(CH_3COO)_i{}^{(3-i)+} + iH^+ \quad \text{IV.9}$$

$$\beta_{acetate,i} = \frac{[Eu(CH_3COO)_i{}^{(3-i)+}][H^+]^i}{[Eu^{3+}][CH_3COOH]^i} \quad \text{IV.10}$$

By definition, the corrected conditional stability constants K'_{cond} correspond to:

$$Eu^{3+} + DFB \overset{K'_{cond}}{\longleftrightarrow} Eu - DFB \quad \text{IV.11}$$

$$K'_{cond} = \frac{[Eu - DFB]}{[Eu^{3+}][DFB]} \quad \text{IV.12}$$

The distribution equilibrium of Eu^{3+} is described as:

$$Eu^{3+} + 3\overline{HTTA} \overset{K_{ex}}{\longleftrightarrow} \overline{Eu(TTA)_3} + 3H^+ \quad \text{IV.13}$$

$$K_{ex} = \frac{[\overline{Eu(TTA)_3}][H^+]^3}{[Eu^{3+}][\overline{HTTA}]^3} \quad \text{IV.14}$$

In the absence of DFB, D_0 can be expressed as:

$$D_0 = \frac{[\overline{Eu(TTA)_3}]}{[Eu^{3+}] + \sum[Eu(TTA)_m{}^{(3-m)+}] + \sum[Eu(CH_3COO)_i{}^{(3-i)+}] + \sum[Eu(OH)_n{}^{(3-n)+}]}$$

$$= \frac{K_{ex}[\overline{HTTA}]^3[H^+]^{-3}}{1 + \sum\beta_{TTA,m}[HTTA]^m[H^+]^{-m} + \sum\beta_{acetate,i}[CH_3COOH]^i[H^+]^{-i} + \sum\beta_{OH,n}[H^+]^{-n}}$$

In the presence of DFB, D can be expressed as:

$$D = \frac{[\overline{Eu(TTA)_3}]}{[Eu^{3+}] + \sum[Eu(TTA)_m{}^{(3-m)+}] + \sum[Eu(CH_3COO)_i{}^{(3-i)+}] + \sum[Eu(OH)_n{}^{(3-n)+}] + [Eu - DFB]}$$

$$= \frac{K_{ex}[\overline{HTTA}]^3[H^+]^{-3}}{1 + \sum\beta_{TTA,m}[HTTA]^m[H^+]^{-m} + \sum\beta_{acetate,i}[CH_3COOH]^i[H^+]^{-i} + \sum\beta_{OH,n}[H^+]^{-n} + K'_{cond}[DFB]}$$

Thus,

$$\frac{D_0}{D} - 1 = \frac{K'_{cond}[DFB]}{1 + \sum \beta_{TTA,m}[HTTA]^m[H^+]^{-m} + \sum \beta_{acetate,i}[CH_3COOH]^i[H^+]^{-i} + \sum \beta_{OH,n}[H^+]^{-n}}$$

$$K'_{cond} = K_{cond} \times (1 + \sum \beta_{TTA,m}[HTTA]^m[H^+]^{-m} + \sum \beta_{acetate,i}[CH_3COOH]^i[H^+]^{-i} + \sum \beta_{OH,n}[H^+]^{-n}) \quad \text{IV.15}$$

In order to determine the stability constants for the equilibrium (**Equation IV.11**), $\beta_{OH,n}$, $\beta_{TTA,m}$ and $\beta_{acetate,i}$ can be used to correct the value of K_{cond} by **Equation IV.15**. However, the unique values of $\beta_{TTA,m}$ are found to be incorrect in the literature [1970IKE]. Thus, only $\beta_{OH,n} = -8.06 \pm 0.08$ and $K_{acetate,1} = 1.97 \pm 0.03$, $K_{acetate,2} = 1.41 \pm 0.04$ ($pK_a = 4.76$) were applied to calculate K'_{cond} [2003RAM] [2006KIT]. The calculated values of conditional stability constants are shown in **Table IV.2**. During the calculation, considering the hydrolysis of Eu(III) does not influence the speciation of Eu(III) in this pC_H domain, but the presence of acetate changes the species distribution of Eu(III) in aqueous phase and further makes the constants decreased.

Table IV.2 Corrected conditional stability constants logK'_{cond} (Equation IV.12) between Eu^{3+} and DFB at different pC_H and comparison with logK_{cond} (Equation IV.3).

pC_H	logK_{cond}	logK'_{cond}
4.75	**2.28±0.03**	**2.5±0.1**
4.6	**2.09±0.03**	**2.2±0.1**
4.2	**1.60±0.03**	**1.7±0.1**

D) Determination of apparent constant K_y

In the pH domain from 4 to 5, the predominant species of DFB is H_4DFB^+ (see **Figure II.12**) and the complexation is expected to occur by the departure of at least one proton of hydroxamate group DFB to form a bond with Eu. Thus, it has been supposed that the overall equilibrium for the 1:1 complex can be described as:

$$Eu^{3+} + H_4DFB^+ \overset{K_y}{\leftrightarrow} Eu\left(H_{4-y}DFB\right)^{(4-y)+} + yH^+ \quad \text{IV.16}$$

$$\text{with } K_y = [Eu\left(H_{4-y}DFB\right)^{(4-y)+}][H^+]^y / [Eu^{3+}][H_4DFB^+] \quad \text{IV.17}$$

where y means the average number of ligand deprotonations occurring during the formation of Eu-DFB complex. It must be emphasized that although there are four possible deprotonations of ligand H_4DFB^+, in fact just three hydrogens of hydroxamate groups can be replaced by Eu(III), which means the maximum value of y is three in the equilibrium. Thus, **Equation IV.17** can be written as:

$$logK_y = log[Eu\left(H_{4-y}DFB\right)^{(4-y)+}]/[Eu^{3+}][H_4DFB^+] + ylog[H^+] \quad \text{IV.18}$$

Using **Equation IV.12**, the following relationship is obtained:

$$K'_{cond} = [Eu - DFB]/[Eu^{3+}][DFB] \quad \text{IV.19}$$

Thus,

$$logK'_{cond} = logK_y - ylog[H^+] \quad \text{IV.20}$$

Figure IV.5 presents the variations of log K'_{cond} as function of pC_H. The linear fitting of the data, according to **Equation IV.20**, leads to y = 1.4 ± 0.1. It means two types of Eu-DFB complex are formed in the system. The corresponding equilibrium is shown below.

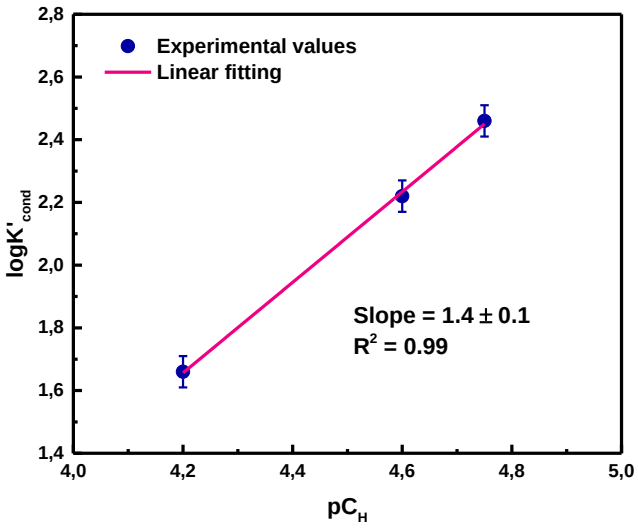

Figure IV.5 Variations of logK'_{cond} as function of pC_H.

$$Eu^{3+} + H_4DFB^+ \overset{K_1}{\leftrightarrow} Eu(H_3DFB)^{3+} + H^+ \quad \text{IV.21}$$

$$\text{with } K_1 = [Eu(H_3DFB)^{3+}][H^+]/[Eu^{3+}][H_4DFB^+] \quad \text{IV.22}$$

$$Eu^{3+} + H_4DFB^+ \overset{K_2}{\leftrightarrow} Eu(H_2DFB)^{2+} + 2H^+ \quad \text{IV.23}$$

$$\text{with } K_2 = [Eu(H_2DFB)^{2+}][H^+]^2/[Eu^{3+}][H_4DFB^+] \quad \text{IV.24}$$

Thus,

$$K'_{cond} = K_1/[H^+] + K_2/[H^+]^2 \qquad \text{IV.25}$$

According to least-square fitting, the values of logβ_{113} and logβ_{112} were obtained and shown in **Table IV.3**. The obtained stability constants are also compared with the literature data. It can be seen that the obtained values are in good agreement with the literature data. But with considering the constants determined from just three experimental points at pC_H = 4.2, 4.6 and 4.75, a relatively large error (0.2) is associated to the constants. The experiments at more pC_H values are needed to be performed in order to verify and accurate the formation constants. According to the current results, this protocol appears promising for an application to the study of the complexation of trivalent actinides with DFB.

Table IV.3 Obtained and published stability constants of $Eu(H_3DFB)^{3+}$ and $Eu(H_2DFB)^{2+}$.

$iM+nL+mH \rightleftharpoons M_iL_nH_m \quad \beta_{inm}=[M_iL_nH_m]/[M]^i[L]^n[H]^m$

[a]logβ_{113}	[b]logβ_{112}	Condition	$C_{Eu(III)}$	Method	Reference
35.4±0.2	**30.9±0.2**	**25 °C 0.7M (Na, $HClO_4$)**	**7×10^{-7} M**	**sol.**	**this work**
35.72±0.06	**30.91±0.06**	**25 °C 0.7M (Na, $HClO_4$)**	**0.04 M**	**pot.**	**[2011CHR]**

a. $\log\beta_{113}=\log K_1+pK_{a1}+pK_{a2}+pK_{a3}+pK_{a4}$

b. $\log\beta_{112}=\log K_2+pK_{a1}+pK_{a2}+pK_{a3}+pK_{a4}$

pKa_1 = 8.54±0.01 pKa_2= 9.06±0.01 pKa_3= 9.70±0.02 pKa_4= 10.89±0.06 [2011CHR]

IV.1.2 Complexation of Ln(III) with DFB studied by UV-visible spectrophotometry

The interaction of Eu(III) and Pr(III) with DFB has been studied by UV-visible absorption spectrophotometry. Eu(III) and Pr(III) have been selected because they possess high molar absorption coefficient in UV-visible range.

First, the validity of Beer-Lambert law relative to Eu(III) and Pr(III) was checked: absorption spectra have been registered at ambient temperature, pH = 4.0, I = 0.5 M with 10^{-3} M ≤ C_{Eu} ≤ 4×10^{-2} M and 6×10^{-4} M ≤ C_{Pr} ≤ 6×10^{-3} M. **Figure IV.6** and **Figure IV.7** presents the corresponding absorption spectra. The absorption bands of DFB appear at the wavelength lower than 300 nm (**Figure A. 5**), which does not interfere with the absorbance of Eu(III) or Pr(III).

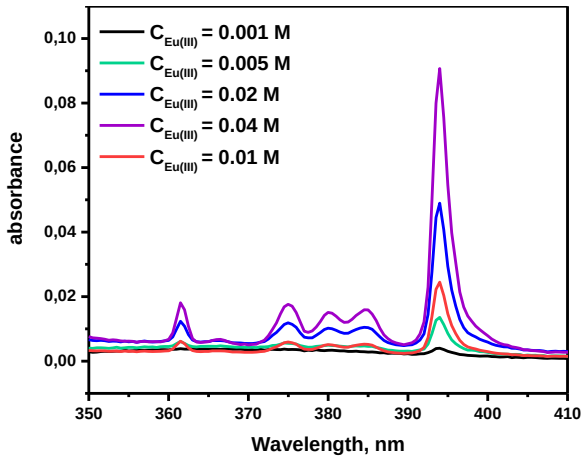

Figure IV.6 Absorption spectra of Eu(III) at different concentrations (pH = 4.0 and I = 0.5 M (Na, $HClO_4$)).

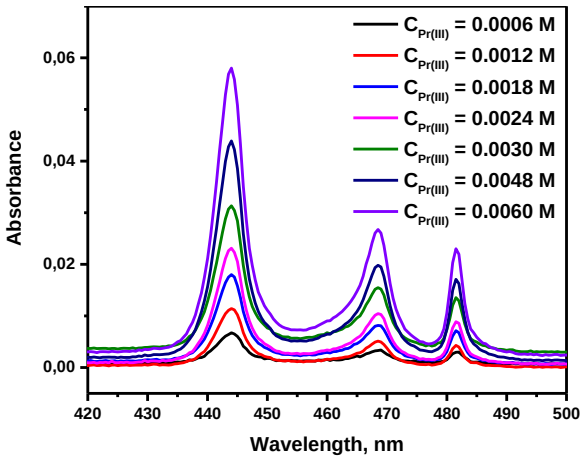

Figure IV.7 Absorption spectra of Pr(III) at different concentrations (pH = 4.0 and I = 0.5 M (Na, $HClO_4$)).

For Eu(III), the absorption maximum has been determined at 394 nm, and for Pr(III), at 444 nm. **Figure IV.8** and **Figure IV.9** present the experimental variations of Eu(III) and Pr(III) absorbance with their concentration and their associated linear fittings. Whatever the element, Beer-Lambert law appears to be valid over the investigated concentration range. The extinction coefficient of $Eu(NO_3)_3$ at 394 nm and $Pr(NO_3)_3$ at 444 nm are calculated to be 2.2 ± 0.2 and 9.2 ± 0.3 $M^{-1}cm^{-1}$, respectively.

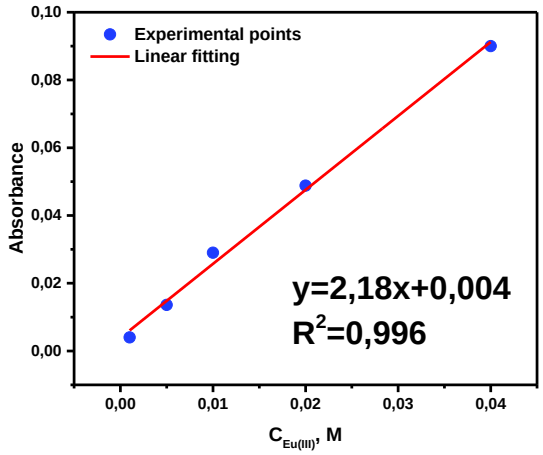

Figure IV.8 Test of Lambert-Beer Law of Eu(III) at the concentration ranging from 10^{-3} to 4×10^{-2} M at pH = 4.0 and I = 0.5 M (Na, $HClO_4$) at the wavelength of 394 nm.

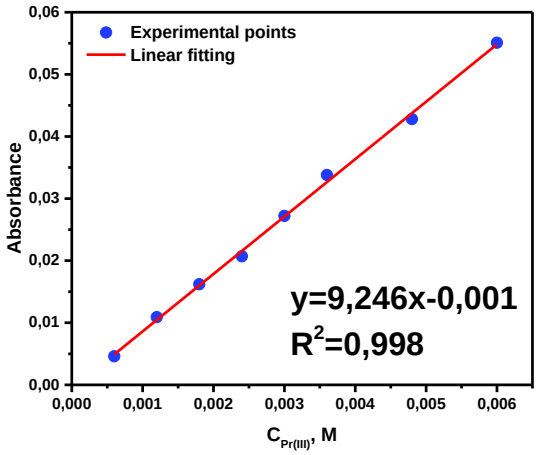

Figure IV.9 Test of Lambert-Beer Law of Pr(III) at the concentration ranging from 6×10^{-4} M to 6×10^{-3} M at pH = 4.0 and I = 0.5 M (H, $NaClO_4$) at the wavelength of 444 nm.

Experiments in the presence of DFB have been performed at pH = 3.7 and 4.5 in the case of Eu(III), and at pH = 4.6 and 5.5 for Pr(III). The metal concentration was fixed at 10^{-2} M and 6×10^{-3} M for Eu(III) and Pr(III), respectively. DFB concentration was varied from 0 to 5.6×10^{-2} M. The UV-Vis absorption spectra of Eu(III) and Pr(III) in the presence of an increasing amount of DFB from 0 to 0.056 M are plotted in **Figure IV.10** and **Figure IV.11**, respectively.

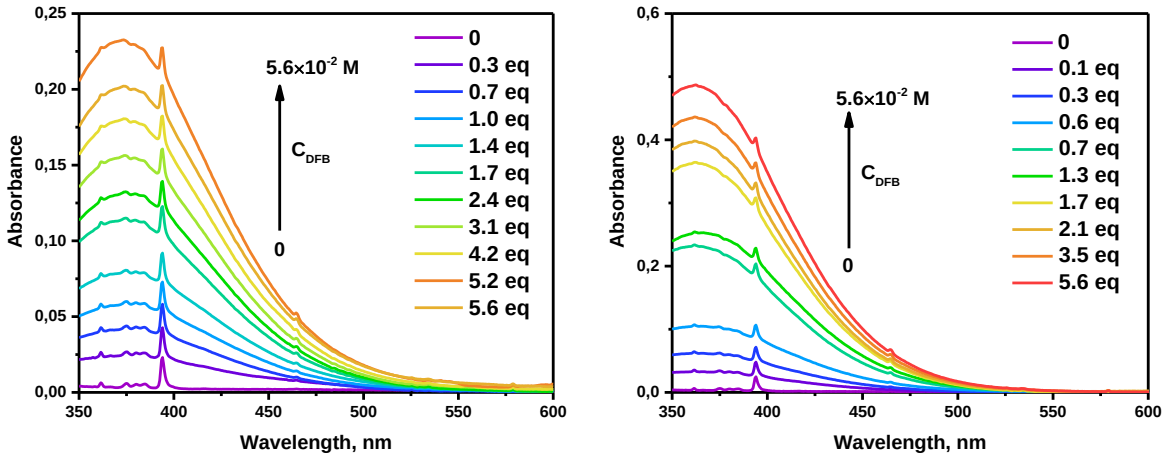

Figure IV.10 Absorption spectra of Eu(III) at 10^{-2} M with increasing amount of DFB at pH = 3.7 (left) and 4.5 (right) (I = 0.5 M, $0 \leq C_{DFB} \leq 5.6\times10^{-2}$ M).

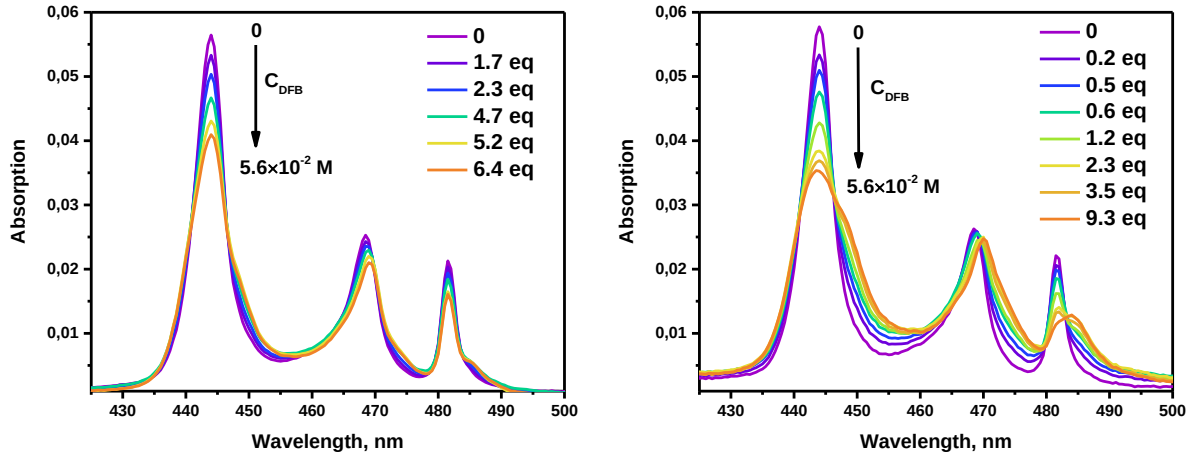

Figure IV.11 Absorption spectra of Pr(III) at 6×10^{-3} M with increasing amount of DFB at pH = 4.6 (left) and 5.5 (right) (I = 0.5 M $0 \leq C_{DFB} \leq 5.6\times10^{-2}$ M).

For the study of Eu-DFB, at pH = 3.7 (**Figure IV.10 left**), it can be seen that as the increase of DFB concentration, the absorption intensity of the broad band from 350 to 550 nm is increasing due to the formation of Eu-DFB complex and a small band is constantly located around 390 nm. In addition, the absorption variation at pH = 4.5 (**Figure IV.10 right**) is more significant than that at pH = 3.7. A larger amount of Eu-DFB complexes is formed at lower acidity with the same Eu(III) concentration range.

For the study of Pr-DFB, at pH = 4.6 (**Figure IV.11 left**), the absorption intensities of the bands at 440, 468 and 481 nm decrease with the increase of DFB concentration due to the formation of Pr-DFB complex. In addition, the band at 468 nm is slightly shifted to the higher wavelength with the increasing DFB concentration. At pH = 5.5 (**Figure IV.11 right**), it can be seen that the band at 444 nm becomes smaller and broader. The band at 468 nm slightly moves to the higher wavelength as the increase of DFB concentration. Additionally, the band at 481 nm disappears and a new band grows up around 484 nm.

All the spectrophotometric data at both of pH were input into the software HypSpec to perform the data analysis. The input protonation constants of DFB as well as complexation constants were determined at I = 0.7 M by E.A. Christenson et al. [2011CHR]. According to their work, the complex LnH_3DFB^{3+} becomes predominant around pH = 3.7. With increasing pH to 4.5, the LnH_2DFB^{2+} complex appears in the solution. Data processing was therefore conducted by assuming the presence of LnH_3DFB^{3+} and LnH_2DFB^{2+}). The output data with HypSpec are the stability constants and the individual spectra of each species. The obtained stability constants are summarized in **Table IV.4**. The molar absorbance of each species in solution is shown in **Figure IV.12** and **Figure IV.13**.

$$DFB^{3-} + Ln^{3+} + 3H^{+} = LnH_3DFB^{3+} \quad \text{IV.26}$$

$$\beta_{113} = \frac{[LnH_3DFB^{3+}]}{[DFB^{3-}][Ln^{3+}][H^{+}]^3} \quad \text{IV.27}$$

$$DFB^{3-} + Ln^{3+} + 2H^{+} = LnH_2DFB^{2+} \quad \text{IV.28}$$

$$\beta_{112} = \frac{[LnH_2DFB^{3+}]}{[DFB^{3-}][Ln^{3+}][H^{+}]^2} \quad \text{IV.29}$$

Table IV.4 Obtained and published stability constants of $Ln(H_3DFB)^{3+}$ and $Ln(H_2DFB)^{2+}$ for Eu(III) and Pr(III).

$iM+nL+mH \rightleftharpoons M_iL_nH_m$ $\beta_{inm}=[M_iL_nH_m]/[M]^i[L]^n[H]^m$

Actinide	Ligand	logβ_{113}	logβ_{112}	Condition[b]	Method	Reference
Eu(III)	**DFB[a]**	**35.6±0.1**	**31.5±0.1**	**20 °C**	**sp.**	**this work**
Eu(III)	**DFB**	**35.72±0.06**	**30.91±0.06**	**25 °C**	**pot.**	**[2011CHR]**
Pr(III)	**DFB[a]**	**35.1±0.1**	**29.9±0.1**	**20 °C**	**sp.**	**this work**
Pr(III)	**DFB**	**35.10**	**29.55**	**25 °C**	**pot.**	**[2011CHR]**

a. Calculated with pKa_1 = 8.54±0.01 pKa_2= 9.06±0.01 pKa_3= 9.70±0.02 pKa_4= 10.89±0.06 [2011CHR]

b. Determined at I = 0.7 M (Na, HClO4)

It can be seen that the obtained stability constants are close to, but slightly different from the literature data determined by potentiometry [2011CHR]. It is probably due to the differences of experimental conditions and techniques. Since the nitrate salt of lanthanide is used in the solution preparation, the electrolyte contains nitrate apart from perchlorate. Additionally, the calculated results can be influenced by the DFB dissociation constants input into HypSpec, but there is no published constants corresponding to the experimental conditions of this work. All the constants in the literature [2011CHR] were used to initialize the calculation of HypSpec. Thus, in spite of the slight difference between the determined constants and the literature data, it can be concluded that the obtained values are in good agreement with the literature data [2011CHR] and this is a useful protocol to determine the stability constant for the further study of trivalent actinides.

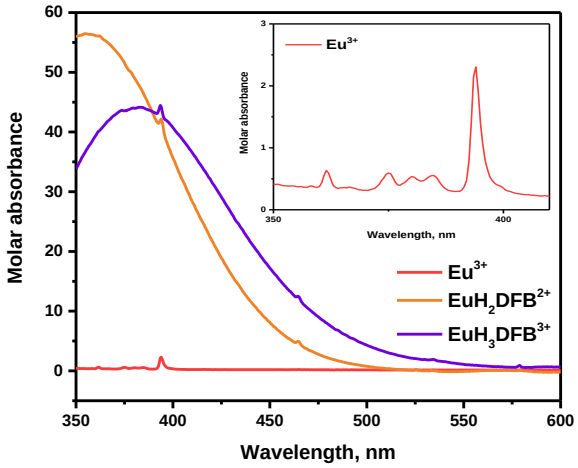

Figure IV.12 Molar absorbance of Eu^{3+}, EuH_3DFB^{3+} and EuH_2DFB^{2+}.

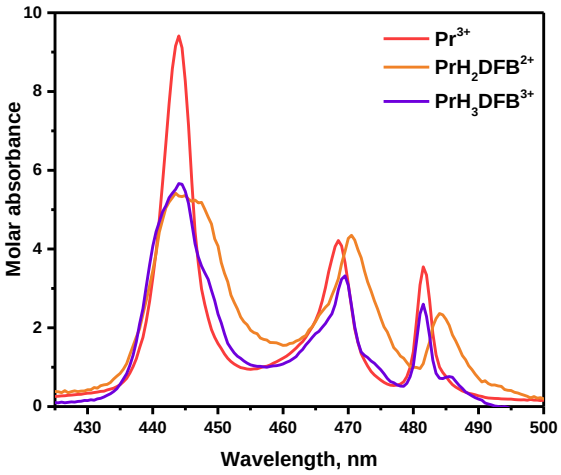

Figure IV.13 Molar absorbance of Pr^{3+}, PrH_3DFB^{3+} and PrH_2DFB^{2+}.

IV.1.3 Complexation of Ln(III) with DFB studied by affinity capillary electrophoresis

The complexation of La and Lu, the lightest and heaviest lanthanide, with DFB has been studied by affinity capillary electrophoresis. By using UV detector to monitor the mobility, some component in the injected sample must display a high extinction coefficient around the wavelength of 200 nm. Instead of lanthanide ions, DFB solution exhibits a strong ultra-violet absorption because of the presence of several absorbing groups [2016WOR]. That is why it was injected into capillary as analyte and its mobility followed by its UV absorption thanks to the diode array detector of the ACE instrument [2006SIM].

Experiments have been conducted at pH = 2.5 and T = 25 °C at two values of ionic strength, 0.1 and 0.5 M (Na, $HClO_4$). The variations of the mobility of the analyte (DFB) as a function of metal ions concentration are presented in **Figure IV.14**.

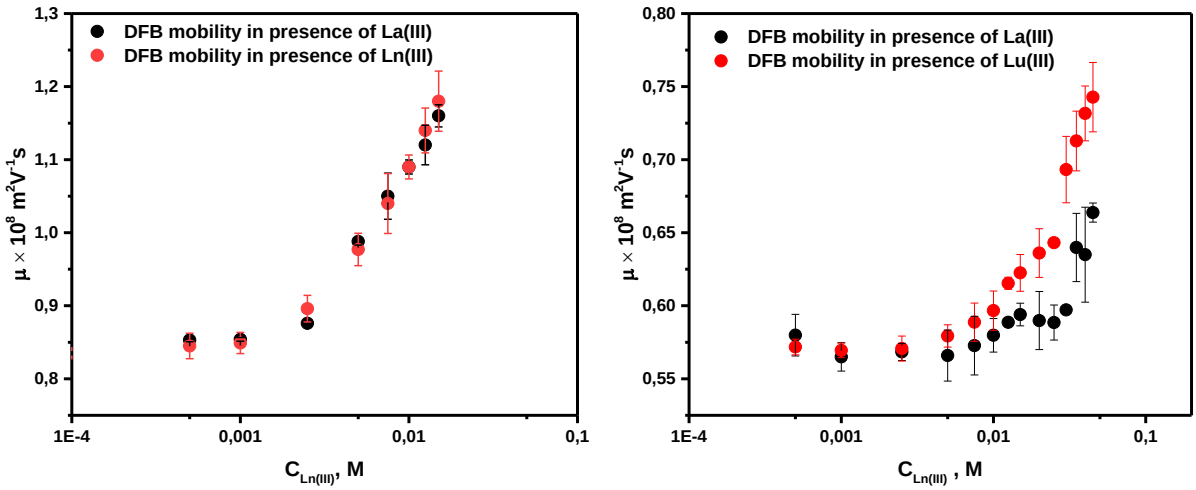

Figure IV.14 Mobility of 1×10^{-4} M DFB as function of La(III) (black points) and Lu(III) (red points) at I = 0.1 M (left) and 0.5 M (right) pH = 2.5, T = 25 °C.

It can be seen that the mobility of injected analyte (DFB) increases with the increase of lanthanide concentration. This can be related to the formation of a complex Ln-DFB that leads to the increase of the total charge of the analyte. Over the narrow range of Ln concentration investigated, the variation of DFB mobility displays a similar tendency in the presence of La(III) and Lu(III). The formed complex is likely to be MH_3DFB^{3+} according to literature data [2011CHR]. Moreover, in this experimental condition (pH = 2.5), the hydrolysis of La^{3+} and Lu^{3+} has been neglected [2000KLU].

The experiments performed at the higher ionic strength (I = 0.5 M), allowed the range of metal concentration to be extended to 0.045 M. However, the high UV absorption of background

electrolyte at the higher concentration of lanthanide ions has been found to interfere with the signal of DMSO (the marker used for determination of electroosmotic migration). In that case, the electroosmotic flow was indicated by H_2O instead of DMSO in order to avoid the slight influence of lanthanides ions on the mobility of DMSO.

The following equilibrium have been considered:

$$H_4DFB^+ + M^{3+} \overset{K_1}{\leftrightarrow} MH_3DFB^{3+} + H^+ \qquad \text{IV.30}$$

$$K_1 = \frac{[MH_3DFB^{3+}][H^+]}{[H_4DFB^+][M^{3+}]} \qquad \text{IV.31}$$

Another way to express the equilibrium is:

$$M^{3+} + DFB^{3-} + 3H^+ \overset{\beta_{113}}{\longleftrightarrow} MH_3DFB^{3+} \qquad \text{IV.32}$$

$$\beta_{113} = \frac{[MH_3DFB^{3+}]}{[M^{3+}][[DFB^{3-}][H^+]^3} \qquad \text{IV.33}$$

In addition, the kinetic of the equilibrium should be fast enough compared to the separation time since the mobility of free DFB and complexed DFB was not distinguished. Thus, the following equation has been used to calculate the equilibrium constant.

$$\mu_{overall} = \mu_{H_4DFB^+} \times \frac{[H_4DFB^+]}{[H_4DFB^+] + [MH_3DFB^{3+}]} + \mu_{MH_3DFB^{3+}} \times \frac{[MH_3DFB^{3+}]}{[H_4DFB^+] + [MH_3DFB^{3+}]}$$

$$= \mu_{H_4DFB^+} \times \frac{1}{1 + K[M^{3+}]/[H^+]} + \mu_{MH_3DFB^{3+}} \times \frac{K_1[M^{3+}]/[H^+]}{1 + K[M^{3+}]/[H^+]}$$

$$\alpha_{H4DFB+} = \frac{1}{1 + K[M^{3+}]/[H^+]}$$

$$\mu_{overall} = \mu_{H_4DFB^+} \times \alpha_{H4DFB+} + \mu_{MH_3DFB^{3+}} \times K_1[M^{3+}]/[H^+] \times \alpha_{H4DFB+} \qquad \text{IV.34}$$

In **Equation IV.34**, $\mu_{overall}$ can be determined experimentally and $\mu_{H_4DFB^+}$ corresponds to the measurements in the absence of lanthanide. The pH was fixed at 2.5. The value of K_1 and $\mu_{MH_3DFB^{3+}}$ can be obtained by a non-linear fitting according to **Equation IV.34**.

The calculation results at I = 0.1 M and T = 25 °C are shown in **Table IV.5**. In order to compare with literature data [2011CHR], the complexation equilibrium constant β_{113} (**Equation IV.33**) was calculated using **Equation IV.35**.

$$log\beta_{113} = logK_1 + pK_{a1} + pK_{a2} + pK_{a3} + pK_{a4} \quad \text{IV.35}$$

Table IV.5 Obtained and published stability constants of $Ln(H_3DFB)^{3+}$ for La(III) and Lu(III).

Lanthanides	La(III)		Lu(III)	
μ_{H4DFB}, m^2/Vs	0.849	-	0.835	-
μ_{MH3DFB}, m^2/Vs	2.11	-	2.32	-
K_1	0.07±0.01	-	0.06±0.01	-
$log\beta_{113}$	36.5±0.1	34.13	36.4±0.1	35.73
T, °C	25	25	25	25
I, M	0.1	0.7	0.1	0.7
Method	ACE.	pot.	ACE.	pot.
Reference	this work	[2011CHR]	this work	[2011CHR]

The used protonation constants of DFB used for normalization of stability constants are the values obtained in I = 0.7 M (Na, $HClO_4$) [2011CHR]. The stability constant K_1 is calculated to be 0.07 ± 0.01 and 0.06 ± 0.01 at I = 0.1 M in the system with La^{3+} and Lu^{3+} respectively. The difference of the interaction strength of DFB with La(III) and Lu(III) cannot be distinguished in this experiment. And the obtained values are much higher than the literature data [2011CHR]. Fitting data at I = 0.5 M, using the same equilibrium (**Equation IV.31**) as I = 0.1 M did not allow to determine the stability constants.

Several reasons can be given to explain the absence of reliable results using ACE. The Ln samples have been prepared by dissolution of a nitrate salt in the electrolyte (Na, $HClO_4$). Although ionic strength has been maintained to 0.1 and 0.5 M, the composition (ratio between nitrate and perchlorate) has continuously varied with increasing Ln concentration. The change in electrolyte composition may affect the viscosity of the buffer. In addition, given the ratio DFB/Ln, the formation of bi- and tri-nuclear species cannot be ruled out. Indeed, the existence of di-nuclear complexes of Ce(III), Nd(III) and Gd(III) have been deduced recently from potentiometric titrations involving metal to ligand ratio equal 2:1 [2013TIR]. A tri-nuclear species of transition element Pb(II) with DFB was also observed by potentiometric titration at 1.5 to 1 metal to ligand ratio [2008FAR].

Further use of capillary electrophoresis to study this system would require an increase of pH to observe a more significant variation of mobility as function of metal concentration. However, using UV-detector, the experiments have to be performed by varying metal concentration in excess over ligand concentration, complicating the curve fitting to find out the proper equilibrium. Thus, it is better to use alternative detector like mass spectrometry to monitor the mobility, so that metal ions can be allowed to be analyte.

Structural study with trivalent lanthanides

IV.1.4 Structural study of the complexation of Eu(III) with DFB by ATR-FTIR

A) IR spectra of free DFB

In order to better understand the complexation of Eu(III) with DFB, IR spectra of the free ligand DFB have been recorded in different conditions. **Figure IV.15** presents the infrared spectra of the desferrioxamine mesylate at pH = 3.1.

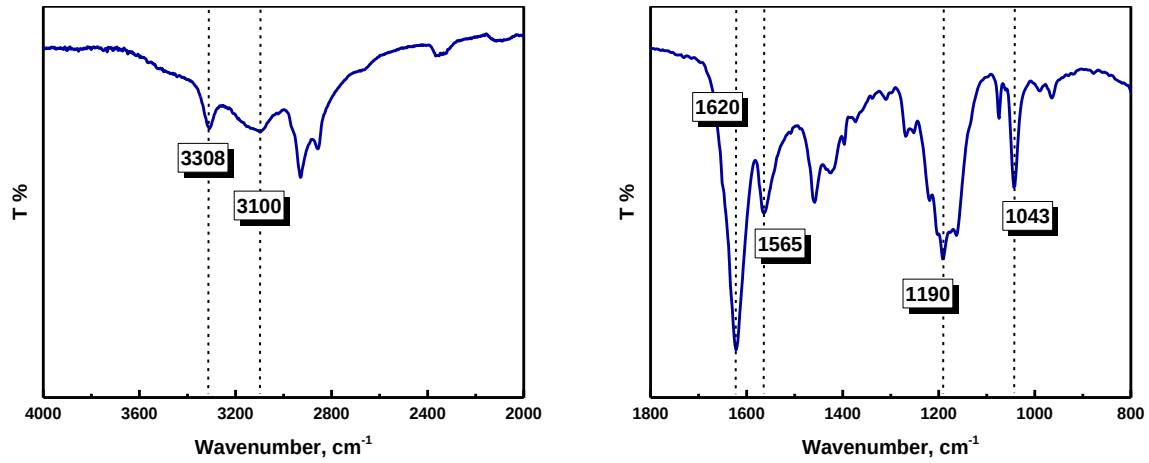

Figure IV.15 IR spectrum of protonated desferrioxamine mesylate at pH=3.1.

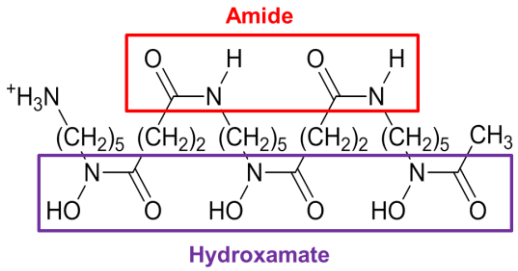

Figure IV.16 Main functional groups of protonated DFB.

The molecule of DFB is composed of several functional groups such as three hydroxamates, two amides, an amine and some alkyl groups. The presence of those functions leads to a significant overlapping of absorption bands in the spectrum, complicating the assignment of each absorption bands. However, DFB spectrum has already been studied and detailed using curve-fitting analyses or calculations [2005EDW] [2005SIE] [2006COZ] [2009BOR]. The main functional groups (hydroxamate groups and secondary amide groups) in DFB are indicated in **Figure IV.16**.

Hydroxamate groups (R-C(=O)-N(OH)-R) are featured by an absorption band of the carbonyl from the ternary amide between 1665-1640 cm^{-1}. In this study, this characteristic band appears at 1620 cm^{-1} (**Figure IV.15 right**). Hydroxamate groups are also featured by the N-OH stretching around 3450-3030 cm^{-1} when they are protonated, but also by the C-N stretching (1175-1055 cm^{-1}) and the bending vibration of N-OH (1420-1330 cm^{-1}). The N-OH vibrations were attributed to the broad band around 3100 cm^{-1} (stretching) (**Figure IV.15 left)** and 1396 cm^{-1} (bending). The band of N-O stretching vibration in hydroxamate groups should appear at 1051cm^{-1} [2006COZ], but it cannot be distinguished due to the interference of mesylate in this case. Because since desferrioxamine mesylate salt powder is used to prepare the solutions, the vibration bands observed at 1043 and 1190 cm^{-1} (**Figure IV.15 right**) correspond to the use of the mesylate salts and prevent the observation of any change in this wavenumber range. The characteristic symmetric and asymmetric bands of the SO_3 functional group are known to be strong stretching vibrations (**Figure IV.17**). They generally appear at 1058 and 1164 cm^{-1} respectively using KBr pellets [2006COZ] or 1049 and 1185 cm^{-1} in solution with an ATR-FTIR [2009BOR].

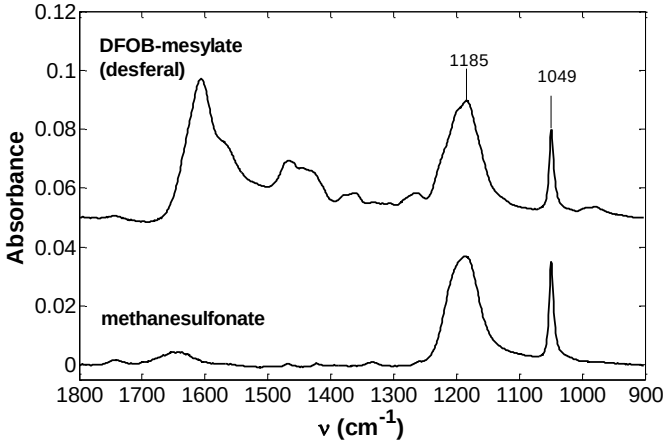

Figure IV.17 IR spectra of solutions containing either the mesylate form of DFB (5×10^{-2} M) at pH = 5.5 or methanesulfonate (5×10^{-2} M) at pH = 4.0 [2009BOR].

Secondary amide group is usually featured by amide carbonyl band among 1695-1615 cm^{-1}, which is around 1651 cm^{-1} for dry samples [2005SIE]. In **Figure IV.15,** this band cannot be distinguished due to the overlapping of the hydroxamate carbonyl band. The carbonyl absorption band from hydroxamate groups is generally sharper and stronger than that from secondary amide groups. The bands from N-H bending and C-N stretching are also observed at 1565 cm^{-1}.

Figure IV.18 presents the mid-infra-red spectra of desferrioxamine mesylate solution (air dried) in absence of Eu(III) at pH from 3.1 to 8.9. Compared to the thermodynamic study, the ionic strength was not fixed at 0.5 M or 0.7 M, preventing the strong influence of the electrolyte in the analysis by drying the samples. In this case, solutions were prepared in pure water and ionic strength was varied due to the pH adjustment. The ionic strength is roughly estimated to be around 2.5×10^{-2} M. In this experiment, the spectra variation due to the deprotonation of hydroxamate groups is expected to be observed, however, the locations of bonding vibrations of DFB are not changed as the increase of pH. It is probably resulted by drying process before the measurements. For the dried powder of DFB, the unique form is always the fully protonated $H_4DFB{\bullet}CH_3SO_3$ and actually it is meaningless to condition the solid using pH or ionic strength.

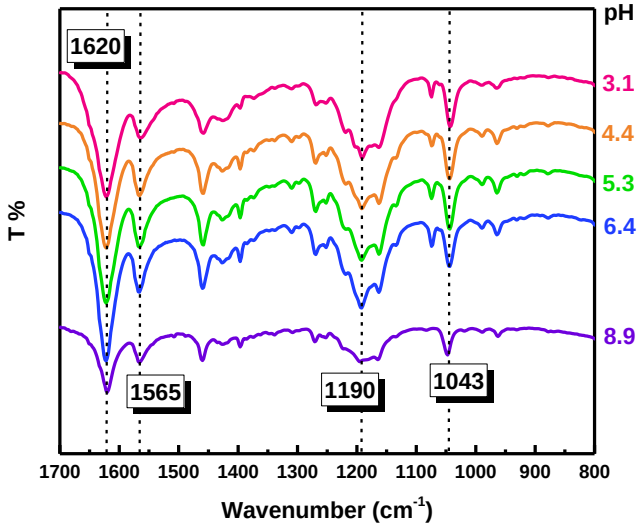

Figure IV.18 IR spectra of the dried DFB solution at 2.5×10^{-2} M in absence of Eu(III) at pH from 3.1 to 8.9.

B) IR spectra of Eu-DFB complexes

Although many works has been done to study the infra-red spectra of DFB in presence of metal ions [2005EDW] [2006COZ] [2009BOR] [2010SIM], it is still difficult to interpret all the bonding vibrations due to the strong couplings of many methylene bridges in DFB and the interference of mesylate in this case. Thus, this work is mainly focused on the bonding variations of hydroxamate groups which possess a strong tendency to coordinate with Eu(III). In addition, it is known that only hydroxamate groups are involved in the complexation [2000NEU], which means the complexation should only affect the infrared absorption of hydroxamate groups.

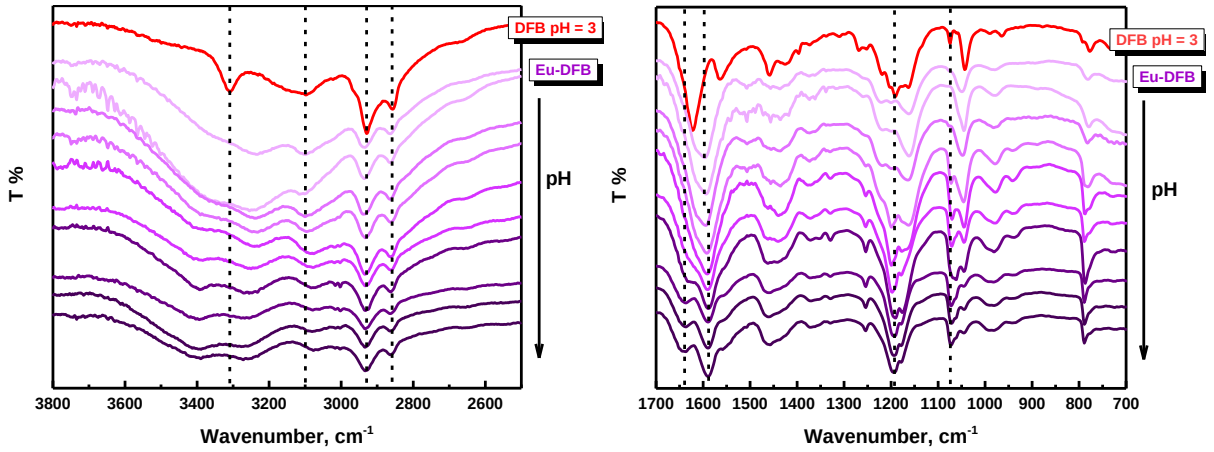

Figure IV.19 FTIR spectra of air-dried Eu(III)-DFB complexes as a function of pH (from 3.1 to 9.4). $C_{Eu(III)} = C_{DFB} = 2.5\times10^{-2}$ M at room temperature.

Figure IV.19 shows the variation of infra-red transmittance spectra of the complexation between Eu(III) and DFB at the stoichiometric ratio 1:1 as function of pH. FTIR spectra have been scaled and offset to facilitate their comparison. It can be seen that the carbonyl bands mentioned above are affected by the complexation with Eu(III). The hydroxamate carbonyl band at 1620 cm^{-1} downshifts to 1597 cm^{-1} due to the complexation with Eu(III) at pH = 3.1. Furthermore, it gradually downshifts to 1589 cm^{-1} as increasing pH to 9.4. It is probably due to the successive deprotonation of hydroxamate groups due to the complexation. Because hydroxamate carbonyl groups increasingly participate to the complexation of Eu(III) with the decreasing acidity. It is very likely that the predominant species of Eu-DFB complex could be varied from EuH_3DFB^{3+} to $EuHDFB^{+}$ as the increase of pH. This result is in agreement with the speciation diagram (**Figure II.15**) plotted using the stability constants from literature [2011CHR]. In addition, increasing the pH leads to the exposure of the amide carbonyl bands at 1637 cm^{-1}, which is assigned to be amide carbonyl bands.

At high frequencies, a broad peak appears at 3400-3500 cm^{-1} from the HOH stretching (water molecules included in the complexes). The frequency of the N-H band of the secondary amide at 3308 cm^{-1} is strongly decreased. However, secondary amine does not participate to the complexation of DFB with Eu(III). This change could be due to intramolecular hydrogen bonds. Finally, the intensity of the broad peak around 3100 cm^{-1} due to the O-H stretch from the hydroxamic groups decreases at lower pH until disappearance at higher pH. Instead, a very broad weak peak slightly shift at 3085 cm^{-1} is seen. This peak can be the C-NH overtone band of the secondary amide which was already reported at 3084 cm^{-1} in ferrioxamine [2005SIE]. The frequencies and assignments of the major bands of H_4DFB^{+} and Eu-DFB complexation are also summarized in **Table IV.6**.

Table IV.6 Frequencies and assignments of the major bands in the IR spectra of H_4DFB^+ at pH = 3 and Eu-DFB complex at pH = 9.1.

Frequency		Assignment
H_4DFB^+	Eu-DFB	
3308	-	ν_{N-H} (amide)
3100	-	ν_{O-H} (hydroxamate)
2930	2933	ν_{CH2} asymmetrical
2856	2864	ν_{CH2} symmetrical
n.r.	1638	$\nu_{C=O}$ (amide)
1565	-	δ_{N-H}, ρ_{C-N-H} (amide)
1458	-	δ_{C-H} (CH_3)
1396	-	δ_{N-OH}, δ_{O-H}
1620	1589	$\nu_{C=O}$ (hydroxamate)

IV.2 Tetravalent actinides

This work is part of the ANR project PLUTON (ANR-17-CE08-0053).

Thermodynamic study with tetravalent actinides

IV.2.1 Complexation of Th(IV) with DFB studied by liquid-liquid extraction

A) Preliminary study in the absence of DFB

TTA is known to extract a wide range of metallic cations from acidic media [1961POS]. With the aim at the determination of the formation constant of Th-DFB in aqueous phase, experimental conditions ensuring a competition between the formation of Th-TTA chelate in organic phase and Th complexation in aqueous phase have to be found. **Figure IV.20** presents the percentage of extracted Th as function of pC_H. It can be seen that the quantitative extraction can be observed at pC_H higher than 1.5.

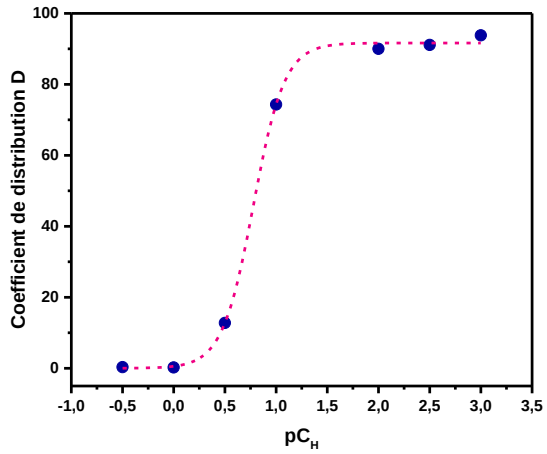

Figure IV.20 Variations of the percentage of extraction of ^{227}Th as function of pC_H (C_{TTA} = 0.08 M in toluene, I = 0.7 M (Na, $HClO_4$), T = 25 °C).

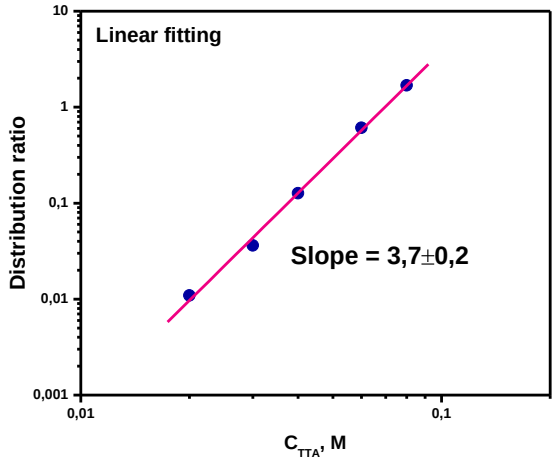

Figure IV.21 Variations of the distribution ratio D of ^{227}Th as function of total TTA concentration in toluene (I = 0.7 M (Na, $HClO_4$), pC_H = 1.0, T = 25 °C).

The variation of the distribution ratio D of ^{227}Th has been determined as function of the total TTA concentration at pC_H = 1.0. In these conditions, Th hydrolysis can be neglected [2008SAS]. DFB solution at pC_H = 1.0 has been proved to be stable within at least one day. The study of DFB stability by UV-visible absorption spectroscopy is described in **Appendix E**. Working at constant ionic strength and temperature allows one to use **Equation III.4** that correlates the

slope of the logarithmic variations of D to the difference in the mean number of TTA molecules per Th atom between species in organic and aqueous phase. The variations in **Figure IV.21** lead to a slope equal 3.7 ± 0.2. Like other tetravalent cations, $Th(TTA)_4$ has been proved to be the only Th-containing species extracted in aromatic diluent [1950DAY] [1951ZEB] [2008SAS]. The value obtained in this work is slightly lower than 4: this could be related to the formation of a small amount of $Th(TTA)^{3+}$ in aqueous phase, as suggested in the literature [1951ZEB] [1952WAG] [1996XIA].

The concentration of HTTA in aqueous phase can be deduced from the distribution ratio of HTTA:

$$D_{HTTA} = \frac{[\overline{HTTA}]}{[HTTA]} \qquad \text{IV.36}$$

The value of [HTTA] corresponding to the experimental conditions of **Figure IV.21** (I = 0.7 M, T = 25 °C) has been estimated by interpolation of the D_{HTTA} values at I = 0.5 and 1.0 M determined by Jaussaud in her systematic study of TTA distribution between toluene and an aqueous solution (Na, $HClO_4$) of fixed acidity (7×10^{-3} M) [2003JAU]. D_{HTTA} does not depend on the initial concentration of TTA since there is no strong interaction between the extractant and the diluent [1992RYD]. Mean value of D for 5.10^{-3} M $\leq C_{TTA}^{tot} \leq$ 0.1 M equal to 35.3 (I = 0.5 M) and 41.6 (I = 1.0 M) were taken from reference [2003JAU]. Moreover, D_{HTTA} does not depend on acidity as long as pH < 4. Thus, D_{HTTA} (**Figure IV.21**) is estimated to be 37.8 ± 0.5.

As weak acid (pK_a = 6.20) [1996RYD], HTTA in aqueous solution undergoes dissociation. Its concentration in aqueous solution can be calculated according to the following equation:

$$[HTTA] = \frac{C_{TTA}^{tot}}{1 + D_{HTTA} + K_a/[H^+]} \qquad \text{IV.37}$$

The values of HTTA and TTA^- concentration in the aqueous phase corresponding to the extreme values of total TTA concentration used in **Figure IV.21** are presented in **Table IV.7**. The amount of $ThTTA^{3+}$ has been estimated using the constant determined by Waggener et al. [1952WAG] according to **Equation IV.38** and **Equation IV.39**. Indeed, in a more recent study, Xia et al propose two values for the complexation of Th according to **Equation IV.40**, but their study has been carried out in C_{NaCl} = 5 M [1996XIA]. Moreover, the values of Waggener et al. are consistent with those of U(IV) and Np(IV) : the affinity between An(IV) and TTA follows the sequence Th< U < Np [1996RYD].

$$Th^{4+} + HTTA \rightleftharpoons Th(TTA)^{3+} + H^{+} \quad \text{IV.38}$$

$$\mathrm{K} = \frac{[Th(TTA)^{3+}][H^{+}]}{[Th^{4+}][HTTA]} = 6.6 \pm 0.3 \ (I = 2\ M) \quad \text{IV.39}$$

$$Th^{4+} + TTA^{-} \rightleftharpoons Th(TTA)^{3+} \quad \text{IV.40}$$

In our experimental conditions (I = 0.7 M, pC_H = 1.0, T= 25 °C) the percentage of the complex $Th(TTA)^{3+}$ lies between 3 and 12 % of total Th(IV) in aqueous solution. This could explain the value lower than 4 obtained in **Figure IV.21**.

Table IV.7 Estimated values of HTTA and TTA^- concentration and $ThTTA^{3+}$ percentage.

$C_{TTA\ tot}$, M	In aqueous phase		
	[HTTA], M	$[TTA^-]$, M	$ThTTA^{3+}$, %
0.02	**5.2×10^{-4}**	**3.3×10^{-9}**	**3**
0.08	**2.1×10^{-3}**	**1.3×10^{-8}**	**12**

Concerning the experimental procedure, the extraction equilibrium can be described as:

$$\overline{Th(TTA)_4} + 4H^{+} \overset{1/K_{ex}}{\longleftrightarrow} Th^{4+} + 4\overline{HTTA} \quad \text{IV.41}$$

$$K_{ex} = \frac{[\overline{Th(TTA)_4}][H^{+}]^4}{[Th^{4+}][\overline{HTTA}]^4} \quad \text{IV.42}$$

B) Determination of conditional stability constants K_{cond}

TTA concentration in toluene was fixed at 0.08 M and DFB concentration in aqueous phase was varied between 0 and 0.07 M. The total concentration of Th(IV) was less than 10^{-12} M at ultra-trace scale where the polymerization of Th(IV) should not take place, but the back-direct extraction experiments were still performed to verify the non-occurrence of Th(IV) condensation in this experiment (**Appendix D**).The experiments have been performed at constant ionic strength (I = 0.7 M, Na, $HClO_4$) and at 25 °C. **Figure IV.22** presents the variation of distribution ratio (D) of ^{227}Th(IV) as function of DFB concentration for different values of pC_H.

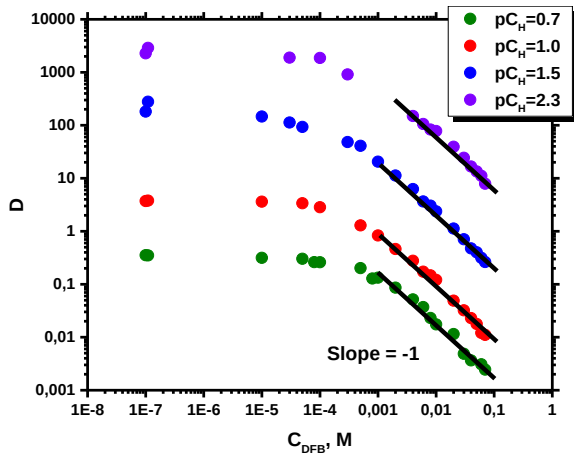

Figure IV.22 Variations of D as a function of DFB concentration at different pC_H (C_{TTA} = 0.08 M, I = 0.7 M (Na, $HClO_4$), T = 25 °C).

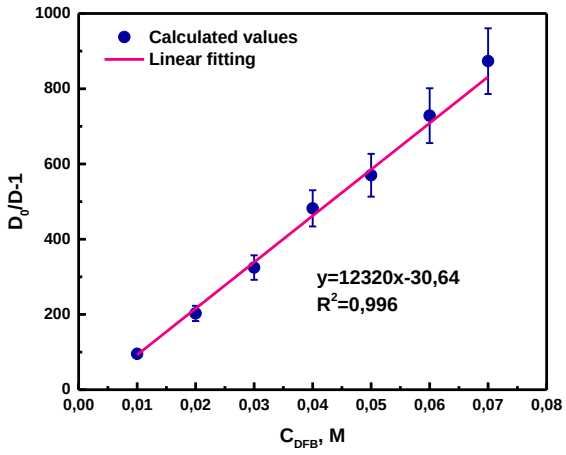

Figure IV.23 Variations of D_0/D-1 as function of DFB concentration (I = 0.7 M (Na, $HClO_4$), T = 25 °C, pC_H = 1.5) and associated linear fitting.

In **Figure IV.22**, the values corresponding to C_{DFB} = 0 (D_0) have been arbitrarily chosen and represented at $C_{DFB} = 10^{-7}$ M. Whatever the pC_H value, the distribution curves exhibit the same trend: at low DFB concentration, a plateau is observed (up to ~10^{-4} M DFB), then the distribution ratios D decrease with the increase in C_{DFB}. This can be related to the formation of a Th-DFB complex in the aqueous phase. The increase of pC_H leads to the increase of D_0. It is very often observed in the work using TTA as the extractant [2003JAU] [2008SAS] [2012LEG].

According to **Equation III.3**, the derivative of logarithmic variations of D with C_{DFB} can be related to the maximum stoichiometry of the complex, equal to 1 in this case. Without considering the precise form of chemical species, the equilibrium in the aqueous phase can be written as:

$$Th(IV) + DFB \overset{K_{cond}}{\longleftrightarrow} Th - DFB \qquad \text{IV.43}$$

$$\text{with } K_{cond} = [Th - DFB]/[Th(IV)][DFB] \qquad \text{IV.44}$$

And the conditional stability constants can be determined according to the following **Equation IV.45**.

$$\frac{D_0}{D} - 1 = K_{cond}[DFB] \qquad \text{IV.45}$$

Figure IV.23 shows an example of calculation of K_{cond} at pC_H = 1.5. According to **Equation IV.45**, the obtained slope deduced from linear fitting represents the conditional stability

constant. The obtained stability constants K_{cond} at $pC_H = 0.7$, 1.0, 1.5 and 2.3 are summarized in **Table IV.8**. It can be seen the values of K_{cond} increase with the increase of pC_H from 0.7 to 1.5.

Table IV.8 Conditional stability constants K_{cond} relative to the formation of Th-DFB at different pC_H.

pC_H	K_{cond}	$\log K_{cond}$
0.7	**2027±186**	**3.31±0.04**
1.0	**5309±521**	**3.72±0.04**
1.5	**12320±1116**	**4.11±0.04**
2.3	**3821±356**	**3.58±0.04**

C) Determination of corrected conditional stability constant K'_{cond}

The aim here is to determine the corrected constant associated to:

$$Th^{4+} + DFB \overset{K'_{cond}}{\longleftrightarrow} Th - DFB \quad \text{IV.46}$$

$$\text{with } K'_{cond} = [Th - DFB]/[Th^{4+}][DFB] \quad \text{IV.47}$$

As with Eu indeed, Th^{4+} is likely to undergo some reactions in aqueous phase, especially hydrolysis and complexation with TTA^-. Although the hydrolytic behavior of Th^{4+} is characterized by the formation of oligomers, these species have not been taken into account since Th was present at tracer scale. The following equilibria have been considered:

$$Th^{4+} + nH_2O \overset{\beta_{OH,n}}{\longleftrightarrow} Th(OH)_n{}^{(4-n)+} + nH^+ \quad \text{IV.48}$$

$$\text{with } \beta_{OH,n} = [Th(OH)_n{}^{(3-n)+}][H^+]^n/[Th^{4+}] \quad \text{IV.49}$$

$$Th^{4+} + mHTTA \overset{\beta_{TTA,m}}{\longleftrightarrow} Th(TTA)_m{}^{(4-m)+} + mH^+ \quad \text{IV.50}$$

$$\text{with } \beta_{TTA,m} = [Th(TTA)_m{}^{(3-m)+}][H^+]^m/[Th^{4+}][HTTA]^m \quad \text{IV.51}$$

In the absence of DFB, D_0 can be expressed as:

$$D_0 = \frac{\left[\overline{Th(TTA)_4}\right]}{[Th^{4+}] + \sum[Th\,(TTA)_m{}^{(4-m)+}] + \sum[Th(OH)_n{}^{(4-n)+}]}$$

$$= \frac{K_{ex}[\overline{HTTA}]^4[H^+]^{-4}}{1 + \sum \beta_{TTA,m}[HTTA]^m[H^+]^{-m} + \sum \beta_{OH,n}[H^+]^{-n}}$$

In the presence of DFB, D can be expressed as:

$$D = \frac{\left[\overline{Th(TTA)_4}\right]}{[Th^{3+}] + \sum[Th\,(TTA)_m{}^{(4-m)+}] + \sum[Th(OH)_n{}^{(4-n)+}] + [Th - DFB]}$$

$$= \frac{K_{ex}[\overline{HTTA}]^4[H^+]^{-4}}{1 + \sum \beta_{TTA,m}[HTTA]^m[H^+]^{-m} + \sum \beta_{OH,n}[H^+]^{-n} + K'_{cond}[DFB]}$$

Thus,

$$\frac{D_0}{D} - 1 = \frac{K'_{cond}[DFB]}{1 + \sum \beta_{TTA,m}[HTTA]^m[H^+]^{-m} + \sum \beta_{OH,n}[H^+]^{-n}}$$

$$K'_{cond} = K_{cond} \times (1 + \sum \beta_{TTA,m}[HTTA]^m[H^+]^{-m} + \sum \beta_{OH,n}[H^+]^{-n}) \qquad \text{IV.52}$$

The selected hydrolysis constants to calculate K'_{cond} are from T. Sasaki et al. ($log\beta_{OH,1} = -2.6 \pm 0.1$) at the ionic strength (I = 0.1 M, $NaClO_4$) by liquid-liquid extraction [2008SAS]. It is the latest data and not included in OECD books. Some other hydrolysis constants were also found in OECD books, but they were not used in this case because they were determined with different techniques and conditions. Since only the stability constant of 1:1 Th-TTA complex was found in the literatures, only $\beta_{TTA,1}[HTTA][H^+]$ was calculated in this case ($\beta_{TTA,1} = 6.6 \pm 0.3$ [1952WAG]). The obtained values of K'_{cond} are listed in **Table IV.9**. The impact of taking into account the hydrolysis species of Th and $Th(TTA)^{3+}$ complex becomes increasingly significant with the increase of pC_H from 0.7 to 2.3. After the correction, the value of K'_{cond} at pC_H = 2.3 is still unreasonably lower than, but closer to that at pC_H = 1.5. If the formation constants of 1:2, 1:3 and 1:4 Th-TTA complexes in aqueous phase are available, a better correction is expected to be conducted. Anyway, due to the seemingly inconsistent result at pC_H = 2.3, this value has not been used in the following calculations.

Table IV.9 Obtained conditional stability constants K'_{cond} (Equation IV.47) between Th^{4+} and DFB at different pC_H and comparison with K_{cond} (Equation IV.44).

pC_H	$\log K_{cond}$	$\log K'_{cond}$
0.7	**3.31±0.04**	**3.3±0.1**
1.0	**3.72±0.04**	**3.8±0.1**
1.5	**4.11±0.04**	**4.3±0.1**
2.3	**3.58±0.04**	**4.2±0.1**

D) Determination of apparent constant K_y

In the pC_H domain from 0.7 to 1.5, the predominant species of DFB is H_4DFB^+. The complexation is expected to occur by the departure at least of one proton of the DFB hydroxamate. It is supposed that the overall equilibrium for the 1:1 complex can be described as:

$$Th^{4+} + H_4DFB^+ \overset{K_y}{\leftrightarrow} Th(H_{4-y}DFB)^{(5-y)+} + yH^+ \qquad \text{IV.53}$$

$$\text{with } K_y = [Th(H_{4-y}DFB)][H^+]^y/[Th^{4+}][H_4DFB^+] \qquad \text{IV.54}$$

Equation IV.54 can be also written as:

$$logK_y = log[Th(H_{4-y}DFB)]/[Th^{4+}][H_4DFB^+] + ylog[H^+] \qquad \text{IV.55}$$

Using **Equation IV.46**, the following relationship is obtained:

$$logK'_{cond} = logK_y - ylog[H^+] \qquad \text{IV.56}$$

The logarithmic variations of the corrected conditional constant as function of proton concentration are plotted on **Figure IV.24**. The slope obtained allows to get y = 1.2 ± 0.2. It means two types of the complexes $Th(H_3DFB)^{4+}$ and $Th(H_2DFB)^{3+}$ are formed in this pC_H domain, which is in good agreement with the literature [1996WHI].

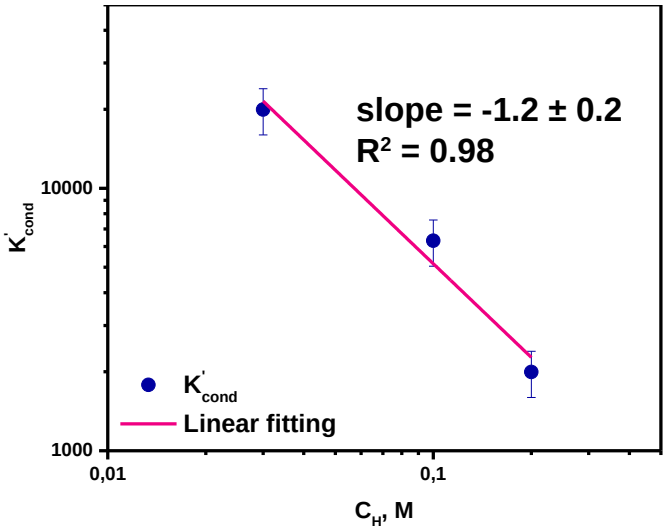

Figure IV.24 Variation of *K'cond* as function of proton concentration.

Thus, the following complexation equilibria can be considered:

$$Th^{4+} + H_4DFB^+ \overset{K_1}{\leftrightarrow} ThH_3DFB^{4+} + H^+ \qquad \text{IV.57}$$

$$K_1 = \frac{[ThH_3DFB^{4+}][H^+]}{[Th^{4+}][H_4DFB^+]} \qquad \text{IV.58}$$

$$Th^{4+} + H_4DFB^{+} \overset{K_2}{\leftrightarrow} ThH_2DFB^{3+} + 2H^{+} \quad \text{IV.59}$$

$$K_2 = \frac{[ThH_2DFB^{3+}][H^+]^2}{[Th^{4+}][H_4DFB^+]} \quad \text{IV.60}$$

Thus,

$$K'_{cond} = K_1/[H^+] + K_2/[H^+]^2 \quad \text{IV.61}$$

According to least-square fitting, the values of logβ_{113} and logβ_{112} were obtained and shown in **Table IV.10**.

Table IV.10 Obtained and published apparent stability constants of $Th(H_3DFB)^{4+}$ and $Th(H_2DFB)^{3+}$.

$iM+nL+mH \rightleftharpoons M_iL_nH_m$ $\beta_{inm}=[M_iL_nH_m]/[M]^i[L]^n[H]^m$

[a]logβ_{113}	[b]logβ_{112}	Condition	$C_{Th(IV)}$	Method	Reference
40.9±0.2	**38.2±0.2**	**25 °C 0.7 M (Na, $HClO_4$)**	**10^{-12} M**	**sol.**	**this work**
42.0±0.1	**40.2±0.1**	**25 °C 0.1 M (KCl)**	**1.25×10^{-3} M**	**pot.**	**[1996WHI]**

a. $\log\beta_{113}=\log K_1+pK_{a1}+pK_{a2}+pK_{a3}+pK_{a4}$

b. $\log\beta_{112}=\log K_2+pK_{a1}+pK_{a2}+pK_{a3}+pK_{a4}$

pKa_1 = 8.54±0.01 pKa_2= 9.06±0.01 pKa_3= 9.70±0.02 pKa_4= 10.89±0.06 [2011CHR]

The obtained stability constant of $Th(H_3DFB)^{4+}$ and $Th(H_2DFB)^{3+}$does not agree well with the literature data [1996WHI]. D.W. Whisenhunt et al. determined this stability constant by potentiometric titration from pH = 2.1 to 10.7. But they mentioned that the slight pH changes in the low pH region related to the formation of $Th(H_2DFB)^+$ and $Th(H_3DFB)^+$ are difficult to extrapolate and they did not consider the first hydrolysis of Th even at pH = 2.1 where Th has been beginning hydrolysis [2008SAS]. In addition, our experimental conditions including ionic strength and its component are also different from the literature. And due to the lack of stability constants of Th-TTA, the formations of 1:2, 1:3 and 1:4 Th-TTA complexes in aqueous phase are not considered in the calculations. Moreover, instead of macro Th(IV) (1.25×10^{-3} M) used in the literature, ultra-trace scale of Th(IV) (10^{-12} M) was applied in this work to avoid polymerization. With considering the constants determined from just three experimental points at pC_H = 0.7, 1.0 and 1.5, a relatively large error (0.2) is associated to the constants. The experiments at more pC_H values are needed to be performed in order to verify and accurate the formation

constants. Overall, this protocol is considered to be a promising protocol for an application to the study of the complexation of other tetravalent actinides with DFB.

IV.2.2 Complexation of U(IV) with BHA, AHA and DFB studied by UV-visible absorption spectrophotometry

A) Complexation of U(IV) with benzohydroxamic acid (BHA) and acetohydroxamic acid (AHA)

The experiments were performed at C_{HCl} = 0.5 M in order to protect U(IV) against hydrolysis or oxidation. The contribution of U(IV), BHA and AHA to the ionic strength has not been taken into account since their concentrations were far lower than that of HCl.

Figure IV.25 and **Figure IV.26** presents the UV-visible absorption spectra of U(IV) at 4.8×10^{-3} M and 9.6×10^{-3} M with increasing amount of BHA from 0 to 5×10^{-2} M and AHA from 0 to 0.8 M, respectively. It can be pointed out that BHA and AHA does not have any absorption in the range from 450 to 700 nm. The variations of the spectra reflect therefore the formation of U(IV)-BHA complex.

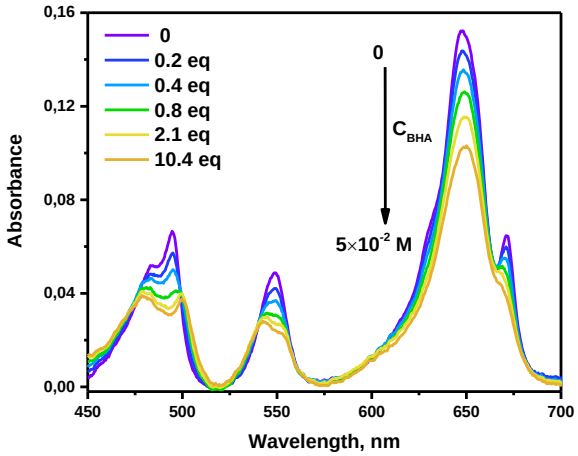

Figure IV.25 UV-visible absorption spectra of U(IV) at 4.8×10^{-3} M with increasing amount of BHA from 0 to 5×10^{-2} M in 0.5 M HCl at 25 °C.

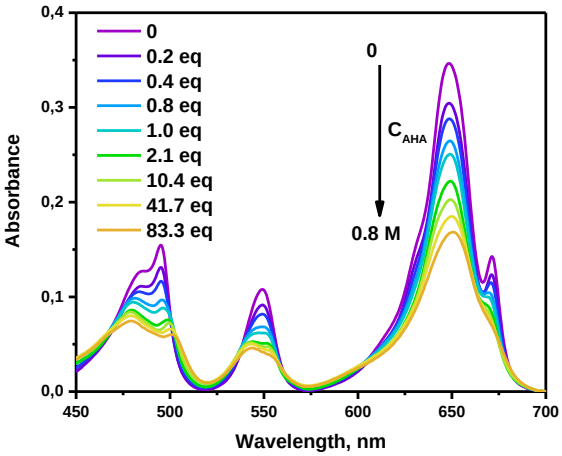

Figure IV.26 UV-visible absorption spectra of U(IV) at 9.6×10^{-3} M with increasing amount of AHA from 0 to 0.8 M in 0.5 M HCl at 25 °C.

On the two figures, the characteristic bands of U(IV) appears at 485, 550 and 650 nm respectively in absence of BHA or AHA, which is in good agreement with the literature [1960COH]. In both cases of BHA and AHA, with the increasing concentration of ligands, the bands around 485, 550, 650 and 675 nm are decreasing. The band around 485 nm is shifted to higher wavelength and the band at 670 nm almost disappears when BHA and AHA concentrations are increased to 5×10^{-2} M and 0.8 M, respectively.

The spectra have been processed with the software HypSpec. In order to start calculation, input parameters (acid dissociation constants of ligand, estimated complexation constants) were introduced into the software. According to principal component analysis (PCA), the number of species existing in solution can be identified. In our condition, one complex with BHA and two complexes with AHA have been observed.

The determined stability constants associated to the equilibrium (**Equation IV.62** and **Equation IV.64**) are summarized in **Table IV.11**.

$$M^{4+} + L^{-} = ML^{3+} \quad \text{IV.62}$$

$$\beta_{110} = \frac{[ML^{3+}]}{[M^{4+}][L^{-}]} \quad \text{IV.63}$$

$$M^{4+} + 2L^{-} = M(L)_2{}^{2+} \quad \text{IV.64}$$

$$\beta_{120} = \frac{[M(L)_2{}^{2+}]}{[M^{4+}][L^{-}]^2} \quad \text{IV.65}$$

Table IV.11 Stability constants β_{110} of $An^{IV}L^{3+}$ (EquationIV.63) and β_{120} of $An^{IV}(L)_2{}^{2+}$ (Equation IV.65).

Ligand	Actinide	logβ_{110}	logβ_{120}	T, °C	I, M	Method	Reference
BHA	Th(IV)	8.97±0.02	17.53	25	0.1($NaNO_3$)	pot.	[2007KHA]
	Th(IV)	9.6	19.81	25	0.1(KNO_3)	pot.	[1966BAR]
	U(IV)	9.89	18.0	25	1.0($KClO_4$)	pot.	[1966BAR]
	U(IV)	11.0±0.1[a]		25	0.5(HCl)	sp.	this work
	U(IV)	11.8±0.1[b]		25	0.5(HCl)	sp.	this work
	Pu(IV)	12.73		25	1.0($HClO_4$)	sol.	[1966BAR]
AHA	Th(IV)	10.50±0.03	19.70	25	0.1($NaNO_3$)	pot.	[2007KHA]
	U(IV)	12.0±0.1[c]	21.1±0.1[c]	25	0.5(HCl)	sp.	this work
	Pu(IV)	14.3±0.03		25±3	1.0($HClO_4$)	sol.	[2010BRO]
	Pu(IV)	14.2±0.2	24.1±0.2	22	2.0($NaNO_3$)	sp.	[2007CAR]

a. Calculated with pKa (BHA) = 8.07±0.06 [2010AKS]

b. Calculated with pKa (BHA) = 8.83±0.01 [2011TUR]

c. Calculated with pKa (AHA) = 9.15 [2011CHU]

Due to the absence of pK_a(BHA) in the literature corresponding to our experimental conditions, the minimum and maximum pK_a(BHA) were used in the calculation of constants. Depending on the pKa value used, up to 2 orders of magnitude are observed in comparison with Baroca's work [1966BAR]. A. Barocas et al. determined the constant of $ThBHA^{3+}$ by potentiometric

titration in the pH range from 2.11 to 5.77. They observed a brown precipitation at pH = 5.77, but the hydrolysis of U(IV) was not mentioned or considered in their work. In the case of AHA, it is failed to find any literature related to the stability constant between U(IV) and AHA.

For binding of electrostatic nature, the interaction strength between An(IV) and organic ligand is known to depend on the ionic radius of metal ion. For the same coordination number, a correlation can be made between the stability constants and the inverse of ionic radius of An(IV) [1976SHA] [1999CHA]. The stability constants of Th(IV) and Pu(IV) available in the literature (**Table IV.11**) were used to represent this correlation considering a coordination number equal to 8 in **Figure IV.27**. The values relative to U(IV) appear fully consistent with those of Th(IV) and Pu(IV).

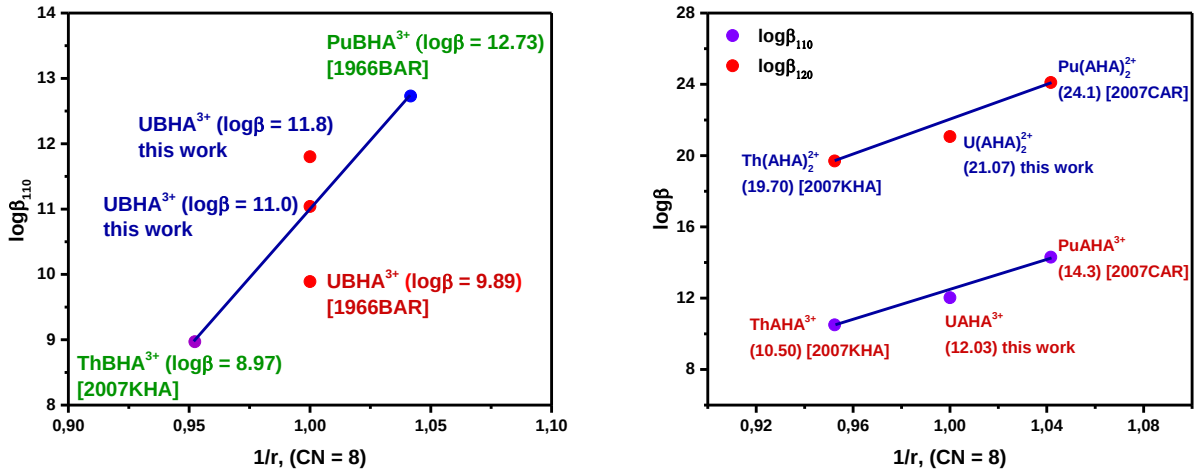

Figure IV.27 Correlation of stability constants of Pu(IV), Th(IV) and U(IV) with BHA (left) and AHA (right).

The molar absorbance spectra of each component for the complex U(IV)-BHA and U(IV)-AHA have also been extracted using HypSpec software and shown in **Figure IV.28** and **Figure IV.29**.

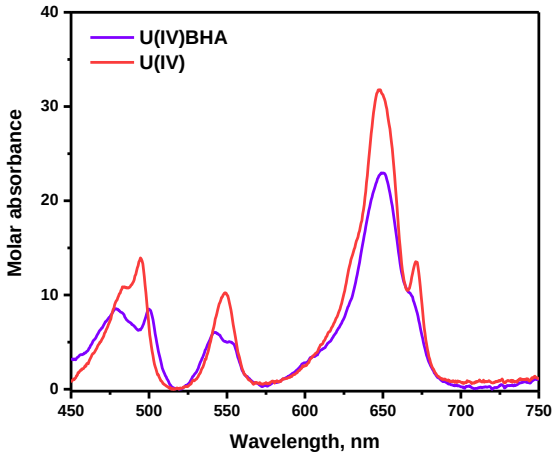

Figure IV.28 Molar absorbance of U^{4+} and $UBHA^{3+}$.

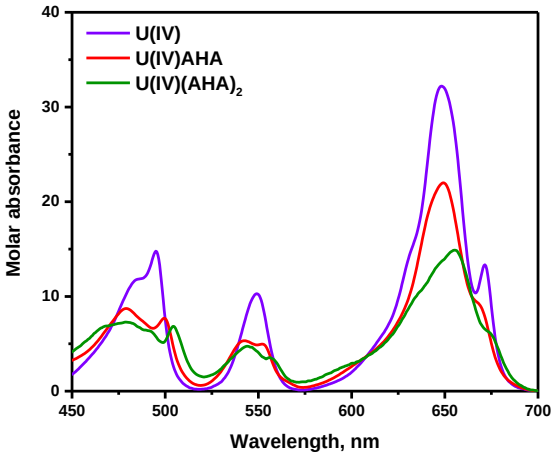

Figure IV.29 Molar absorbance of U^{4+}, $UAHA^{3+}$ and $U(AHA)_2^{2+}$.

B) Complexation of U(IV) with DFB

Figure IV.30 presents the variation of U(IV) absorption spectra as a function of DFB concentration. There is no absorption of DFB in the range from 400 to 700 nm. The variations observed on the figure arise from the formation of the complexation of U(IV) with DFB. The solutions were measured immediately after the preparation, in order to avoid the hydrolysis of DFB at high proton concentration (**Appendix E**). However, when the ligand equivalence is increased from one to two, no apparent variation of absorption was observed, similarly to the case of the complex Pu(IV)-DFB [2007NEU]. Therefore, the complex U(IV)-DFB formed in acidic media (C_{HCl} = 0.5 M) is not significantly influenced by the U(IV)/DFB ratio.

Figure IV.31 presents the variation of U(IV) absorption spectra as function pC_H. It can be seen that as the increase of pC_H, the absorption tends to be decreasing due to the formation of U(IV)-DFB complex, exhibiting the similar tendency as the system U(IV) with AHA or BHA (**Figure IV.26** and **Figure IV.25**). Increasing either pC_H or ligand concentration favor the formation of complex, leading to the decrease of absorption.

Overall, it is failed to observe a gradual and significant variation of U(IV) absorption in the presence of DFB. Because U(IV) is quantitatively complexed with DFB and no free U(IV) can be detectable by UV-vis spectrophotometer. Additionally, due to the degradation of DFB in acidic solution, it is not possible to increase the acidity over 0.5 M HCl to weaken the complexing ability of DFB. Thus, it is impossible to determine the stability constant of U(IV) with DFB by direct UV-vis spectrophotometric titration. Alternatively, competition UV-vis spectrophotometric titration can be applied in the future work. This technique has been ever applied to study the interaction between Pu(IV) and DFB in the presence of EDTA by Boukhalfa et al.

[2007BOU]. Moreover, D.W. Whisenhunt et al. have also determined the stability constants of Th(IV) and Pu(IV) with DFB and its derivatives by using indirect UV-vis spectrophotometric titration competing with EDTA [1996WHI].

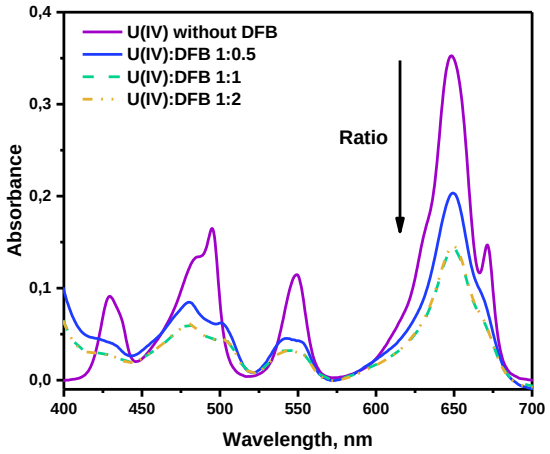

Figure IV.30 Absorption spectra of U(IV) at 9.6×10^{-3} M with different ratio U:DFB at C_{HCl} = 0.5 M in 0.5 M HCl.

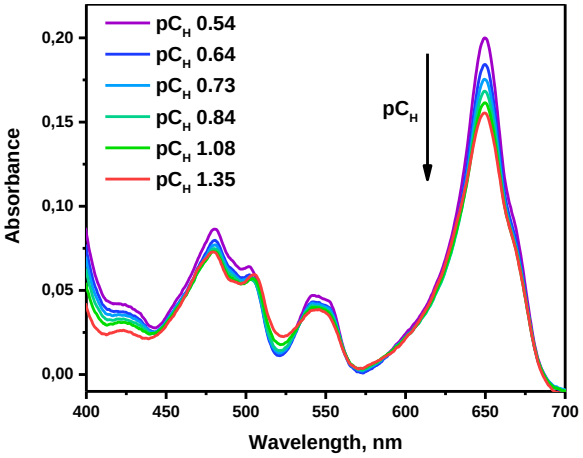

Figure IV.31 Variation of U(IV) absorption spectra as a function of pC_H (pC_H from 1.35 to 0.54, $C_U = 9.6\times10^{-3}$ M, $C_{DFB} = 1.1\times10^{-2}$ M).

Structural study with tetravalent actinides

IV.2.3 Structural study of the complexation of Th(IV) with DFB by ATR-FTIR

The IR spectra of free ligand has been investigated and illustrated in **Section IV.1.2.1**. **Figure IV.32** presents the variation of infra-red absorption spectra of the complexation between Th(IV) and DFB at the stoichiometric ratio 1:1 as a function of pH. Spectra have been scaled and offset to facilitate their comparison.

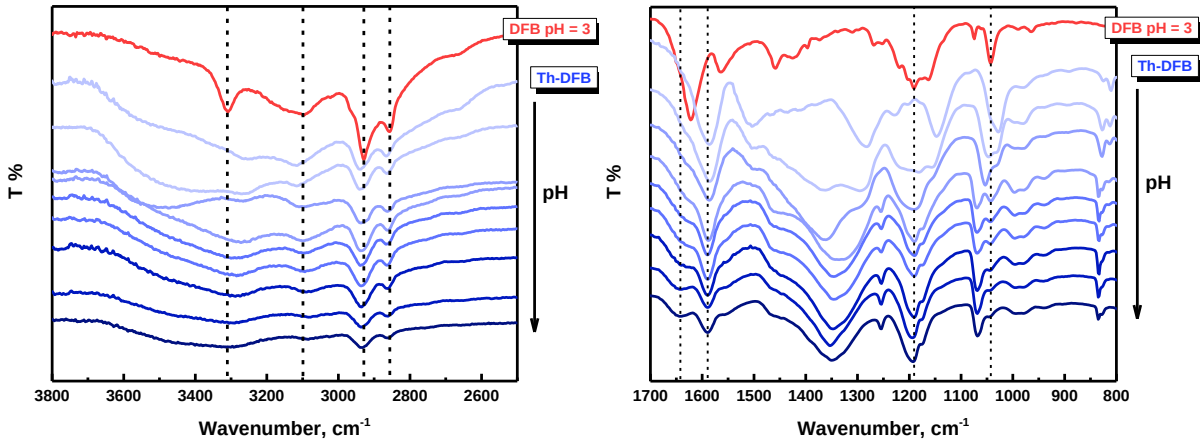

Figure IV.32 FTIR spectra of the air-dried Th(IV)-DFB complexes as a function of pH (from 1.3 to 9.1) $C_{Th(IV)} = C_{DFB} = 2.5\times10^{-2}$ M at room temperature.

The most noticeable effect upon complexation with thorium is the shift of the absorption band from 1620 cm^{-1} to 1589 cm^{-1} due to the coordination of thorium with the hydroxamate groups. The hydroxamate carbonyl bands are affected due to the complexation with Th(IV). This shift is observed even at low pH and the same shift is also observed when DFB is deprotonated [2005EDW] [2010SIM]. By increasing the pH, the shift to lower frequencies is more significant and leads to the exposure of the amide carbonyl bands at 1643 cm^{-1} and a disappearance of N-H band at 1565 cm^{-1}. The same behavior has been observed with successive deprotonation of DFB [2005EDW] [2010SIM]. The amide carbonyl bands are not well resolved for the H_4DFB^+ and H_3DFB species due to the overlapping with the hydroxamate carbonyl bands. The IR spectra variation of Th-DFB complex at high frequencies is almost same as Eu-DFB complex (**Figure IV.19 left**).

An evidence of the thorium chelation with the hydroxamate groups is also the disappearance of the OH deformation band at 1396 cm^{-1} and the shift at higher frequencies of the N-O bands as it can be observed in ferrioxamine spectra [2005SIE].

From pH = 3, no significant change is observed in the FTIR spectra. The only difference is between pH = 6.5 and 7.6 where the band of the amide carbonyl at 1643 cm^{-1} is better resolved. From study on the deprotonation of DFB, it is known that spectra of DFB^{3-} and $HDFB^{2-}$ are nearly identical since the last deprotonation is from the terminal amine group. Indeed, the N-H deformation bands related to this functional group is weak and broad [2005EDW] [2010SIM]. It seems that from pH = 3, $Th(HDFB)^{2+}$ or/and $Th(DFB)^{+}$ are the main species in solutions, and that from pH = 7, $Th(DFB)^{+}$ becomes the majority complex. This result is in agreement with the speciation diagram (**Figure II.16**) plotted using the stability constants obtained by Whisenhunt et al.11 [1996WHI] that depicts the presence of more than 50% of $Th(HDFB)^{2+}$ at pH = 3 and the appearance of $Th(DFB)^{+}$ at pH = 7.

Unfortunately, all the bands could not be assigned. An intense band was observed at 1349 cm^{-1}. This band is present from pH = 1.3 but is shifted until pH = 3. This is also the case for the band at 835 cm^{-1}. Those bands were only observed in presence of thorium which was not the case in presence of iron or other studied metals. More experiments or calculations would be needed to better understand those vibration bands. Hydrolysis or formations of hydrogen bonds due to the drying process were suspected. However, in the case of $Th(OH)_4$, stretching bands of Th-O and O-H were observed at 528 and 3750 cm^{-1} respectively [2005WAN]. The assigned vibrations of Th-DFB complexation are also summarized in **Table IV.12** and compared with Eu-DFB complexation.

The noticeable differences between Th-DFB and Eu-DFB complexes are the frequencies of CH_2 symmetrical and amide carbonyl vibrations. For a given ligand DFB, the size of hexadentate chelation ring can be different depending on the specific center metal atom. It can probably affect the length of the carbon chain and further lead to the variation of CH_2 vibrations.

It is unreasonable to observe the difference of amide carbonyl vibrations between Th-DFB and Eu-DFB complexes. The amide carbonyl groups should not be involved in the complexation, which has been proved by XRD using a very similar ligand as DFB [2000NEU]. One possibility is due to the interference of the stronger and sharper bands from hydroxamate carbonyl groups nearby. Moreover, it can be probably explained by the formation of hydrogen bonds in the secondary amide. The samples of Th-DFB and Eu-DFB complexes were measured at different pH, 9.1 and 9.4, respectively. And the pH was not determined precisely without considering the ionic strength.

Table IV.12 Frequencies and assignments of the major bands in the IR spectra of H_4DFB^+ at pH = 3 and Th-DFB complex at pH = 9.1 Comparison with Eu-DFB complex at pH = 9.4.

Frequency			Assignment
H_4DFB^+	Th-DFB	Eu-DFB	
3308	-	-	ν_{N-H} (amide)
3100	-	-	ν_{O-H} (hydroxamate)
2930	2933	2933	ν_{CH2} asymmetrical
2856	2860	2864	ν_{CH2} symmetrical
n.r.	1643	1638	$\nu_{C=O}$ (amide)
1565	-	-	δ_{N-H}, ρ_{C-N-H} (amide)
1458	-	-	δ_{C-H} (CH_3)
1396	-	-	δ_{N-OH}, δ_{O-H}
1620	1589	1589	$\nu_{C=O}$ (hydroxamate)

IV.2.4 Structural study of the complexation of An(IV) with DFB by theoretical calculations and EXAFS

This work has been carried out in close cooperation with Melody MALOUBIER (IPNO-PACS) and Jérôme ROQUES (IPNO-Radiochimie).

A) Complexation of Th(IV) with DFB studied by DFT calculations

A.1 Computational details

All structures were optimized using density functional theory (DFT) approach as implemented in the Gaussian09 package [2009FRI]. Calculations were performed using the hybrid B3LYP functional [1993BEC]. MWB60 Stuttgart relativistic effective core potentials were used to describe thorium atoms while the 6-31+G* basis set was used for others. To take into account part of the solvent effect, solvation was introduced using a dielectric continuum model of permittivity $\varepsilon = 80$. The conductor-like polarizable continuum model implemented in Gaussian09 was used. Vibrational harmonic frequencies, corresponding to the optimized structures, were also calculated and compared to the experimental ones.

A.2 Deprotonation of ligand DFB

Since one DFB molecule contains three geometrically different hydroxamate groups (**Figure IV.33**), the deprotonation process of ligand DFB alone is expected to be known by theoretical calculation. However, the overall energy of the optimized structures of ligand DFB deprotonated at Site 1, 2 and 3 (**Figure IV.34**) are the same, indicating that they exhibit the same stability. The overall energy of the structure of ligand DFB deprotonated at amine (**Figure IV.34**) is 0.4 eV higher than those deprotonated at hydroxamate groups. It means that the deprotonation at amine should take place lastly, which is in good agreement with the dissociation constants of DFB that pK_a (amine) is larger than pK_a (hydroxamate) [2010SIM] [2011CHR] [2013TIR].

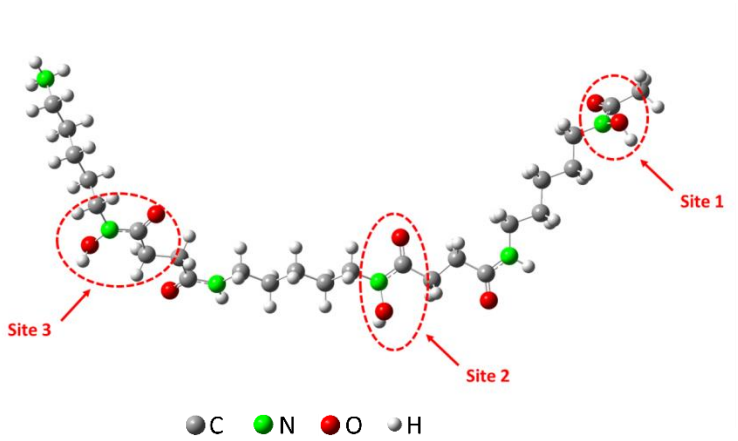

Figure IV.33 Optimized structure of ligand DFB.

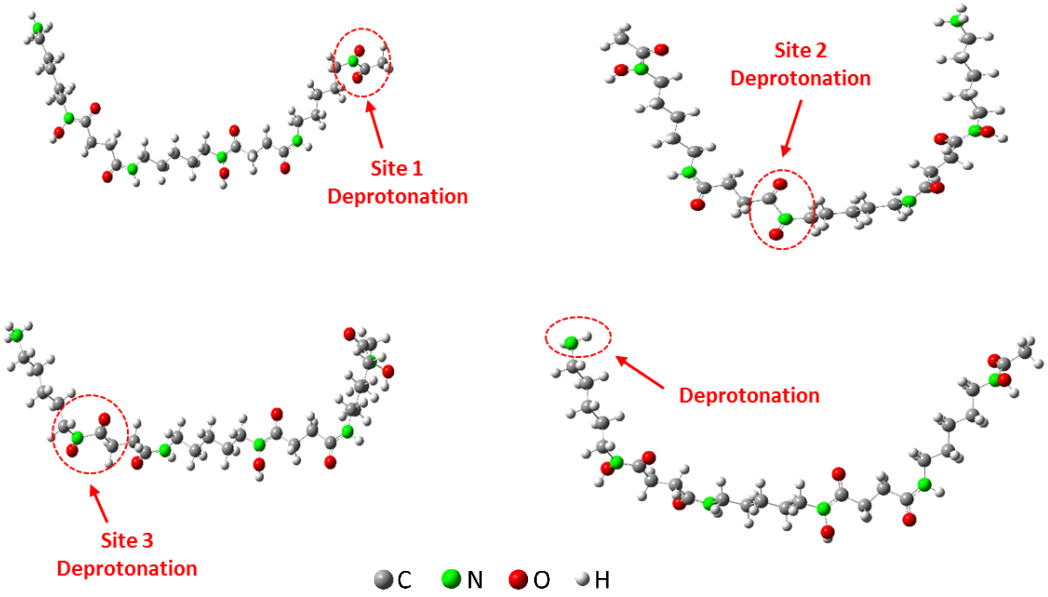

Figure IV.34 Optimized structures of ligand DFB with different deprotonation.

A.3 Study of coordination number of Th in the first solvation sphere

The structure optimization of Th with one hydroxamate group was performed with different number of water molecules in the first solvation sphere of thorium. When oxygens binding to Th are increased from 8 to 9, one water molecule is moved outside the first coordination sphere of thorium (**Figure IV.35**). Thus, the Th coordination number used in the further calculations will be 8.

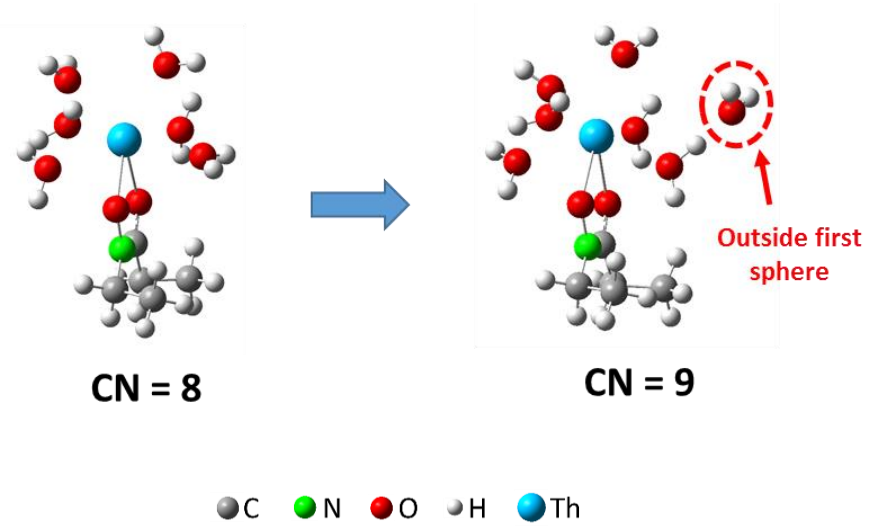

Figure IV.35 Optimized structures of Th with one hydroxamate group at coordination number = 8 (left) and 9 (right).

A.4 Stability investigation of the complex Th(H_3DFB)

The optimized structures of the complex of Th with only one hydroxamate group (bidentate) at different sites are presented in **Figure IV.36** and the associated geometrical parameters are summarized in **Table IV.13**. Whatever the one site coordinated to Th, the overall energy of the complex Th(H_3DFB) is the same. Additionally, the average bond distances Th-O (H_2O) and Th-O (hydroxamate) for different coordination sites are also very close. Thus, the complexes of Th binding to one hydroxamate group (Site 1, 2 or 3) exhibit the approximately same stability ($\Delta E < 0.003$ eV). The distances of Th-O (hydroxamate) are always larger than Th-O (H_2O). It is because Th displays higher interaction strength with hydroxamate groups than water molecules.

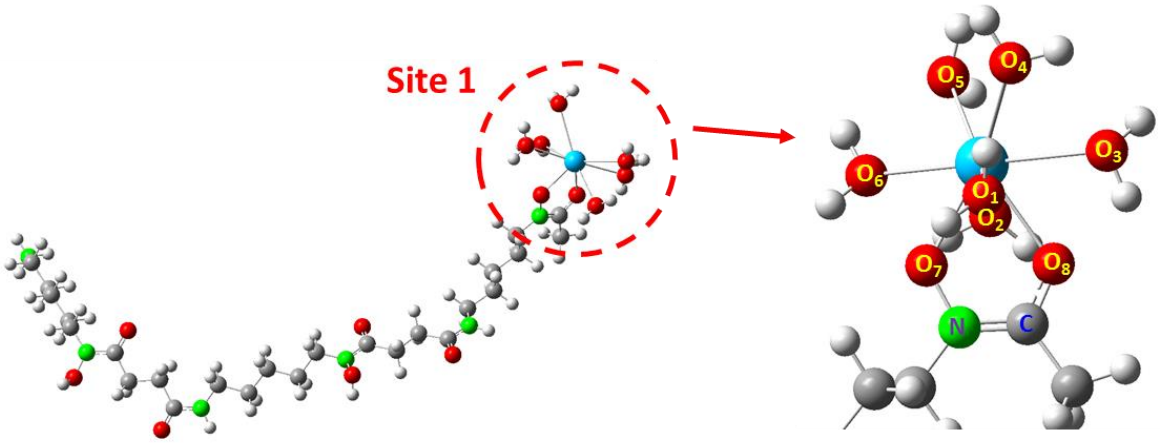

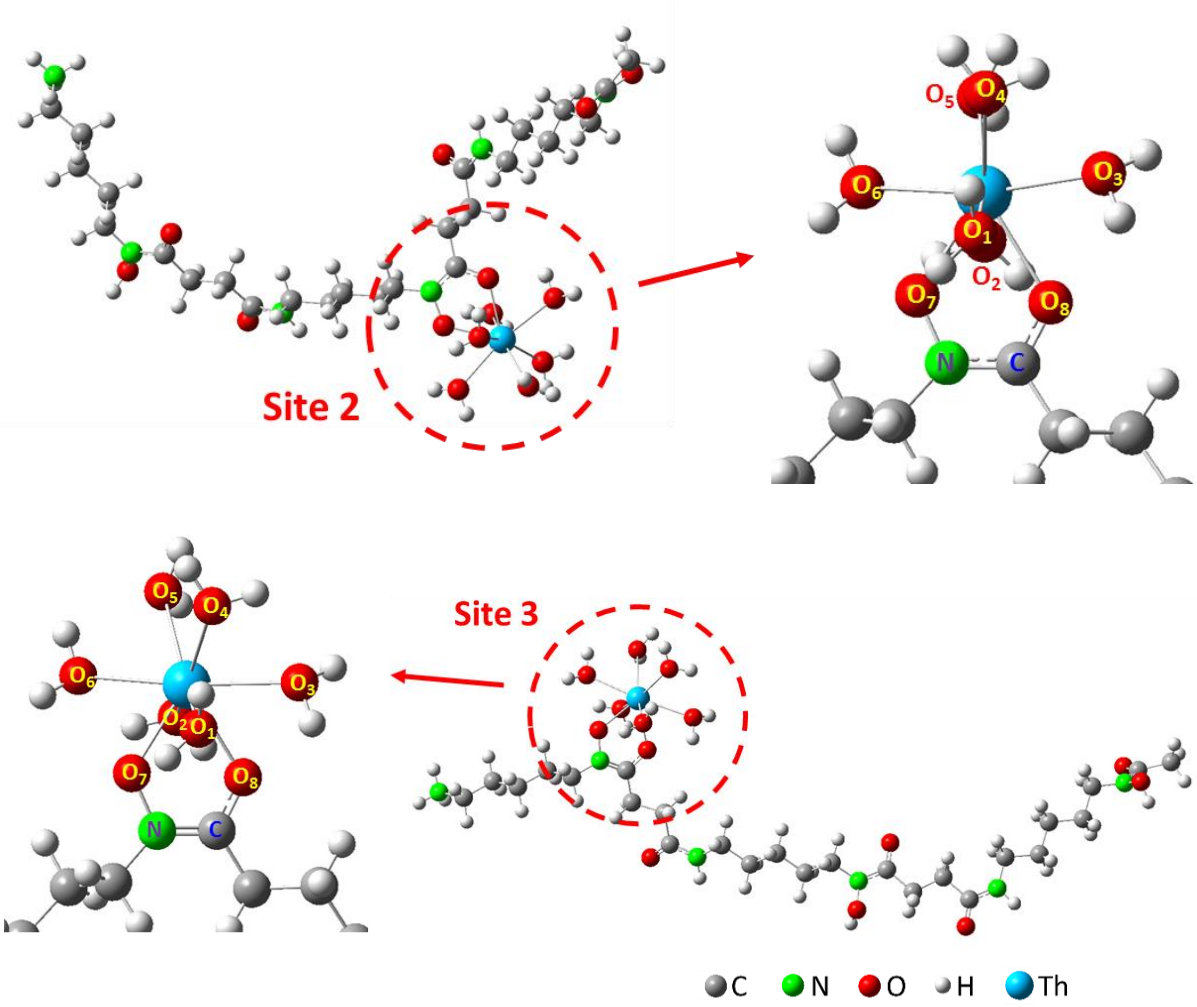

Figure IV.36 Optimized structures of the complex of Th with one hydroxamate group at Site 1 (first figure), Site 2 (second figure) and Site 3 (third figure).

Table IV.13 Geometrical parameters associated with Figure IV.36 obtained by DFT calculations.

Distance	Th(H_3DFB)		
	Site 1, Å	Site 2, Å	Site3, Å
Th-O_1 (H_2O)	2.57	2.59	2.58
Th-O_2 (H_2O)	2.60	2.64	2.64
Th-O_3 (H_2O)	2.69	2.69	2.69
Th-O_4 (H_2O)	2.95	2.84	2.83
Th-O_5 (H_2O)	2.86	2.64	2.86
Th-O_6 (H_2O)	2.59	2.62	2.64
Average Th-O (H_2O)	2.71	2.67	2.71
Th-O_7N	2.27	2.26	2.26
Th-O_8C	2.40	2.38	2.37
Average Th-O (hydroxamate)	2.33	2.32	2.31

A.5 Stability investigation of the complex Th(H_2DFB)

All the possibility of the complex of Th coordinated with two hydroxamate groups (bidentate) were investigated. The most stable Th(H_2DFB) complex is formed by binding to two bidentate hydroxamate groups at Site 1 and Site 2. The optimized structure of the most stable Th(H_2DFB) complex is presented in **Figure IV.37** and the associated geometrical parameters are summarized in **Table IV.14**. It can be seen that the distances of Th-O (hydroxamate) for the same site are increased. For instant, at Site 1, the distances of Th-O_5N (2.28 Å) and Th-O_6C (2.45 Å) in the complexation with two bidentate hydroxamate groups are larger than those (2.27 Å and 2.40 Å) in the complexation with only one bidentate hydroxamate groups. It is led by the steric effect in the complexation with two bidentate hydroxamate groups.

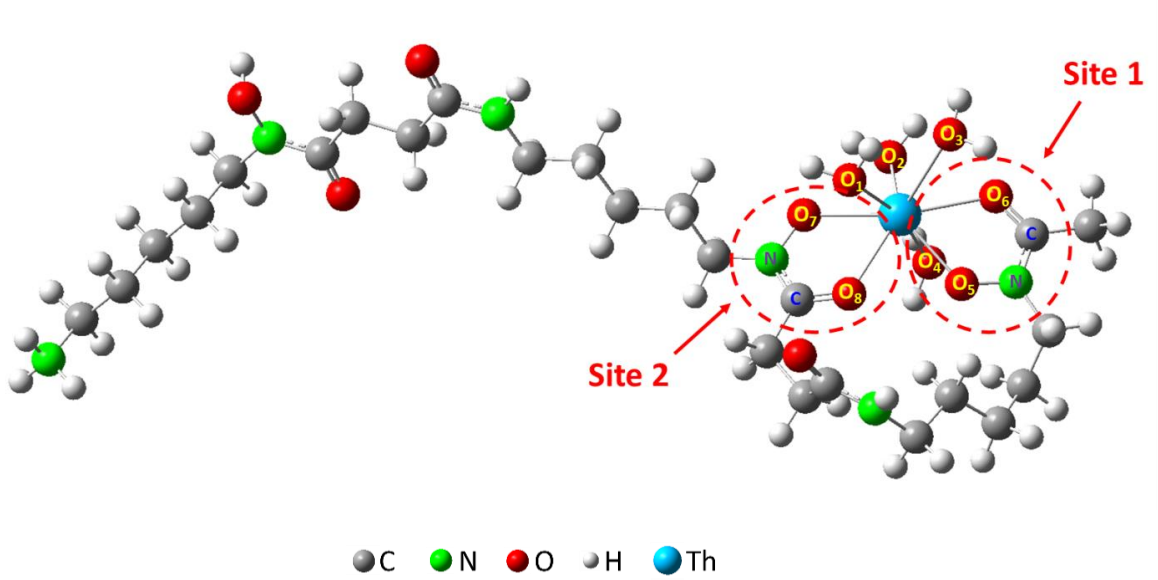

Figure IV.37 Optimized structure of Th(H_2DFB) complex obtained by DFT calculation.

Table IV.14 Geometrical parameters associated with Figure IV.37 obtained by DFT calculations.

Distance	Th(H_2DFB) Site 1 and Site 2, Å	Distance	Th(H_2DFB) Site 1 and Site 2, Å
Th-O_1 (H_2O)	2.64	Th-O_5N (Site 1)	2.28
Th-O_2 (H_2O)	2.79	Th-O_6C (Site 1)	2.45
Th-O_3 (H_2O)	2.91	Th-O_7N (Site 2)	2.35
Th-O_4 (H_2O)	2.77	Th-O_8C (Site 2)	2.43
Average Th-O (H_2O)	2.78	Average Th-O (hydroxamate)	2.38

A.6 Stability investigation of the complex Th(HDFB)

The optimized structure of the most stable Th(HDFB) complex where Th is coordinated with three hydroxamate groups (bidentate) is presented in **Figure IV.38** and the associated geometrical parameters are summarized in **Table IV.15**. It can be seen that the average distance of Th-O (2.43 Å) (hydroxamate) in the complexation with three bidentate hydroxamate groups is larger than that (2.38 Å) in the complexation with two bidentate hydroxamate gourps. Thus, the distances are further increased due to the increasing steric constraint in the complexation with three bidentate sites.

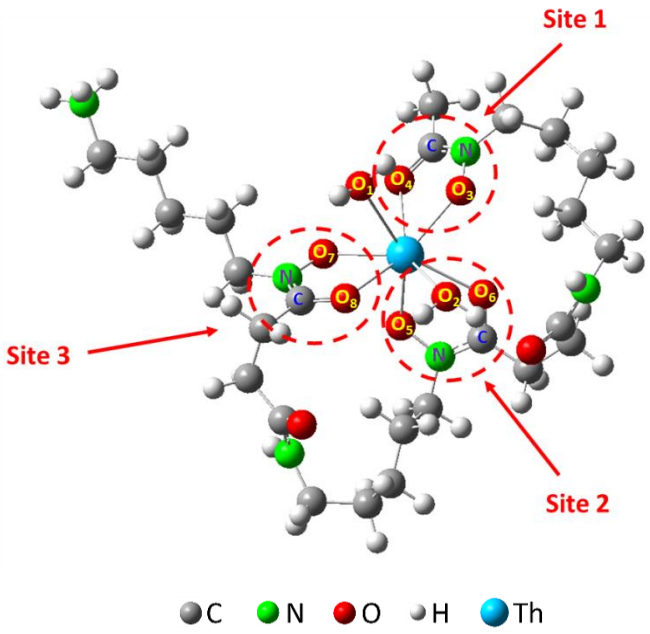

Figure IV.38 Optimized structure of Th(HDFB) complex (three bidendate hydroxamates) obtained by DFT calculations.

Table IV.15 Geometrical parameters associated with Figure IV.38 obtained by DFT calculations.

Distance	Th(HDFB)
	Site 1 Site 2 and Site 3 (bidentate)
Th-O_1 (H_2O)	2.73
Th-O_2 (H_2O)	2.65
Average Th-O (H_2O)	2.69
Th-O_3N (Site 1)	2.37
Th-O_4C (Site 1)	2.51
Th-O_5N (Site 2)	2.37
Th-O_6C (Site 2)	2.46
Th-O_7N (Site 3)	2.36
Th-O_8C (Site 3)	2.49
Average Th-O (hydroxamate)	2.43

The complex structure of Th coordinated with three hydroxamate groups (monodentate and bidentate) was also studied by DFB calculation. The optimized structure of the most stable Th(HDFB) complex is presented in **Figure IV.39** and the associated geometrical parameters are summarized in **Table IV.16**. The distances of Th-O_5N (2.26 Å) and Th-O_8N (2.22 Å) at monodentate sites (Site 1 and Site 3) are shorter than Th-O_6N (2.36 Å) at bidentate Site 2, indicating a higher coordination potential with monodentate sites. However, according to the

EXAFS results, the use of monodentate coordination fashion did not allowed to obtain a better fit.

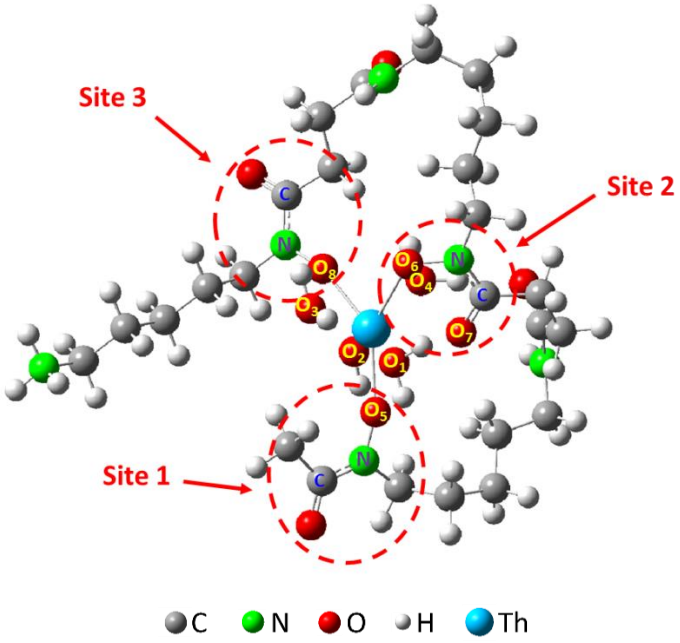

Figure IV.39 Optimized structure of Th(HDFB) complex (one bidentate and two monodentate hydroxamates) obtained by DFT calculations.

Table IV.16 Geometrical parameters associated with Figure IV.39 obtained by DFT calculations.

Distance	Th(HDFB)	Distance	Th(HDFB)
	Site 1 and Site 3 (monondentate) Site 2 (bidentate)		Site 1 and Site 3 (monondentate) Site 2 (bidentate)
Th-O_1 (H_2O)	2.78	Th-O_5N (Site 1)	2.26
Th-O_2 (H_2O)	2.70	Th-O_6N (Site 2)	2.36
Th-O_3 (H_2O)	2.70	Th-O_7C (Site 2)	2.44
Th-O_4 (H_2O)	2.71	Th-O_8N (Site 3)	2.22
Average Th-O (H_2O)	2.72	Average Th-O (hydroxamate)	2.32

B) Complexation of Th(IV) and U(IV) with DFB studied by EXAFS

According to the speciation diagram (**Figure II.16**) plotted using literature data [1996WHI], the species of $Th(H_3DFB)^{4+}$ and $Th(HDFB)^{2+}$ are predominant at pH = 0.5 and 5, respectively. Due to the instability of DFB at pH = 0.5, the structure of the Th(IV)-DFB complex has been studied at pH = 5 using X-ray absorption fine structure. The EXAFS spectrum as well as its

corresponding Fourier transform is presented in **Figure IV.40**. The experimental spectrum was adjusted using the calculated structure (**Figure IV.38**) with the three hydroxamate sites (bidentate) coordinated to thorium. Indeed, both speciation diagrams and FTIR analysis seem to indicate the formation of the deprotonated complex $Th(HDFB)^{2+}$ at pH = 5. The EXAFS FT modulus exhibits an intense peak at $R+\phi \approx 1.9$ Å (non phase shift corrected distance). This first peak corresponds to a first oxygen shell around 2.3-2.5 Å. This oxygen contribution could not be fitted with only one oxygen shell. Two distinct oxygen shells were observed, one at 2.36 Å with 3 oxygen atoms and a longer one at 2.45 Å with 5 oxygen atoms (**Table IV.17**). The total coordination number of thorium was fixed at 8, according to the DFT calculations results. Unlike the DFT calculations, the difference between Th-O_N and Th-O_C lengths (hydroxamate) is due to the negative charge on O_N atom, rather than due to the radial resolution ($\Delta R = \pi/2\Delta k$ = 0.13 Å). However, the average bond length (2.42 Å) is in agreement with the one calculated from the DFT calculations (2.43 Å) (**Table IV.15**). The results obtained from the first coordination sphere seems to be in good agreement with the presence of the $Th(HDFB)^{2+}$ with two water molecules. However, the adjustment of the second coordination sphere (Th⋯C/N) leads to a coordination number of 4. The distance Th⋯N/C was evaluated at 3.31 Å, which is in good agreement with calculations (Th⋯C/N = 3.30 Å). Even if the quality factor seems to indicate a good adjustment of the spectrum ($\Delta\chi^2 = 5.3$), the number of carbon and nitrogen atoms around the thorium does not indicate that the thorium is coordinated to three hydroxamate groups in bidentate fashion. However, the uncertainty obtained on this coordination number is significant. The observation of the EXAFS FT moduli pinpoints a contribution not well fitted around $R+\phi \approx 3.2$ Å. Gong et al. studied the speciation of U(VI) dioxo-diacetohydroxamate complex using several techniques [2007GON]. They observed that in aqueous solution, according to the pH, both binding fashion (monodentate and bidentate) were present. The Th-DFB spectrum was also adjusted by considering at least one monodentate hydroxamate group. The use of monodentate coordination fashion did not allow to obtain a better fit. In conclusion, the complex configuration of Th with three bidentate hydroxamate groups in DFB well corresponds to the experimental results of EXAFS.

It is important to notify that at the end of the EXAFS analyses, the thorium solution took a bright orange color. The same coloration was not observed for the same solution not exposed to the X-ray beam. However, no change was observed on the EXAFS spectra over time.

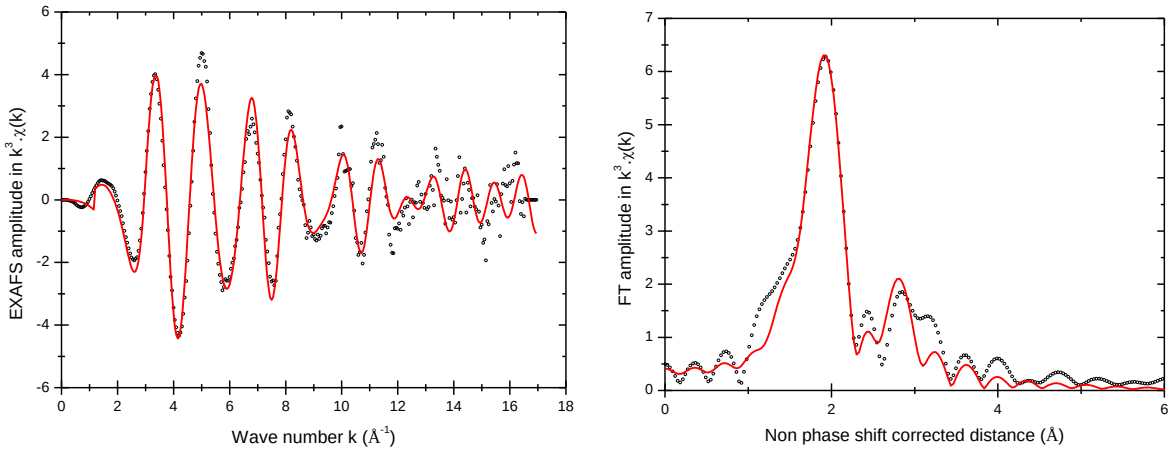

Figure IV.40 k^3-weighted EXAFS spectra and their corresponding Fourier transform at the Th L_{III} edge of a solution of Th-DFB at pH = 5. Experimental spectrum (circles) and adjustment (red line).

Table IV.17 EXAFS best fit parameters for the Th(IV) and U(IV)-DFB solutions at pH = 5. s_0^2 is the EXAFS global amplitude factor and is fixed to 1; ε is the average noise, $\Delta\chi^2$ is the quality factor and R_f(%) is the agreement factor of the fit.

	Shell	CN	R(Å)	σ^2(Å^2)	Δe_0(eV)	ε(k)	R_f(%)	$\Delta\chi^2$
Th(IV)-DFB	O_N	3	2.36(1)	0.0084				
pH = 5, [Th(IV)] = 5 mM, [DFB] = 6 mM	O_C+O_{H2O}	3+2	2.45(2)	0.0063	3.1	0.00052	0.3	5.3
	C/N	6	3.31(1)	0.0039				
U(IV)-DFB	O	6.2(2)	2.34(1)	0.0057				
pH = 5, [U(IV)] = 5 mM, [DFB] = 6 mM	O_{H2O}	1.8(2)	2.46(2)	0.0066	-2.9	0.00051	0.1	4.2
	C/N	6.2(2)	3.25(1)	0.0030				

The analogy with other tetravalent actinides was verified by studying the speciation of uranium(IV) in presence of DFB at the same pH. In this way a solution of uranium(IV) with DFB was prepared in the same conditions than the solution of Th(IV) with DFB ([U(IV)] = 5×10^{-3} M, [DFB] = 6×10^{-3} M, pH = 5). Because of the instability of U(IV), rongalite was introduced in the solution to maintain the oxidation state to +IV. Possible redox reactions under large photon flux were expected, so the U(IV) samples were prepared at the last moment and analyzed as soon as possible. The monitoring of the XANES spectra during the measurement did not indicate the formation of significant amount of U(VI) under the beam (**Supplementary figure in Appendix E**). The uranium sample does not show any U=O contribution from an oxo shell around 1.80 Å. **Figure IV.41** shows the EXAFS spectra of the U(IV)-DFB complex with its

corresponding Fourier transforms (FT). The best fit parameters are reported in **Table IV.17**. As the thorium sample, the spectrum was adjusted by considering a three bidentate coordination configuration. A better adjustment was obtained with a coordination number set to nine instead of eight. In this case, uranium(IV) has a similar behavior than plutonium(IV) with the siderophore DFE [2000NEU]. DFE is a cyclic siderophore with functional groups to those in DFB.

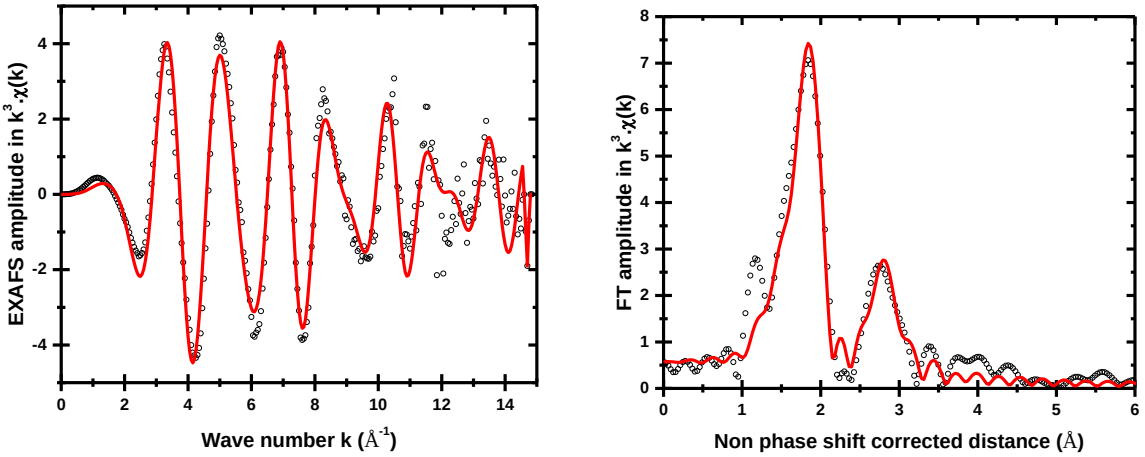

Figure IV.41 k^3-weighted EXAFS spectra and their corresponding Fourier transform at the U L_{III} edge of a solution of U(IV)-DFB at pH = 5. Experimental spectrum (circles) and adjustment (red line).

Thus, for uranium, the intense peak at R+ϕ ≈ 1.9 Å was fitted by 6 oxygen atoms at 2.34 Å and 3 oxygen atoms at 2.46 Å characteristics of three water molecules. A better fit could be obtained by using several U-O distances to distinguish oxygen atoms bonded to N or C; however, the bond length resolution is also limited at 0.13 Å (ΔR = π/2Δk). The second coordination sphere was fitted with 6 carbon and/or nitrogen atoms at 3.25 Å. Those values are in good agreement with the distances determined by Neu et al. for the structure of Pu(IV)-desferrioxamine E [2000NEU]. Three Pu-O bonds were isolated. The Pu-O_{H2O} was evaluated at 2.46 Å, Pu-O_N at 2.31 Å and Pu-O_C at 2.36 Å leading to an average bond length for hydroxamates equal to 2.33 Å. The Pu-C and Pu-N distances were calculated at 3.21 Å.

The bond length difference between U-O, Pu-O and Th-O is mainly due to the difference of the effective ionic radii. The effective ionic radii of those actinides are evaluated at 0.96, 1.00 and 1.05 for Pu^{4+}, U^{4+} and Th^{4+} respectively [1976SHA].

IV.3 Summary

The formation constants of $Ln(H_3DFB)^{3+}$ and $Ln(H_2DFB)^{2+}$ have been determined using two different techniques (liquid-liquid extraction and UV-Vis absorption spectrophotometry) and two different metal concentrations (tracer scale and macro-amount). The values obtained are consistent and agree well with literature data. However, results from affinity capillary electrophoresis were found inconclusive. ATR-FTIR spectroscopy measurements were also performed on solutions of equimolar Eu and DFB. The shift of the carbonyl band of hydroxamate group with increasing pH has been correlated to the successive deprotonation of hydroxamate groups due to the complexation, and thus to the successive formation of the complexes $Eu(H_3DFB)^{3+}$, $Eu(H_2DFB)^{2+}$ and $Eu(HDFB)^{+}$ in agreement with the speciation diagram.

The formation constants of $Th(H_3DFB)^{4+}$ and $Th(H_2DFB)^{3+}$ have been deduced from liquid-liquid extraction experiments with ^{227}Th. And those of $U(BHA)^{3+}$, $U(AHA)^{3+}$ and $U(AHA)_2^{2+}$ have been deduced from UV-Vis absorption spectrophotometry measurements. The values obtained are presented in **Table IV.18** with the available literature data. The discrepancy observed on the system Th-DFB could be explained not only by the difference in techniques, concentrations and medium composition but also by the fact that several auxiliary data have been used when calculating the stability constants.

Table IV.18 Formation constants obtained in this work and available in the literatures.

$iM+nL+mH \rightleftharpoons M_iL_nH_m \quad \beta_{inm}=[M_iL_nH_m]/[M]^i[L]^n[H]^m$

Actinide	Ligand	logβ_{110}	logβ_{120}	Condition[e]	Method	Reference
^{227}Th(IV)	DFB[a]	40.9±0.1	38.2±0.1	0.7 M (Na, HClO4)	LLE	this work
Th(IV)	DFB[a]	42.0±0.1	40.2±0.1	0.1 M (KCl)	pot.	[1996WHI]
U(IV)	BHA[b]	11.0±0.1		0.5 M (HCl)	sp.	this work
U(IV)	BHA[c]	11.8±0.1		0.5 M (HCl)	sp.	this work
U(IV)	AHA[d]	12.0±0.1	21.1±0.1	0.5 M (HCl)	sp.	this work

a. Calculated with pKa_1 = 8.54±0.01 pKa_2= 9.06±0.01 pKa_3= 9.70±0.02 pKa_4= 10.89±0.06 [2011CHR]

b. Calculated with pKa (BHA) = 8.07±0.06 [2010AKS]

c. Calculated with pKa (BHA) = 8.83±0.01 [2011TUR]

d. Calculated with pKa (AHA) = 9.15 [2011CHU]

e. Determined at T = 25 °C

EXAFS spectra have been registered on the complexes Th(IV)-DFB and U(IV)-DFB at pH = 5, where the species $M(HDFB)^{+}$ is expected to be predominant. For Th(IV), the spectrum was adjusted using optimized structures deduced from DFT calculations. The best fitting has been

obtained by considering a bidendate coordination of 3 hydroxamate groups. The coordination sphere was completed by 2 and 3 oxygen atoms of water molecules for Th(IV) and U(IV), respectively.

V. Conclusion

The aim of this work was to determine thermodynamic and structural data on the complexation of tri-and tetra-valent actinides with hydroxamate ligands, especially desferrioxamine B, a natural occurring organic ligand. These fundamental data indeed are essential to improve models of actinides behavior in the environment.

Trivalent lanthanides were used to simulate trivalent actinides, whereas Th(IV) and U(IV) were considered as Pu(IV) analogues. The thermodynamic study has been conducted using different techniques and different metal concentration:

- Liquid-liquid extraction experiments combined with gamma spectroscopy were carried out with ^{152}Eu (commercial) and ^{227}Th (purified at IPNO). In both cases, only complexes of stoichiometry 1:1 have been identified, and the formation constants of two complexes $Eu(H_3DFB)^{3+}$ / $Eu(H_2DFB)^{2+}$ and $Th(H_3DFB)^{4+}$ / $Th(H_2DFB)^{3+}$ have been determined.

- Affinity capillary electrophoresis with UV detector was used to investigate the complexation of La and Lu with DFB. But no conclusive results were obtained. Since UV detector can only monitor the mobility of DFB, experiments were performed with the metal in excess over DFB. Multi-nuclear species can be probably formed, complicating data analysis.

- UV-Visible absorption spectrophotometry was used to study the complexation of Eu(III), Pr(III), U(IV) with DFB and also aceto-and benzo-hydroxamate (AHA, BHA). The constants of the complex $Ln(H_3DFB)^{3+}$ and $Ln(H_2DFB)^{2+}$ were obtained for two pH values using HypSpec software. The stability constants of $U(BHA)^{3+}$, $U(AHA)^{3+}$ and $U(AHA)_2^{2+}$ have been determined in 0.5 M HCl. But the complexation constants of U(IV) with DFB could not be determined because of their strong interaction.

The thermodynamic data obtained in the present work are in agreement with the scarce available literature data (**Table V.1**) However, auxiliary data (hydrolysis constants, complexation constants with acetate, TTA, acidity constants of DFB) and differences in the techniques and media used are likely to increase sometimes discrepancies. Nevertheless, the protocols used in liquid-liquid extraction and UV-Vis absorption spectrophotometry appear to be valid for further studies with trivalent actinides. Concerning Pu(IV), the use of UV-Vis spectrophotometry will require the development of a new method involving a competition with an organic ligand like DTPA. Moreover, performing liquid-liquid extraction experiments with Pu at tracer scale should include a step that ensure that Pu remains at the +IV oxidation state.

Table V.1 Obtained formation constants between trivalent lanthanides and DFB

$iM+nL+mH \rightleftharpoons M_iL_nH_m$ $\beta_{inm}=[M_iL_nH_m]/[M]^i[L]^n[H]^m$

Actinide	Ligand	logβ_{113}	logβ_{112}	Condition[b]	Method	Reference
^{152}Eu(III)	DFB[a]	35.4±0.2	30.9±0.2	25 °C	LLE	this work
Eu(III)	DFB[a]	35.6±0.1	31.5±0.1	20 °C	sp.	this work
Eu(III)	DFB[a]	35.72±0.06	30.91±0.06	25 °C	pot.	[2011CHR]
Pr(III)	DFB[a]	35.1±0.1	29.9±0.1	20 °C	sp.	this work
Pr(III)	DFB[a]	35.10	29.55	25 °C	pot.	[2011CHR]
Actinide	**Ligand**	**logβ_{113}**	**logβ_{112}**	**Condition**	**Method**	**Reference**
^{227}Th(IV)	DFB[a]	40.9±0.1	38.2±0.1	25 °C 0.7 M ($Na,HClO_4$)	LLE	this work
Th(IV)	DFB[a]	42.0±0.1	40.2±0.1	25 °C 0.1 M (KCl)	pot.	[1996WHI]
Actinide	**Ligand**	**logβ_{110}**	**logβ_{120}**	**Condition[f]**	**Method**	**reference**
U(IV)	BHA[c]	11.0±0.1		0.5 M (HCl)	sp.	this work
U(IV)	BHA[d]	11.8±0.1		0.5 M (HCl)	sp.	this work
U(IV)	AHA[e]	12.0±0.1	21.1±0.1	0.5 M (HCl)	sp.	this work

a. Calculated with pKa_1 = 8.54±0.01 pKa_2= 9.06±0.01 pKa_3= 9.70±0.02 pKa_4= 10.89±0.06 [2011CHR]

b. Determined at I = 0.7 M (Na, HClO4)

c. Calculated with pKa (BHA) = 8.07±0.06 [2010AKS]

d. Calculated with pKa (BHA) = 8.83±0.01 [2011TUR]

e. Calculated with pKa (AHA) = 9.15 [2011CHU]

f. Determined at T = 25 °C

The structural study has been carried out on DFB complexes of Eu(III), Th(IV) and U(IV) using infrared and X-ray absorption spectroscopies combined with quantum chemistry calculations:

- By using ATR-FTIR spectroscopy, the main bands of DFB and its complex with Eu(III) and Th(IV) have been assigned. In particular, the gradual shift of the hydroxamate carbonyl band with increasing pH has been correlated to the successive deprotonation of hydroxamate groups leading to the formation of $Eu(H_3DFB)^{3+}$ to $Eu(HDFB)^{+}$, and $Th(H_3DFB)^{4+}$ to $Th(HDFB)^{2+}$.

- The structure of the possible Th-DFB complexes: $Th(H_3DFB)$, $Th(H_2DFB)$ and Th(HDFB), have been optimized using DFT calculations, with a coordination number equal 8. In the case of Th(HDFB) where the 3 hydroxamate groups are involved in bondings, bidentate and monodentate have been considered.

- EXAFS measurements have been performed on samples of Th(IV) and U(IV) with DFB at pH = 5 (predominance of $Th(HDFB)^{2+}$). For Th(IV), EXAFS spectra were adjusted using the calculated structure of of Th(HDFB). Th(IV) was shown to be coordinated by 3 bidendate hydroxamates and 2 water molecules (**Figure V.1**). In the case of U(IV), a better adjustment was obtained with a coordination number set to nine. The obtained distance are in good agreement with the those of the complex Pu(IV)-desferrioxamine E [2000NEU].

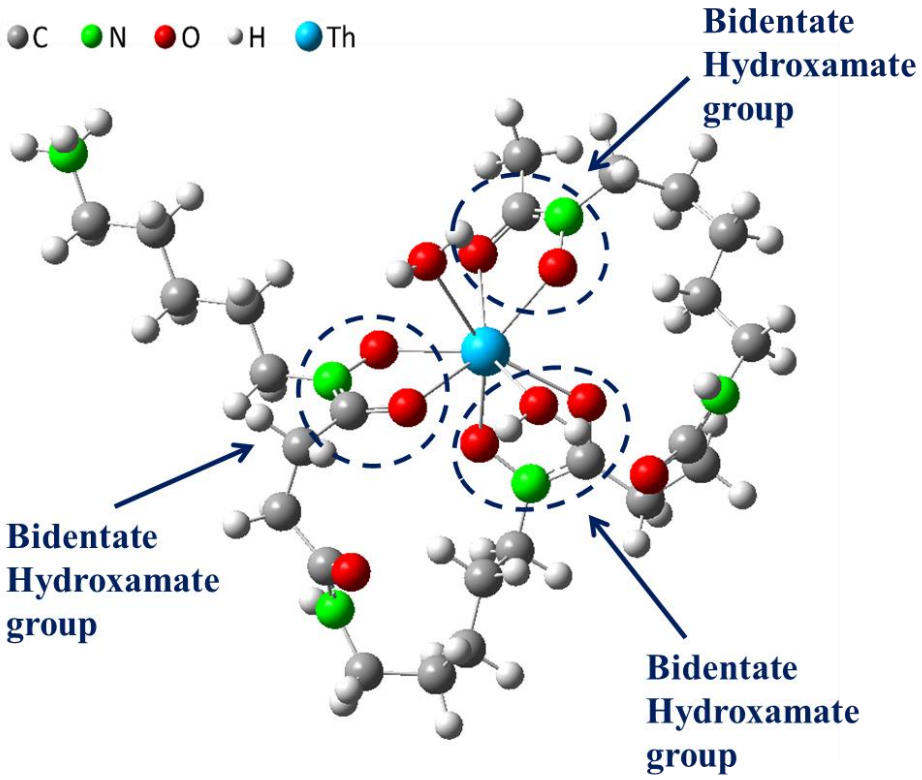

Figure V.1 Structure of the complex Th(HDFB).

Microbial siderophores like DFB are strong chelating agents that are likely to influence the mobility of actinides (IV) in the environment, otherwise rather characterized by their insolubility. Studying such systems remains challenging since on one hand, hydroxamates are not stable in acidic media, and on the other hand, An(IV) exhibit a strong tendency towards hydrolysis leading to polymers and colloids formation. Further thermodynamic studies should be performed at higher pH than in the present work. For that purpose, new experimental protocols have to be developed.

Appendix

Appendix A: Preparation of solutions

1) $HClO_4$ solution

A stock solution of perchloric acid (~3M) was prepared by dilution of concentrated perchloric acid (70%, ACS Reagent, Sigma-Aldrich). Its concentration was determined by acid-base titration with fresh standard solution of 0.1 M NaOH.

2) $NaClO_4$ solution

The stock solution of sodium perchlorate was prepared by dissolution of the monohydrate salt $NaClO_4 \cdot H_2O$ (≥ 99%, Fluka) in deionized water. The resulting solution was filtered on Millipore Stericup Unit (0.2 µm). Its concentration was determined by gravimetry on 3 samples. The error associated to the $NaClO_4$ concentration was derived from the mean value of the 3 weighted masses of the monohydrate salt obtained after drying of 500 µL of the stock solution.

3) TTA (2-Thenoyltrifluoroacetone) solution

The commercial TTA product (99%, Sigma-Aldrich) was contacted with deionized water for 7 days in order to get TTA in the hydrated form [1951KIN]. The hydrated TTA (P.M. 240.2 g/mol) was recrystallized twice from diethyl ether [2003JAU]. The so-purified TTA was stored in a glass bottle in a fridge at 8°C. The organic phases (TTA dissolved in toluene –Analytical Reagent Grade, Fisher Chemical) were prepared just prior to use.

4) Ligand (AHA, BHA and DFB) solution

Acetohydroxamic acid (>98%, Sigma-Aldrich) and benzohydroxamic acid (> 98%, Alfa Aesar) solutions have been prepared by solubilization of each reagent in electrolyte.

Desferriooxamine mesylate (>98.7%, Apollo Scientific) have been prepared in ionized water or in electrolyte.

5) Stable lanthanide (La, Pr, Eu, Lu) solution

The stock solutions were prepared in deionized water or in electrolyte by dissolution of the salt of $La(NO_3)_3 \cdot 6H_2O$, $Pr(NO_3)_3 \cdot 5H_2O$, $Eu(NO_3)_3 \cdot 5H_2O$ and $Lu(NO_3)_3 \cdot 5H_2O$ (>99%, ACS Reagent, Sigma-Aldrich), respectively.

6) Isotope ^{152}Eu solution

The commercial solution of ^{152}Eu (CERCA-LEA) is packaged in HCl in a sealed ampoule. In a glove box, the whole solution has been evaporated and the residue taken up in 0.1 M $HClO_4$. At the time of its use, the ^{152}Eu concentration was 7×10^{-7} M. Just prior to liquid-liquid extraction experiments, a few µL of this stock solution was evaporated in a PTFE crucible and taken up with 1300 µL of $HClO_4$ solution which concentration corresponds to the pC_H value under study. This fresh solution was distributed over the twenty samples used for extraction and three reference for mass balance.

7) Organic and aqueous solutions for liquid-liquid extraction

Experiments of ^{152}Eu(III)-DFB:

Organic phase: Toluene was used as the diluent and was pre-equilibrated with the electrolyte for two days. The TTA stock solution was prepared by dissolution of TTA hydrate in pre-equilibrated toluene and was filtered on WHATMAN filter (grade 3).

Aqueous phase: The electrolyte at I = 0.7 M was prepared with deionized water by dilution of $NaClO_4$ stock solution. The proton concentration of the electrolyte was adjusted to the desired value with addition of 3 M $HClO_4$ solution. The determination of proton concentration is described in **Appendix C**. The DFB stock solution was prepared by dissolution of the salt in the electrolyte of given ionic strength and pC_H. Then dilution was carried out with same electrolyte.

Experiments of ^{227}Th(IV)-DFB:

Organic phase: Toluene was used as the diluent and was pre-equilibrated with the electrolyte for two days. The TTA stock solution was prepared by dissolution of TTA hydrate in pre-equilibrated toluene. This organic phase was contacted with aqueous solution of ^{227}Th(IV) (at a given ionic strength and pC_H) overnight away from light. After separation, 50 µL of this ^{227}Th(IV) loaded organic phase where introduced in samples for extraction experiments.

Aqueous phase: The electrolyte at I = 0.7 M was prepared with deionized water by dilution of $NaClO_4$ stock solution. The electrolyte was prepared at the desired value with addition of 3 M $HClO_4$ solution and 7 M $NaClO_4$. The DFB stock solution was prepared by dissolution of the salt in the electrolyte of given ionic strength and pC_H. Then dilution was carried out with same electrolyte.

Experiments were performed in glass vials covered by galxyl-parylene (Comelec).

Appendix B: Influence of γ-ray energy for counting

The self-absorption (gamma-ray) is related to sample size, shape, density, chemical composition and emitted photon energy. In this work, 0.5 ml of aqueous solution or organic phase (TTA in toluene) is measured with identical geometry by gamma-spectroscopy.

Figure A. 1 presents the distribution values (D_0) of ^{152}Eu between organic and aqueous phases at pC_H = 4.0 and 4.2 as function of energy (γ-ray characteristic peak of ^{152}Eu).

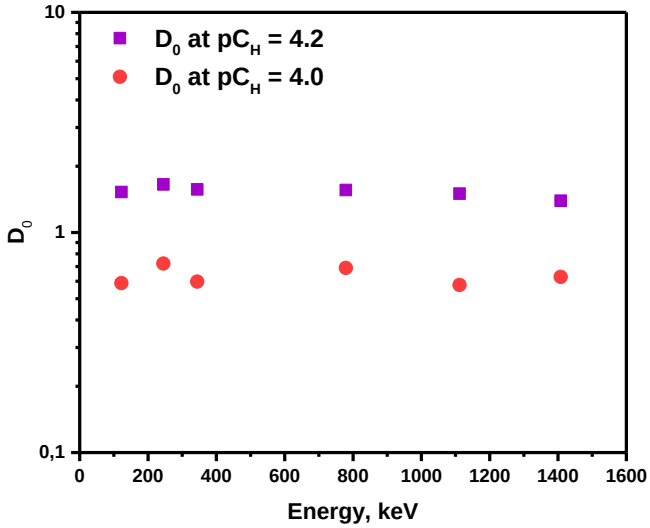

Figure A. 1 Distribution values (D_0) of ^{152}Eu at pC_H = 4.0 and 4.2 as function of energy (γ-ray characteristic peak of ^{152}Eu).

It can be seen that the distribution values (D_0) are almost constant with the increase of counting energy, indicating that the energy for counting in this work does not impact the distribution value.

Appendix C: Determination of proton concentration

The measurements of the proton concentration were carried out by a conventional assembly: pH-meter and a glass electrode combined with a reference Ag/AgCl with saturated 3M NaCl solution. However, the ionic strength of the studied solutions was different from commercial buffer solutions. Thus, a range of buffer solution was prepared by mixing the stock solution of $NaClO_4$ and $HClO_4$, in order to obtain the solutions at I = 0.7 M (Na, $HClO_4$) with known proton concentrations (C_H = 0.1, 0.01 and 0.001 M). The potential (ΔE) was measured for each solution, allowing plotting a calibration line. Thus, the value of pC_H can be calculated by measuring ΔE of the solution according to the calibration line [2012LEG].

Appendix D: Back and direct extraction of Th(IV)

At first, the equilibrium time between TTA solution (C_{TTA} = 0.08 M) charged by ^{227}Th in toluene and DFB aqueous solution (C_{DFB} = 0.07 M, I = 0.7 M (Na, $HClO_4$)) was determined at T = 25 °C at 50 rpm stirring speed. **Figure A. 2** presents the variation of D as function of contacting time. It can be seen that the D value became stable after three hours, indicating the equilibrium was reached. Thus, in the case of Th-DFB, the organic and aqueous phases were separated immediately after contacting for 3 hours, which is consistent with Sasaki et al.'s work [2008SAS].

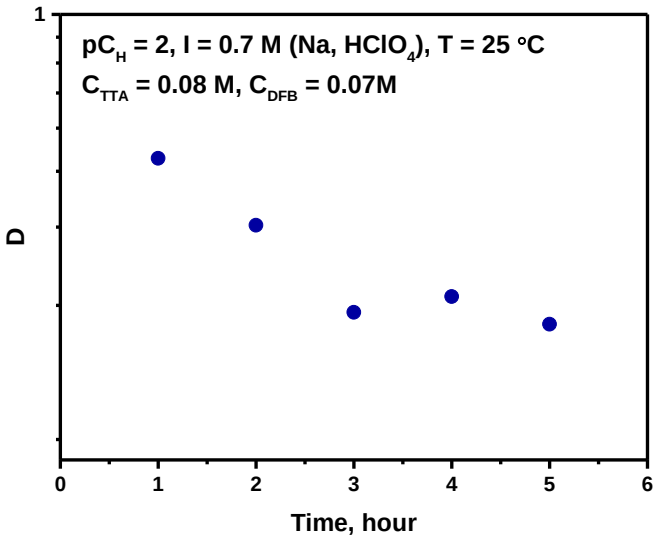

Figure A. 2 Variation of D as function of contacting time.

Like other An(IV), Th(IV) exhibits a strong tendency to hydrolysis that favors the formation of oligomer and colloids. The condensation of hydrolyzed actinides can impact liquid-liquid extraction experiments [1963BRO]. If the distribution coefficients in both direct and back extraction are not equal, it means the inextractable poly-nuclear complex indeed exists in the aquatic system [1965TAK].

Figure A. 3 presents the experimental procedure back and direct extraction of Th(IV). First, 2 mL organic phase (^{227}Th and 0.08 M TTA in toluene) was contacted with 2 mL aqueous phase. After reaching equilibrium, 1 mL of each phase was taken to contact with 1 mL fresh aqueous phase and organic phase, respectively.

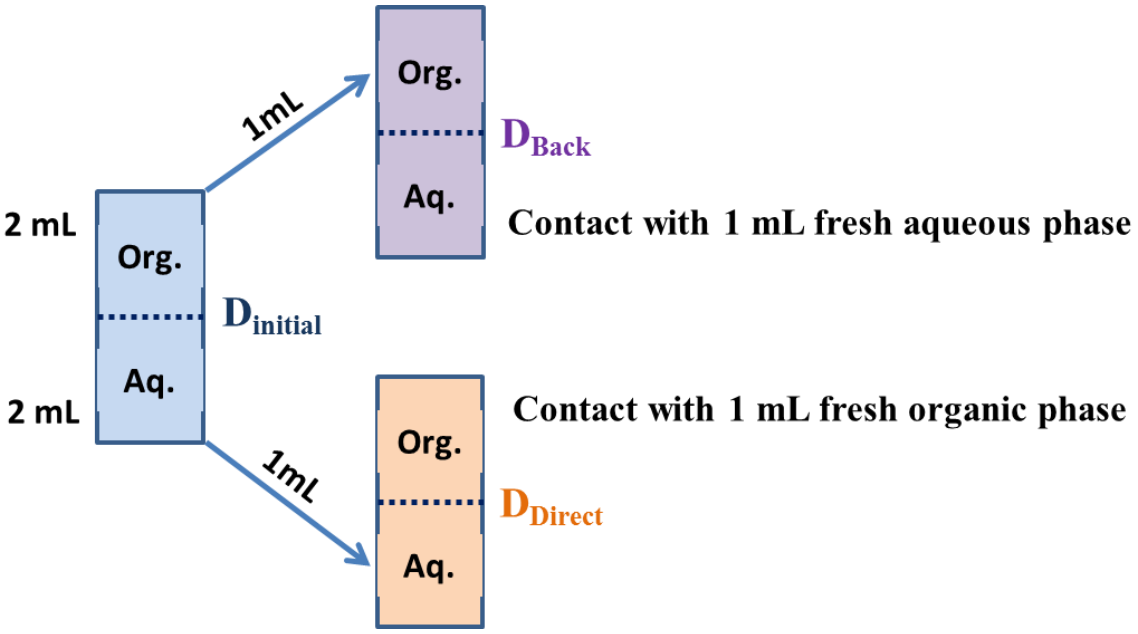

Figure A. 3 Experimental procedure of back and direct extraction of Th(IV)

Figure A. 4 presents the values of D in the back and direct extraction of Th(IV) at pC_H = 1, I = 0.7 M (Na, $HClO_4$) without DFB and at pC_H = 2, I = 0.7 M (Na, $HClO_4$) with 0.07 M DFB. It can be seen that the values of $D_{initial}$, D_{direct} and D_{back} are close to each other in the absence of DFB, as well as in its presence. It is suggested that the inextractable poly-nuclear species of Th(IV) is not significantly observed in this condition.

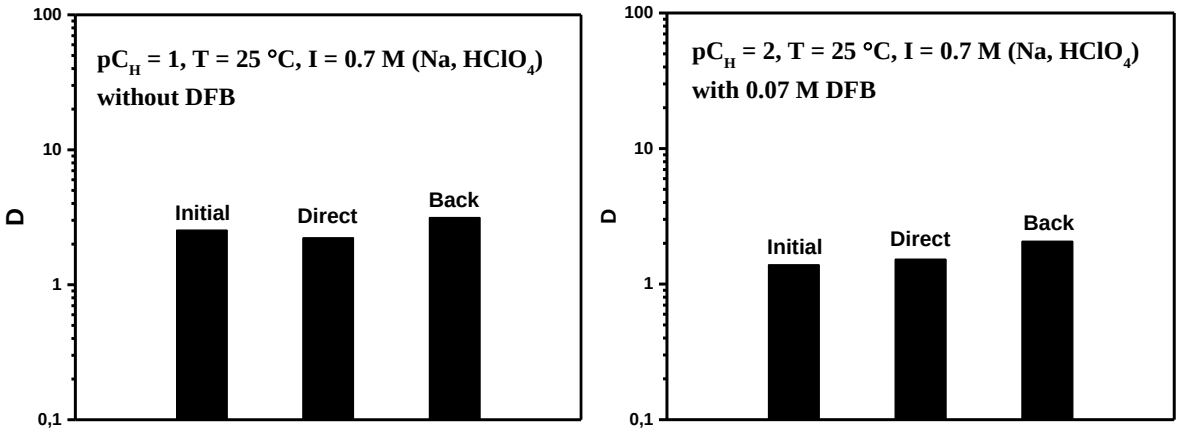

Figure A. 4 Values of D in the back and direct extraction of Th(IV) at pC_H = 1, I = 0.7 M (Na, $HClO_4$) without DFB (left) and at pC_H = 2, I = 0.7 M (Na, $HClO_4$) with 0.07 M DFB (right).

Appendix E: Study of DFB Stability

In order to avoid the hydrolysis of tetravalent actinides, the solutions have been prepared in acidic media. But DFB and hydroxamic acid are not stable [1959PLA]. The degradation of DFB was studied in acidic media by UV-visible spectrophotometry.

First, the validity of Beer-Lambert law relative to DFB was checked: absorption spectra have been registered at ambient temperature, pH = 4.0, I = 0.5 M with 10^{-5} M ≤ C_{DFB} ≤ 5×10^{-6} M. Figure A. 5 presents the corresponding absorption spectra. Figure A. 6 presents the experimental variations of DFB absorbance at 200, 210 and 220 nm with its concentration and linear fittings. Whatever the wavelength, Beer-Lambert law appears to be valid over the investigated concentration.

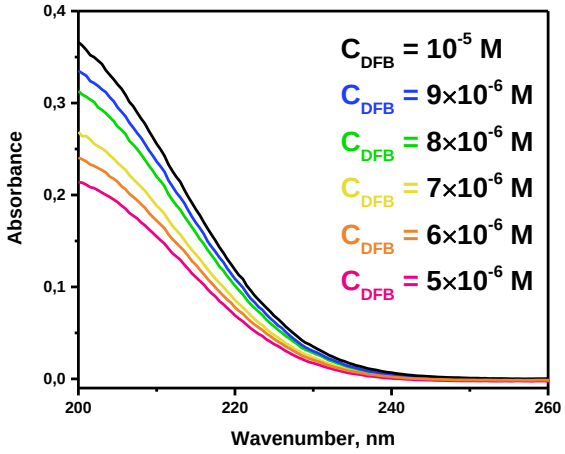

Figure A. 5 Absorption spectra of DFB at different concentrations (pH = 4.0 and I = 0.5 M (Na, $HClO_4$)).

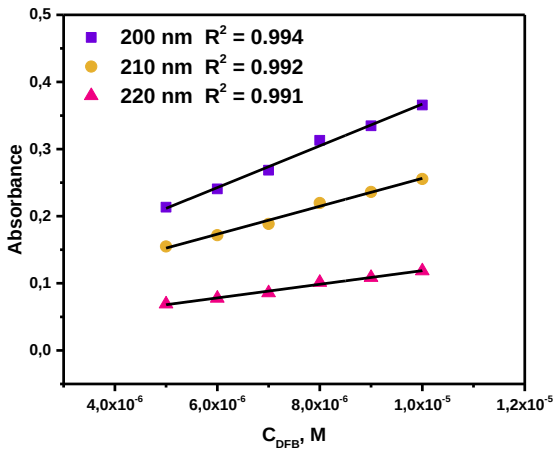

Figure A. 6 Test of Lambert-Beer Law of DFB at the concentration ranging from 10^{-5} to 5×10^{-6} M at pH = 4.0 and I = 0.5 M (Na, $HClO_4$) at the wavelength of 200, 210 and 220 nm.

The UV absorption of 1×10^{-5} M DFB solution at 200 nm was recorded as function of time at the acidity 1 and 0.01 M as shown in **Figure A. 7**.

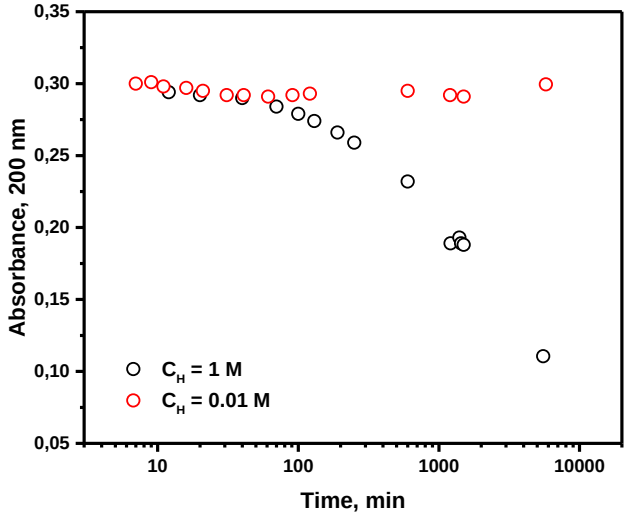

Figure A. 7 Variation of UV absorbance of 1×10^{-5} M DFB solution at 200 nm as function of time.

It can be seen that DFB solution is almost stable at C_H = 0.01 M ($HClO_4$) and a visible degradation at C_H = 1.0 M ($HClO_4$) can be observed after 40 min. The degradation of 1×10^{-5} M DFB at C_H = 0.1 M was also examined. The initial absorbance and the absorbance after one day were compared and no significant difference is observed. Thus, it is not necessary to consider the degradation of DFB at $C_H \leq 0.1$ M in this work.

The high acidities used in the experiments were 0.2 M ($HClO_4$) for liquid-liquid extraction (Th-DFB) and 0.5 M (HCl) for UV-vis absorption spectroscopy. The UV absorption of 2×10^{-5} M DFB solution (pC_H = 0.7) at 200, 210 and 220 nm was recorded as the increase of time. The collected table is shown in **Table A. 1**.

The contacting time for liquid-liquid extraction (Th-DFB) is to be 3 hours. According to the recorded values in the table, approximate 5 % of DFB is degraded at pC_H = 0.7 from 3 to 4 hours. Thus, 5% degradation of DFB has been taken into account during the data treatment.

Table A. 1 UV absorbance of 2×10^{-5} M DFB solution (pC_H = 0.7) at 200, 210 and 220 nm as function of time.

Time, min	Absorbance					
	200nm	Degradation	210nm	Degradation	220nm	Degradation
0	0.5268	0.00%	0.3280	0.00%	0.1451	0.00%
30	0.5195	1.39%	0.3226	1.65%	0.1422	2.00%
60	0.5165	1.96%	0.3194	2.62%	0.1419	2.21%
90	0.5137	2.49%	0.3160	3.66%	0.1411	2.76%
120	0.5125	2.71%	0.3136	4.39%	0.1410	2.83%
150	0.5090	3.38%	0.3126	4.70%	0.1400	3.51%
180	0.5043	4.27%	0.3098	5.55%	0.1393	4.00%
210	0.5033	4.46%	0.3085	5.95%	0.1369	5.65%
240	0.4963	5.79%	0.3073	6.31%	0.1369	5.65%

Supplementary figure for page 102:

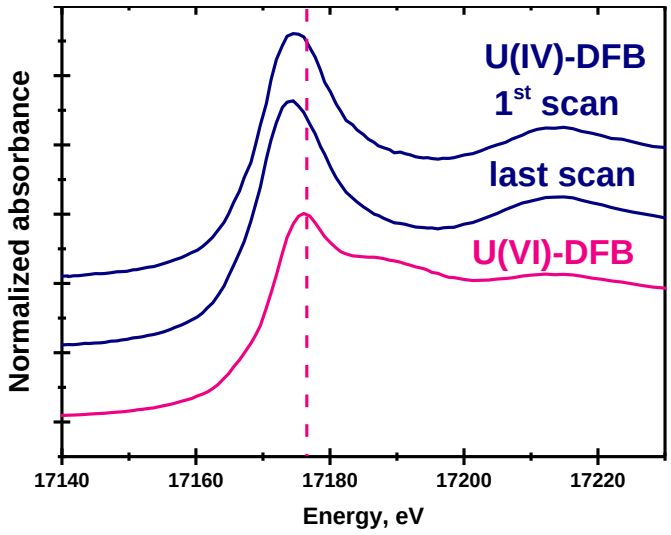

Supplementary figure for page 102: XANES spectra of U(IV)-DFB and U(VI)-DFB complexes.

In the XANES spectra of U(IV)-DFB, no significant variation between the first and last scans is observed. The absorption edge and the dioxo shoulder band of UO_2^{2+} is not clearly observed in the XANES spectra of U(IV)-DFB, which indicates that no significant amount of U(VI) was formed under the beam.

Reference

[1945SEA] Seaborg, G. T. (**1945**). The chemical and radioactive properties of the heavy elements. Chemical & Engineering News Archive, 23(23), 2190-2193.

[1950DAY] Day, R. A., & Stoughton, R. W. (**1950**). Chemistry of thorium in aqueous solutions. I. Some organic and inorganic complexes. Journal of the American Chemical Society, 72(12), 5662-5666.

[1951KIN] King, E. L., & Reas, W. H. (**1951**). The hydration of thenoyltrifluoroacetone in benzene solution. Journal of the American Chemical Society, 73(4), 1806-1808.

[1951ZEB] Zebroski, E. L., Alter, H. W., & Heumann, F. K. (**1951**). Thorium complexes with chloride, fluoride, nitrate, phosphate and sulfate. Journal of the American Chemical Society, 73(12), 5646-5650.

[1952WAG] Waggener, W. C., & Stoughton, R. W. (**1952**). Chemistry of Thorium in Aqueous Solutions. II. Chloride Complexing as A Function of Ionic Strength. The Journal of Physical Chemistry, 56(1), 1-5.

[1956KRA] Kraus, K. A., Moore, G. E., & Nelson, F. (**1956**). Anion-exchange Studies. XXI. Th (IV) and U (IV) in hydrochloric acid. Separation of thorium, protactinium and uranium. Journal of the American Chemical Society, 78(12), 2692-2695.

[1959ISH] Ishimori, T., & Nakamura, E. (**1959**). Distribution of neptunium between TBP and some mineral acids. Bulletin of the Chemical Society of Japan, 32(7), 713-720.

[1959NEW] Newton, T., & Rabideau, S. (**1959**). A review of the kinetics of the aqueous oxidation–reduction reactions of uranium, neptunium, And plutonium. Journal of Physical Chemistry, 63(3), 365-370.

[1959PLA] Plapinger, R. E. (**1959**). Ultraviolet absorption spectra of some hydroxamic acids and hydroxamic acid derivatives. Journal of Organic Chemistry, 24(6), 802-804.

[1960COH] Cohen, D., & Carnall, W. T. (**1960**). Absorption spectra of uranium (iii) and uranium (IV) in $DClO_4$ solution. Journal of Physical Chemistry, 64(12), 1933-1936.

[1961POS] Poskanzer, A., & Foreman Jr, B. (**1961**). A summary of TTA extraction coefficients. Journal of Inorganic and Nuclear Chemistry, 16(3-4), 323-336.

[1963AND] Anderegg, G., Schwarzenbach, G., & Leplatte.F. (**1963**). Hydroxamatkomplexe .2. Die Anwendung der pH-Methode. Helvetica Chimica Acta, 46(4), 1400-&.

[1963BRO] Brown, D., & Maddock, A. G. (**1963**). Protactinium. Quarterly Reviews, Chemical Society, 17(3), 289-341.

[1963SCH] Schwarzenbach, G., & Schwarzenbach, K. (**1963**). Hydroxamatkomplexe i. Die Stabilität der Eisen(iii)-Komplexe einfacher Hydroxamsäuren und des Ferrioxamins b. Helvetica Chimica Acta, 46(4).

[1965TAK] Takagi, J., & Shimojima, H. (**1965**). Studies on protactinium (V) in sulphuric acid solution—I: Centrifugation study. Journal of Inorganic and Nuclear Chemistry, 27(2), 405-409.

[1966BAR] Barocas, A., Baroncelli, F., Biondi, G., & Grossi, G. (**1966**). The complexing power of hydroxamic acids and its effect on behaviour of organic extractants in the reprocessing of irradiated fuels—II: The complexes between benzohydroxamic acid and thorium, uranium (IV) and plutonium (IV). Journal of Inorganic and Nuclear Chemistry, 28(12), 2961-2967.

[1968CAR] Carey, G. H., & Martell, A. E. (**1968**). Formation, hydrolysis, and olation of uranium (IV) chelates. Journal of the American Chemical Society, 90(1), 32-38.

[1969EDR] Edroth, B. (**1969**). Adsorption of thorium and its TTA-complexes from aqueous solutions. Acta Chem. Scand, 23(8), 6.

[1969NOR] Noren, B. (**1969**). Solvent extraction studies of the formation of fluoride and sulphate complexes of zirconium (IV). Acta Chem. Scand, 23(2).

[1970CLE] Cleveland, J. M. (**1970**). The Chemistry of Plutonium. Gordon and Beach. New York, USA.

[1970IKE] Ikeda, N., Kimura, K., Asai, H., & Oshima, N. (**1970**). Extraction behavior of europium with thenoyltrifluoroacetone (TTA). Radioisotopes, 19(1), 1-6.

[1972MET] Metivier, H., Guillaumont, R. (**1972**). Hydrolyse du plutonium tétravalent. Radiochem. Radioanal. Lett., 10, 27-35.

[1974SIL] Silva, R., McDowell, W., Keller, O., & Tarrant, J. (**1974**). Comparative solution chemistry, ionic radius, and single ion hydration energy of nobelium. Inorganic Chemistry, 13(9), 2233-2237.

[1975DAV] Davydov, Yu.P., & Efremenkov, V.M. (**1975**). Investigation of the hydrolytic properties of tetravalent uranium: II. Conditions of formation of mononuclear and polynuclear hydroxo complexesof U(IV). Sov. Radiochem., 17, 160-164.

[1975LIU] Liu, C. Y., & Sun, P. J. (**1975**). Studies of rare-earth metal-complexes of hydroxamic acids. Journal of the Chinese Chemical Society, 22(4), 317-330.

[1976SHA] Shannon, R. D. (**1976**). Revised effective ionic-radii and systematic studies of interatomic distances in halides and chalcogenides. Acta Crystallographica Section A, 32, 751-767.

[1978JOH] Johnson, G. L., & Toth, L. M. (**1978**). Plutonium (IV) and thorium (IV) hydrous polymer chemistry. Oak Ridge National Lab. Tennessee, USA.

[1978PYY] Pyykkö, P. (**1978**). Relativistic Quantum Chemistry. Advances in Quantum Chemistry (Vol. 11, pp. 353-409). Academic Press.

[1980PER] Perkins, R. W., & Thomas, C. W. (**1980**). Worldwilde Fallout. In: Transuranic Elements in the Environment Worldwide Fallout (ed. W. C. Hanson), Technical Information Center, Department of Energy, Springfield, MO, pp. 53–82.

[1980POW] Powell, P. E., Cline, G. R., Reid, C. P. P., & Szaniszlo, P. J. (**1980**). Occurrence of hydroxamate siderophore iron chelators in soils. Nature, 287(5785), 833-834.

[1982JEN] Jensen, W. B. (**1982**). The positions of lanthanum (actinium) and lutetium (lawrencium) in the periodic table. Journal of Chemical Education, 59, 634, 1982.

[1983CAC] Caceci, M. S., & Choppin, G. R. (**1983**). The determination of the 1st hydrolysis constant of Eu(III) and Am(III). Radiochimica Acta, 33(2-3), 101-104.

[1983CHO] Choppin, G. R. (**1983**). Solution chemistry of the actinides. Radiochimica Acta, 32(1-3), 43-53.

[1986KAT] Katz, J. J., Seaborg, G. T., & Morss, L. R. (**1986**). Summary and comparative aspects of the actinide elements. The chemistry of the actinide elements. Springer Netherlands. New York, USA.

[1988PYY] Pyykko, P. (**1988**). Relativistic effects in structural chemistry. Chemical Reviews, 88(3), 563-594.

[1989BOR] Borgias, B., Hugi, A. D., & Raymond, K. N. (**1989**). Isomerization and solution structures of desferrioxamine B complexes of aluminum(3+) and gallium(3+). Inorganic Chemistry, 28(18), 3538-3545.

[1989EVE] Evers, A., Hancock, R. D., Martell, A. E., & Motekaitis, R. J. (**1989**). Metal-ion recognition in ligands with negatively charged oxygen donor groups - complexation of Fe(iii), Ga(iii), In(iii), Al(iii), and other highly charged metal-ions. Inorganic Chemistry, 28(11), 2189-2195.

[1989HAR] Harris, D. C., & Bertolucci, M. D. (**1989**). Symmetry and spectroscopy: an introduction to vibrational and electronic spectroscopy. Courier Corporation.

[1989KOI] Koide, Y., Uchino, M., Shosenji, H., & Yamada, K. (**1989**). Studies of collectors .10. Complexing ability of amino hydroxamic acid ligands with dioxouranium(IV) in aqueous-solution. Bulletin of the Chemical Society of Japan, 62(11), 3714-3715.

[1989MOH] Mohapatra, P., & Khopkar, P. (**1989**). Hydrolysis of actinides and lanthanides: hydrolysis of some trivalent actinide and lanthanide ions studied by extraction with thenoyltrifluoroacetone. Polyhedron, 8(16), 2071-2076.

[1989ROS] Rosch, F., Reimann, T., Buklanov, G. V., Milanov, M., & Khalkin, V. A. (**1989**). Electromigration of carrier-free radionuclides .8. Hydrolysis of Cf-249(III) in aqueous-solution. Radiochimica Acta, 47(4), 187-189.

[1992BRA] Brainard, J. R., Strietelmeier, B. A., Smith, P. H., Langstonunkefer, P. J., Barr, M. E., & Ryan, R. R. (**1992**). Actinide binding and solubilization by microbial siderophores. Radiochimica Acta, 58-9, 357-363.

[1992GRE] Grenthe, I., Wanner, H., Forest, I., & Agency, O. N. E. (**1992**). Chemical thermodynamics of uranium. North-Holland. Amsterdam, Netherlands.

[1992HEN] Henry, M., Jolivet, J. P., & Livage, J. (**1992**). Aqueous chemistry of metal-cations - hydrolysis, condensation and complexation. Structure and Bonding, 77, 153-206.

[1992RYD] Rydberg, J., Cox, M., Musikas, C.& Choppin, G.R. (**1992**). Principles and practices of solvent extradction. Marcel Dekker. New York, USA.

[1993ADL] Adloff, J. P. (**2018**). Fundamentals of Radiochemistry. CRC Press. Boca Raton, USA.

[1993BEC] Becke, A. D. (**1993**). Density-functional thermochemistry. III. The role of exact exchange. J. Chem. Phys. 98, 5648.

[1993CLA] Clark, B. J., Frost, T., & Russell, M. A. (**1993**). UV Spectroscopy: Techniques, instrumentation and data handling (Vol. 4). Springer Science & Business Media. Suffolk, UK.

[1993GUZ] Guzman, N. A. (**1993**). Capillary electrophoresis technology (Vol. 64). CRC Press. New York, USA.

[1993MIR] Mirabella Jr, F. M. (**1993**). Practical spectroscopy series. Internal reflection spectroscopy: Theory and Applications, 17-52. Marcel Dekker. New York, USA.

[1994BAL] Balasubramanian, K. (**1994**). Relativistic effects and electronic structure of lanthanide and actinide molecules. In "Handbook on the physics and chemistry of rare earths" (vol. 18, pp. 29-158): Elsevier. Online.

[1995NEI] Neilands, J. B. (**1995**). Siderophores - structure and function of microbial iron transport compounds. Journal of Biological Chemistry, 270(45), 26723-26726.

[1995YAT] Yatsimirskii, K. B. (**1995**). Relativistic effects in chemistry. Theoretical and Experimental Chemistry, 31(3), 153-168.

[1996AIH] AlHashimi, A., Evans, G. J., & Cox, B. (**1996**). Aspects of the permanent storage of uranium tailings. Water Air and Soil Pollution, 88(1-2), 83-92.

[1996BER] Bernhard, G., Geipel, G., Brendler, V., & Nitsche, H. (**1996**). Speciation of uranium in seepage waters of a mine tailing pile studied by time-resolved laser-induced fluorescence spectroscopy (TRLFS). Radiochimica Acta, 74(s1), 87-92.

[1996GAN] Gans, P., Sabatini, A., & Vacca, A. (**1996**). Investigation of equilibria in solution. Determination of equilibrium constants with the HYPERQUAD suite of programs. Talanta, 43(10), 1739-1753.

[1996HER] Hernlem, B. J., Vane, L. M., & Sayles, G. D. (**1996**). Stability constants for complexes of the siderophore desferrioxamine B with selected heavy metal cations. Inorganica Chimica Acta, 244(2), 179-184.

[1996RYD] Rydberg, J. (**1996**). Hydrophilic actinide complexation studied by solvent extraction radiotracer technique. SKB Technical Report. SKB-TR-96-17.

[1996WHI] Whisenhunt, D. W., Neu, M. P., Hou, Z. G., Xu, J., Hoffman, D. C., & Raymond, K. N. (**1996**). Specific sequestering agents for the actinides .29. Stability of the thorium(IV) complexes of desferrioxamine B (DFO) and three octadentate catecholate or hydroxypyridinonate DFO derivatives: DFOMTA, DFOCAMC, and DFO-1,2-HOPO. Comparative stability of the plutonium(IV) DFOMTA complex. Inorganic Chemistry, 35(14), 4128-4136.

[1996XIA] Xia, Y. X., Chen, J. F., & Choppin, G. R. (**1996**). Solubility, dissociation and complexation with Nd(III) and Th(IV) of oxine, thenoyltrifluoroacetone and 1,10-phenanthroline in 5.0 m NaCl. Talanta, 43(12), 2073-2081.

[1997DAC] Dacheux, N., & Aupiais, J. (**1997**). Determination of uranium, thorium, plutonium, americium, and curium ultratraces by photon electron rejecting α liquid scintillation. Analytical Chemistry, 69(13), 2275-2282.

[1997MCN] McNaught, A. D., & McNaught, A. D. (**1997**). Compendium of chemical terminology (Vol. 1669). Blackwell Science Oxford.

[1997PEA] Pearson, R.G. (**1997**). Chemical Hardness. Wiley-VCH. Weinheim, Germany.

[1998BEA] Beasley, T. M., Kelley, J. M., Maiti, T. C., & Bond, L. A. (**1998**). 237Np 239Pu atom ratios in integrated global fallout: a reassessment of the production of 237Np. Journal of Environmental Radioactivity, 38(2), 133-146.

[1998CON] Conradson, S. D., AlMahamid, I., Clark, D. L., Hess, N. J., Hudson, E. A., Neu, M. P., Palmer, P. D., Runde, W. H., & Tait, C. D. (**1998**). Oxidation state determination of plutonium aquo ions using X-ray absorption spectroscopy. Polyhedron 17, 599-602.

[1998TAY] Taylor, R. J., May, I., Wallwork, A. L., Denniss, I. S., Hill, N. J., Galkin, B. Y., ... & Fedorov, Y. S. (**1998**). The applications of formo-and aceto-hydroxamic acids in nuclear fuel reprocessing. Journal of Alloys and Compounds, 271, 534-537.

[1999CHA] Chaudhuri, N. K., Sawant, R. M., & Sood, D. D. (**1999**). A critical review on the stability constants of the fluoride complexes of actinides in aqueous solution and their correlation with fundamental properties of the ions. Journal of Radioanalytical and Nuclear Chemistry, 240(3), 993-1011.

[1999FAR] Farkas, E., Enyedy, E. A., & Csoka, H. (**1999**). A comparison between the chelating properties of some dihydroxamic acids, desferrioxamine B and acetohydroxamic acid. Polyhedron, 18(18), 2391-2398.

[1999KER] Kersting, A. B., Efurd, D. W., Finnegan, D. L., Rokop, D. J., Smith, D. K., & Thompson, J. L. (**1999**). Migration of plutonium in ground water at the Nevada Test Site. Nature, 397(6714), 56-59.

[1999MOL] Moll, H., Denecke, M. A., Jalilehvand, F., Sandstrom, M., & Grenthe, I. (**1999**). Structure of the aqua ions and fluoride complexes of uranium(IV) and thorium(IV) in aqueous solution: an EXAFS study. Inorganic Chemistry, 38(8), 1795-1799.

[2000CLA] Clark, D. L. (**2000**). The chemical complexities of plutonium. Los Alamos Science, 26, 364-381.

[2000EKB] Ekberg, C., Albinsson, Y., Comarmond, M. J., & Brown, P. L. (**2000**). Studies on the complexation behavior of thorium(IV). 1. Hydrolysis equilibria. Journal of Solution Chemistry, 29(1), 63-86.

[2000KLU] Klungness, G. D., & Byrne, R. H. (**2000**). Comparative hydrolysis behavior of the rare earths and yttrium: the influence of temperature and ionic strength. Polyhedron, 19(1), 99-107.

[2000NEU] Neu, M. P., Matonic, J. H., Ruggiero, C. E., & Scott, B. L. (**2000**). Structural characterization of a plutonium (IV) siderophore complex: single-crystal structure of pu-desferrioxamine E. Angewandte Chemie International Edition, 39(8), 1442-1444.

[2000OBR] O'Brien, E. C., Farkas, E., Gil, M. J., Fitzgerald, D., Castineras, A., & Nolan, K. B. (**2000**). Metal complexes of salicylhydroxamic acid (H(2)Sha), anthranilic hydroxamic acid and benzohydroxamic acid. Crystal and molecular structure of Cu(phen)(2)(Cl) Cl center dot H(2)Sha, a model for a peroxidase-inhibitor complex. Journal of Inorganic Biochemistry, 79(1-4), 47-51.

[2000STU] Stuart, B. (**2000**). Infrared spectroscopy. Kirk-Othmer encyclopedia of chemical technology. John Wiley & Sons. Online.

[2001ANT] Antonio, M. R., Soderholm, L., Williams, C. W., Blaudeau, J. P., & Bursten, B. E. (**2001**). Neptunium redox speciation. Radiochimica Acta, 89(1), 17-25.

[2001LEM] Lemire, R. J. (**2001**). Chemical thermodynamics of neptunium and plutonium (Vol. 4).

[2002MAD] Madic, C., Lecomte, M., Baron, P., & Boullis, B. (**2002**). Separation of long-lived radionuclides from high active nuclear waste. Comptes Rendus Physique, 3(7-8), 797-811.

[2002NEC] Neck, V., Muller, R., Bouby, M., Altmaier, M., Rothe, J., Denecke, M. A., & Kim, J. I. (**2002**). Solubility of amorphous Th(IV) hydroxide - application of LIBD to determine the solubility product and EXAFS for aqueous speciation. Radiochimica Acta, 90(9-11), 485-494.

[2002ROT] Rothe, J., Denecke, M. A., Neck, V., Muller, R., & Kim, J. I. (**2002**). XAFS investigation of the structure of aqueous thorium(IV) species, colloids, and solid thorium(IV) oxide/hydroxide. Inorganic Chemistry, 41(2), 249-258.

[2002SAN] Santschi, P. H., Roberts, K. A., & Guo, L. D. (**2002**). Organic mature of colloidal actinides transported in surface water environments. Environmental Science & Technology, 36(17), 3711-3719.

[2002SIN] Sinkov, S., & Choppin, G. (**2002**). Acetohydroxamic acid complexes with trivalent f-block metal cations. Journal of Nuclear Science and Technology, 39, 359-362.

[2003GUI] Guillaumont, R. et al. (**2003**). Update on the chemical thermodynamic of uranium, neptunium, plutonium, americium and technetium, Elsevier, OCDE, Amsterdan

[2003JAU] Jaussaud, C. (**2003**). Contribution à l'étude thermodynamique de l'hydrolyse de Pa (V) à l'échelle des traces par la technique d'extraction liquide-liquide avec la thenoyltrifluoroacetone (TTA): caractérisation du partage de la thenoyltrifluoroacetone dans le système TTA/H2O/toluène/Na+/H+/ClO4- (Doctoral dissertation, Paris 11).

[2003RAM] Ramírez-García, J. J., Jiménez-Reyes, M., Solache-Ríos, M., Fernández-Ramírez, E., López-González, H., & Rojas-Hernández, A. (**2003**). Solubility and first hydrolysis constants of europium at different ionic strength and 303 K. Journal of Radioanalytical and Nuclear Chemistry, 257(2), 299-303.

[2004LAN] Landa, E. R. (**2004**). Uranium mill tailings: nuclear waste and natural laboratory for geochemical and radioecological investigations. Journal of Environmental Radioactivity, 77(1), 1-27.

[2005BUG] Buglyo, P., & Potari, N. (**2005**). Study of the interaction between oxovanadium(IV) and hydroxamic acids. Polyhedron, 24(7), 837-845.

[2005DUC] Duckworth, O. W., & Sposito, G. (**2005**). Siderophore−manganese(III) interactions. I. Air-oxidation of manganese(II) promoted by desferrioxamine B. Environmental Science & Technology, 39(16), 6037-6044.

[2005EDW] Edwards, D. C., Nielsen, S. B., Jarzęcki, A. A., Spiro, T. G., & Myneni, S. C. B. (**2005**). Experimental and theoretical vibrational spectroscopy studies of acetohydroxamic acid and desferrioxamine B in aqueous solution: Effects of pH and iron complexation. Geochimica Et Cosmochimica Acta, 69(13), 3237-3248.

[2005LEN] Le Naour, C., Trubert, D., Di Giandomenico, M. V., Fillaux, C., Den Auwer, C., Moisy, P., & Hennig, C. (**2005**). First structural characterization of a protactinium (V) single oxo bond in aqueous media. Inorganic Chemistry, 44(25), 9542-9546.

[2005RAV] Ravel, B., & Newville, M. (**2005**). ATHENA, ARTEMIS, HEPHAESTUS: data analysis for X-ray absorption spectroscopy using IFEFFIT. Journal of Synchrotron Radiation, 12, 537-541.

[2005SIE] Siebner-Freibach, H., Yariv, S., Lapides, Y., Hadar, Y., & Chen, Y. N. (**2005**). Thermo-FTIR spectroscopic study of the siderophore ferrioxamine B: Spectral analysis and stereochemical implications of iron chelation, pH, and temperature. Journal of Agricultural and Food Chemistry, 53(9), 3434-3443.

[2005TAK] Takeno, N. (**2005**). Atlas of Eh-pH diagrams. Geological Survey of Japan Open File report, 419, 102.

[2005WAN] Wang, X. F., & Andrews, L. (**2005**). Infrared spectra and structures of the Th(OH)(2) and Th(OH)(4) molecules. Physical Chemistry Chemical Physics, 7(22), 3834-3838.

[2006COZ] Cozar, O., Leopold, N., Jelic, C., Chiş, V., David, L., Mocanu, A., & Tomoaia-Cotişel, M. (**2006**). IR, Raman and surface-enhanced Raman study of desferrioxamine B and its Fe(III) complex, ferrioxamine B. Journal of Molecular Structure, 788(1), 1-6.

[2006KIT] Kitano, H., Onishi, Y., Kirishima, A., Sato, N., & Tochiyama, O. (**2006**). Determination of the thermodynamic quantities of complexation between Eu(III) and carboxylic acids by microcalorimetry. Radiochimica Acta, 94(9-11), 541-547.

[2006NOV] Novikov, A. P., Kalmykov, S. N., Utsunomiya, S., Ewing, R. C., Horreard, F., Merkulov, A., Myasoedov, B. F. (**2006**). Colloid transport of plutonium in the far-field of the Mayak production association. Russia. Science, 314(5799), 638-641.

[2006SIM] Simionato, A. V. C., Cantú, M. D., & Carrilho, E. (**2006**). Characterization of metal-deferoxamine complexes by continuous variation method: A new approach using capillary zone electrophoresis. Microchemical Journal, 82(2), 214-219.

[2006SZA] Szabo, Z., Toraishi, T., Vallet, V., & Grenthe, I. (**2006**). Solution coordination chemistry of actinides: Thermodynamics, structure and reaction mechanisms. Coordination Chemistry Reviews, 250(7-8), 784-815.

[2007BOU] Boukhalfa, H., Reilly, S. D., & Neu, M. P. (**2007**). Complexation of Pu(IV) with the natural siderophore desferrioxamine B and the redox properties of Pu(IV)(siderophore) complexes. Inorganic Chemistry, 46(3), 1018-1026.

[2007CAR] Carrott, M. J., Fox, O. D., Maher, C. J., Mason, C., & Taylor, R. J. (**2007**). Solvent extraction behavior of plutonium (IV) ions in the presence of simple hydroxamic acids. Solvent Extraction and Ion Exchange, 25(6), 723-745.

[2007CHO] Choppin, G. R. (**2007**). Actinide speciation in the environment. Journal of Radioanalytical and Nuclear Chemistry, 273(3), 695-703.

[2007GLO] Glorius, M., Moll, H., & Bernhard, G. (**2007**). Complexation of uranium(VI) with aromatic acids in aqueous solution - a comparison of hydroxamic acids and benzoic acid. Radiochimica Acta, 95(3), 151-157.

[2007GON] Gong, C. M. S., Poineau, F., & Czerwinski, K. R. (**2007**). Synthesis and characterization of the solid uranium(VI) dioxo-diacetohydroxamate complex. Radiochimica Acta, 95(8), 439-450.

[2007HEN] Hennig, C., Schmeide, K., Brendler, V., Moll, H., Tsushima, S., & Scheinost, A. C. (**2007**). EXAFS investigation of U(VI), U(IV), and Th(IV) sulfato complexes in aqueous solution. Inorganic Chemistry, 46(15), 5882-5892.

[2007KHA] Khalil, M. M., El-Deeb, M. M., & Mahmoud, R. K. (**2007**). Equilibrium studies of binary systems involving lanthanide and actinide metal ions and some selected aliphatic and aromatic monohydroxamic acids. Journal of Chemical and Engineering Data, 52(5), 1571-1579.

[2007SIN] Sinkov, S. I., Choppin, G. R., & Taylor, R. J. (**2007**). Spectrophotometry and luminescence spectroscopy of acetohydroxamate complexes of trivalent lanthanide and actinide ions. Journal of Solution Chemistry, 36(6), 815-830.

[2008CHE] Chen, Z., & Weber, S. G. (**2008**). Determination of binding constants by affinity capillary electrophoresis, electrospray ionization mass spectrometry and phase-distribution methods. Trends in Analytical Chemistry, 27(9), 738-748.

[2008CAR] Carrott, M. J., Fox, O. D., LeGurun, G., Jones, C. J., Mason, C., Taylor, R. J., ... & Boxall, C. (**2008**). Oxidation–reduction reactions of simple hydroxamic acids and plutonium (IV) ions in nitric acid. Radiochimica Acta, 96(6), 333-343.

[2008FAR] Farkas, E., Batka, D., Kremper, G., & Pocsi, I. (**2008**). Structure-based differences between the metal ion selectivity of two siderophores desferrioxamine B (DFB) and desferricoprogen (DFC): Why DFC is much better Pb(II) sequestering agent than DFB? Journal of Inorganic Biochemistry, 102(8), 1654-1659.

[2008LAV] Lavelle, L. (**2008**). Lanthanum (La) and actinium (Ac) should remain in the d-block. Journal of Chemical Education, 85(11), 1482.

[2008RAN] Rand, M. H., Mompean, F. J., Perrone, J., & Illemassène, M. (**2008**). Chemical Thermodynamics of Thorium. OECD Publications, Paris, France.

[2008SAS] Sasaki, T., Takaoka, Y., Kobayashi, T., Fujii, T., Takagi, I., & Moriyama, H. (**2008**). Hydrolysis constants and complexation of Th(IV) with carboxylates. Radiochimica Acta, 96(12), 799-803.

[2009BOR] Borer, P., Hug, S. J., Sulzberger, B., Kraemer, S. M., & Kretzschmar, R. (**2009**). ATR-FTIR spectroscopic study of the adsorption of desferrioxamine B and aerobactin to the surface of lepidocrocite (γ-FeOOH). Geochimica Et Cosmochimica Acta, 73(16), 4661-4672.

[2009FRI] Frisch, M. J., Trucks, G. W., Schlegel, H. B., Scuseria, G. E., Robb, M., Cheeseman, J. R., ... & Nakatsuji, H. (**2009**). Gaussian 09, Revision D. 01, Gaussian. Inc.: Wallingford, CT.

[2009IKE] Ikeda-Ohno, A., Hennig, C., Tsushima, S., Scheinost, A. C., Bernhard, G., & Yaita, T. (**2009**). Speciation and structural study of U(IV) and -(VI) in perchloric and nitric acid solutions. Inorganic Chemistry, 48(15), 7201-7210.

[2009MIC] Alain, M., Jacques, M., Diane, M. B., & Karine, P. (**2009**). MAX: Multiplatform Applications for XAFS. In A. DiCicco & A. Filipponi (Eds.), 14th International Conference on X-Ray Absorption Fine Structure (Vol. 190). Bristol: Iop Publishing Ltd. Camerino, Italy.

[2009PRA] Prat, O., Vercouter, T., Ansoborlo, E., Fichet, P., Perret, P., Kurttio, P., & Salonen, L. (**2009**). Uranium speciation in drinking water from drilled wells in southern Finland and its potential links to health effects. Environmental science & Technology, 43(10), 3941-3946.

[2009TOP] Topin, S., Aupiais, J., Baglan, N., Vercouter, T., Vitorge, P., & Moisy, P. (**2009**). Trace metal speciation by capillary electrophoresis hyphenated to inductively coupled plasma mass spectrometry: sulfate and chloride complexes of Np (V) and Pu (V). Analytical Chemistry, 81(13), 5354-5363.

[2009TOR] Torapava, N., Persson, I., Eriksson, L., & Lundberg, D. (**2009**). Hydration and hydrolysis of thorium(IV) in aqueous solution and the structures of two crystalline thorium(IV) hydrates. Inorganic Chemistry, 48(24), 11712-11723.

[2009WAL] Walther, C., Rothe, J., Brendebach, B., Fuss, M., Altmaier, M., Marquardt, C. M., Seibert, A. (**2009**). New insights in the formation processes of Pu(IV) colloids. Radiochimica Acta, 97(4-5), 199-207.

[2010AKS] Aksoy, M. S. (**2010**). Study of the interaction between chromium(III) and hydroxamic acids. Journal of Chemical and Engineering Data, 55(6), 2252-2256.

[2010BRO] Brown, M. A., Paulenova, A., & Tkac, P. (**2010**). Investigation of Pu (IV)-acetohydroxamic acid complex by solvent extraction with di (2-ethylhexyl) phosphoric acid. Paper presented at the IOP Conference Series: Materials Science and Engineering.

[2010CHO] Choppin, G.R., & Jensen, M.P. (**2010**). Actinides in Solution: Complexation and Kinetics. The Chemistry of the Actinide and Transactinide Elements, 4th edition L.R. Mors, N.M. Edelstein and J. Fuger Eds, Springer, Dordrecht, The Netherlands, pp. 2524-2611.

[2010GAL] Galbis, E., Hernandez-Cobos, J., den Auwer, C., Le Naour, C., Guillaumont, D., Simoni, E., Marcos, E. S. (**2010**). Solving the hydration structure of the heaviest actinide aqua ion known: the californium(III) case. Angewandte Chemie-International Edition, 49(22), 3811-3815.

[2010HU] Hu, Q. H., Weng, J. Q., & Wang, J. S. (**2010**). Sources of anthropogenic radionuclides in the environment: a review. Journal of Environmental Radioactivity, 101(6), 426-437.

[2010KIR] Kirby, H.W. & Morss, L.R. (**2010**). Actinium. The chemistry of actinides and transactinides elements. 4th edition, L.R. Mors, N.M. Edelstein and J. Fuger Eds, Springer, Dordrecht; The Netherlands, pp. 18-51

[2010REH] Rehr, J. J., Kas, J. J., Vila, F. D., Prange, M. P., & Jorissen, K. (**2010**). Parameter-free calculations of X-ray spectra with FEFF9. Physical Chemistry Chemical Physics, 12(21), 5503-5513.

[2010RUN] Runde, W., & Neu, M. P. (**2010**). Actinides in the Geosphere. "The chemistry of the actinide and transactinide elements" (pp. 3475-3593). Springer, Dordrecht.

[2010SIM] Simanova, A. A., Persson, P., & Loring, J. S. (**2010**). Evidence for ligand hydrolysis and Fe(III) reduction in the dissolution of goethite by desferrioxamine-B. Geochimica Et Cosmochimica Acta, 74(23), 6706-6720.

[2011CHA] Chaboy, J., & Díaz-Moreno, S. (**2011**). Ab initio X-ray absorption spectroscopy study of the solvation structure of Th(IV), U(IV), and Np(IV) in aqueous solution. The Journal of Physical Chemistry A, 115(11), 2345-2349.

[2011CHR] Christenson, E. A., & Schijf, J. (**2011**). Stability of YREE complexes with the trihydroxamate siderophore desferrioxamine B at seawater ionic strength. Geochimica Et Cosmochimica Acta, 75(22), 7047-7062.

[2011CHU] Chung, D. Y., Choi, E. K., Lee, E. H., & Kim, K. W. (**2011**). Complexation of U(VI), Ce(III) and Nd(III) with acetohydroxamic acid in perchlorate aqueous solution. Journal of Radioanalytical and Nuclear Chemistry, 289(2), 315-319.

[2011EDE] Edelstein, N. M., Fuger, J., Katz, J. J., & Morss, L. R. (**2011**). Summary and comparison of properties of the actinide and transactinide elements. The chemistry of the Actinide and Transactinide Elements (pp. 1753-1835): Springer.

[2011SZA] Szabo, O., & Farkas, E. (**2011**). Characterization of Mn(II) and Mn(III) binding capability of natural siderophores desferrioxamine B and desferricoprogen as well as model hydroxamic acids. Inorganica Chimica Acta, 376(1), 500-508.

[2011TUR] Turkel, N. (**2011**). Stability of Metal Chelates of Some Hydroxamic Acid Ligands. Journal of Chemical and Engineering Data, 56(5), 2337-2342.

[2012KNO] Knope, K. E., Vasiliu, M., Dixon, D. A., & Soderholm, L. (**2012**). Thorium(IV)-selenate clusters containing an octanuclear Th(IV) hydroxide/oxide core. Inorganic Chemistry, 51(7), 4239-4249.

[2012LEG] Leguay, S. (**2012**). Complexation of the actinides (III, IV and V) with organic acids. (Doctoral dissertation, Paris 11).

[2013ABD] Abdel-Fattah, A. I., Zhou, D. X., Boukhalfa, H., Tarimala, S., Ware, S. D., & Keller, A. A. (**2013**). Dispersion stability and electrokinetic properties of intrinsic plutonium colloids: implications for subsurface transport. Environmental Science & Technology, 47(11), 5626-5634.

[2013ATW] Atwood, D. A. (**2013**). Radionuclides in the Environment. John Wiley & Sons. Chichester, UK.

[2013KER] Kersting, A. B. (**2013**). Plutonium transport in the environment. Inorganic Chemistry, 52(7), 3533-3546.

[2013KNO] Knope, K. E., & Soderholm, L. (**2013**). Solution and solid-state structural chemistry of actinide hydrates and their hydrolysis and condensation products. Chemical Reviews, 113(2), 944-994.

[2013MAH] Maher, K., Bargar, J. R., & Brown, G. E. (**2013**). Environmental speciation of actinides. Inorganic Chemistry, 52(7), 3510-3532.

[2013MIC] Michalowicz, A., Moscovici, J., Muller-Bouvet, D., & Provost, K. (**2013**). MAX (multiplatform applications for XAFS) new features. Journal of Physics: Conference Series. Beijing, China.

[2013TIR] Tircso, G., Garda, Z., Kalman, F. K., Baranyai, Z., Pocsi, I., Balla, G., & Toth, I. (**2013**). Lanthanide(III) complexes of some natural siderophores: A thermodynamic, kinetic and relaxometric study. Journal of Inorganic Biochemistry, 127, 53-61.

[2014AHM] Ahmed, E., & Holmstrom, S. J. M. (**2014**). Siderophores in environmental research: roles and applications. Microbial Biotechnology, 7(3), 196-208.

[2014BOG] Boggs, M. A., Mason, H., Arai, Y., Powell, B. A., Kersting, A. B., & Zavarin, M. (**2014**). Nuclear magnetic resonance spectroscopy of aqueous plutonium (IV) desferrioxamine B complexes. European Journal of Inorganic Chemistry, 21, 3312-3321.

[2015GRA] Gralla, F., Abson, D. J., Moller, A. P., Lang, D. J., Vilsmaier, U., Sovacool, B. K., & von Wehrden, H. (**2015**). Nuclear accidents call for transdisciplinary nuclear energy research. Sustainability Science, 10(1), 179-183.

[2015MAL] Maloubier, M., Solari, P. L., Moisy, P., Monfort, M., Den Auwer, C., & Moulin, C. (**2015**). XAS and TRLIF spectroscopy of uranium and neptunium in seawater. Dalton Transactions, 44(12), 5417-5427.

[2016SLA] Sladkov, V. (**2016**). Affinity capillary electrophoresis in studying the complex formation equilibria of radionuclides in aqueous solutions. Electrophoresis, 37(19), 2558-2566.

[2016WOR] Workman Jr, J. J. J. (**2016**). Concise Handbook Of Analytical Spectroscopy, The: Theory, Applications, And Reference Materials. World Scientific. Singapore.

[2017SKO] Skoog, D. A., Holler, F. J., & Crouch, S. R. (**2017**). Principles of instrumental analysis. Cengage learning. Boston, USA.

[2018DEN] Denecke, M., Bryan, N., Kalmykov, S., Morris, K., & Quinto, F. (**2018**). Sources and Behaviour of Actinide Elements in the Environment. In "Experimental and Theoretical Approaches to Actinide Chemistry". John Wiley & Sons.

[2018GUO] Guo, N., Pottier, F., Aupiais, J., Alliot, C., Montavon, G., & Champion, J. (**2018**). Evidence for the Heaviest Expected Halide Species in Aqueous Solution, At^-, by Electromobility Measurements. Inorganic Chemistry, 57(9), 4926-4933.

[2018MOR] Morrison, K. D., Jiao, Y., Kersting, A. B., & Zavarin, M. (**2018**). Reduction of Plutonium (VI) to (V) by Hydroxamate Compounds at Environmentally Relevant pH. Environmental Science & Technology, 52(11), 6448-6456.

[2019IUP] International Union of Pure and Applied Chemistry https://iupac.org/what-we-do/periodic-table-of-elements/.

Résumé en français

Les applications civiles et militaires de l'énergie nucléaire sont à l'origine d'une dissémination d'actinides dans l'environnement, principalement U, Np, Pu et Am. Ces éléments se caractérisent par une toxicité chimique et radiologique élevée. Pour des raisons de sûreté, il est indispensable de disposer de données thermodynamiques et structurales sur les complexes d'actinides susceptibles d'être présents afin de disposer de modèles prédictifs de leur comportement dans l'environnement. Par ailleurs, ces actinides du début de série se caractérisent par une chimie complexe en raison de leur aptitude à exister sous différents degrés d'oxydation (+III à +VI) en solution aqueuse, chacun présentant une réactivité spécifique, notamment vis-à-vis de ligands présents naturellement dans les eaux souterraines comme de surface et dans les sols.

La complexation des actinides par des ligands organiques en milieu aqueux a fait l'objet de nombreuses études qui ont permis la création de bases de données thermodynamiques. Cependant, des incohérences peuvent être relevées, notamment lorsqu'il s'agit d'acides organiques faibles pour lesquels il existe autant de formes complexantes que de constantes d'acidité.

Ce travail de thèse est axé sur l'étude de la complexation d'actinides tri- et tétra-valents avec un ligand organique naturel appartenant à la classe des sidérophores. Ces composés, sécrétés par des microorganismes tels que des bactéries et des levures, sont de puissants chélateurs du fer qui, en permettant la solubilisation d'hydroxydes ferriques, assurent leur approvisionnement en fer. Les sidérophores peuvent être divisés en trois classes principales selon leur groupe fonctionnel : hydroxamate (**figure 1a**), catécholate et carboxylate. Les sidérophores hydroxamates sont le plus souvent observés dans les eaux naturelles. Ils forment des complexes très stables avec le fer(III), la complexation s'effectuant de manière bidentate. Le rapport charge/taille similaire pour Fe^{3+} et Pu^{4+}, et la réactivité des actinides tétravalents, laissent supposer une coordination voisine pour les deux éléments et une stabilité élevée des complexes formés, en particulier avec la desferrioxamine B (DFB, **figure 1b**). La DFB possède en effet trois groupes hydroxamates pouvant se lier aux ions métalliques. La formation de ces chélates très stables peut ainsi favoriser la migration des actinides dans la géosphère. Dans ce travail, nous avons étudié la complexation des actinides aux états d'oxydation +III et +IV avec la desferrioxamine B.

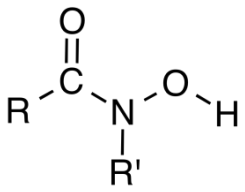

Figure 1a : Acide hydroxamique

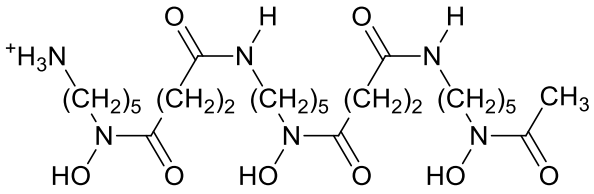

Figure 1b : Desferrioxamine B

Des lanthanides d'une part, Th(IV) et U(IV) d'autre part, ont été utilisés en tant qu'analogues des actinides trivalents et de Pu(IV) respectivement. L'étude de l'interaction entre ces éléments et la DFB a été conduite selon une double approche, thermodynamique et structurale, en mettant en jeu différentes échelles de concentration selon les techniques utilisées. Les constantes de formation des complexes ont été déduites d'expériences d'extraction liquide-liquide avec l'élément à l'échelle des ultra-traces, de spectrophotométrie d'absorption UV-visible et d'électrophorèse capillaire d'affinité. Pour l'étude structurale, les données issues de spectroscopie infrarouge et d'absorption des rayons X, ont été complétées par des calculs de chimie quantique.

Complexation de lanthanides avec la DFB

Une étude systématique des variations du coefficient de distribution (D) de ^{152}Eu en fonction du pCH et de la concentration de ligand a été conduite dans le système TTA/toluène/(H,Na)ClO_4/H_2O à température constante (25°C) et à force ionique fixée (0,7 M). Les courbes d'extraction, illustrées sur la **figure 2** mettent en évidence la formation d'un complexe de stoechiométrie 1:1 (pente $\frac{\partial logD}{\partial \log [DFB]} = -1$), dont la constante de formation conditionnelle a pu être déduite des variations de [D_0/D-1], D_0 étant la valeur du coefficient de distribution en absence de ligand (**figure 3**). Par suite, les constantes apparentes K_1 et K_2 (**Eq. 1 et 2**) ont été déterminées et se sont avérées en très bon accord avec les données de la littérature. Le protocole développé dans ce travail permet ainsi d'envisager l'étude directe de la complexation d'actinides trivalents à l'échelle des ultra-traces, comme ^{241}Am et ^{249}Cf par exemple.

$$Eu^{3+} + H_4DFB^+ \overset{K_1}{\leftrightarrow} Eu(H_3DFB)^{3+} + H^+ \qquad (1)$$

$$Eu^{3+} + H_4DFB^+ \overset{K_2}{\leftrightarrow} Eu(H_2DFB)^{2+} + 2H^+ \qquad (2)$$

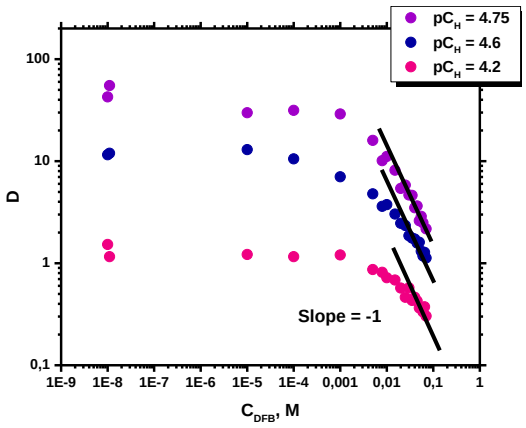

Figure 2 : Variations du coefficient de distribution de ^{152}Eu en fonction de la concentration totale de DFB (25°C, I = 0,7 M).

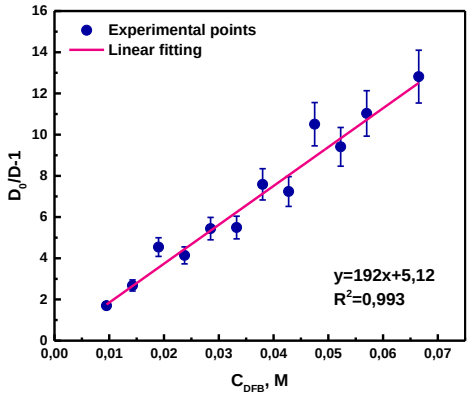

Figure 3 : Variations de [D_0/D-1] en fonction de la concentration totale de DFB (25°C, I = 0,7 M) et ajustement associé.

L'interaction entre La et Lu en macro-concentration, avec la DFB, a été étudiée par électrophorèse capillaire d'affinité couplée à un détecteur UV, en suivant la mobilité du ligand en présence d'un excès de lanthanide. Malheureusement, les variations trop faibles de mobilité observées n'ont pas permis la détermination de constantes de stabilité.

En revanche, par spectrophotométrie d'absorption UV-Vis, les variations des spectres de Eu(III) et Pr(III) en fonction de la concentration de DFB ont pu être exploitées à l'aide du logiciel Hypspec. La **figure 4** illustre les variations du spectre d'absorption de Pr avec l'augmentation de la concentration de DFB. L'analyse en composantes principales a permis de mettre en évidence l'existence de 3 espèces : l'ion aquo et deux complexes, dont les spectres individuels sont présentés sur la **figure 5**. Les constantes de formation de $Ln(H_3DFB)^{3+}$ et $Ln(H_2DFB)^{2+}$ ainsi obtenues pour les deux lanthanides sont en très bon accord avec les données de la littérature. Il faut souligner ici que dans le cas de l'europium, les données recueillies avec l'élément à l'échelle des ultra-traces par extraction liquide-liquide et avec l'élément en macro-concentration par spectrophotométrie d'absorption sont parfaitement cohérentes (**tableau 1**).

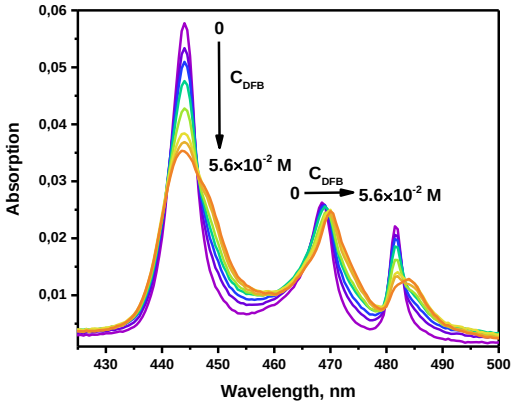

Figure 4 : Spectres d'absorption de Pr(III) 6×10^{-4}M en présence de quantités croissantes de DFB (pH = 5,5, I = 0,5 M $0 \leq C_{DFB} \leq 5{,}6\times10^{-2}$ M)

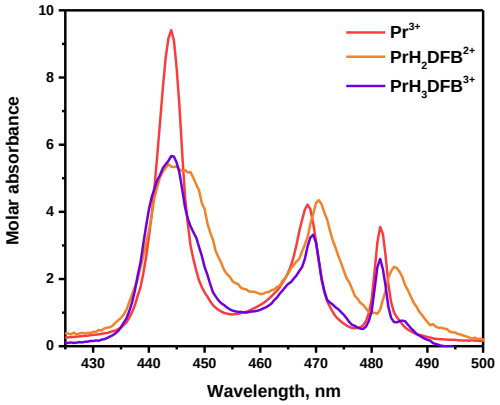

Figure 5 : Coefficient d'extinction molaire de Pr^{3+}, PrH_3DFB^{3+} et PrH_2DFB^{2+}.

Tableau 1 : Constantes de formations de complexes Eu et Pr avec la DFB (I = 0,7 M $NaClO_4$).

Cation	logβ_{13}	logβ_{12}	Température	Méthode	Référence
^{152}Eu	35,4 ± 0,2	30,9 ± 0,2	25°C	ELL	ce travail
Eu	35,6 ± 0,1	31,5 ± 0,1	20°C	sp	ce travail
Eu	35,72 ± 0,06	30,91 ± 0,06	25°C	pot.	[1]
Pr	35,1 ± 0,1	29,9 ± 0,1	20°C	sp.	ce travail
Pr	35,1	29,55	25°C	pot.	[1]

$M^{3+}+nDFB^{3-} + mH^+ \leftrightarrow M(DFB)_nH_m^{(3+m-3n)+}$ (β_{nm})

Complexation d'actinides (IV) : Th(IV) et U(IV)

L'étude thermodynamique de la complexation de Th par la DFB a été réalisée par extraction liquide-liquide couplée à la spectrométrie gamma, avec le thorium à l'échelle des ultra-traces sous forme de l'isotope ^{227}Th. Comme pour l'europium, un complexe de stoechiométrie 1:1 est observé (**figures 6 et 7**) et les constantes apparentes de formation des complexes $Th(H_3DFB)^{4+}$ et $Th(H_2DFB)^{3+}$ ont été déterminées. Les valeurs obtenues sont d'environ un ordre de grandeur inférieur aux seules données disponibles dans la littérature, déterminées par potentiométrie en présence de macro-concentration de Th.

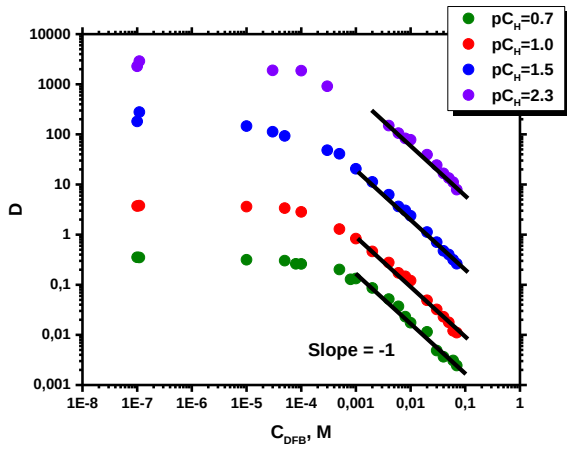

Figure 6 : Variations du coefficient de distribution de ^{227}Th en fonction de la concentration totale de DFB (C_{TTA} = 0,08 M, 25°C, I = 0,7 M).

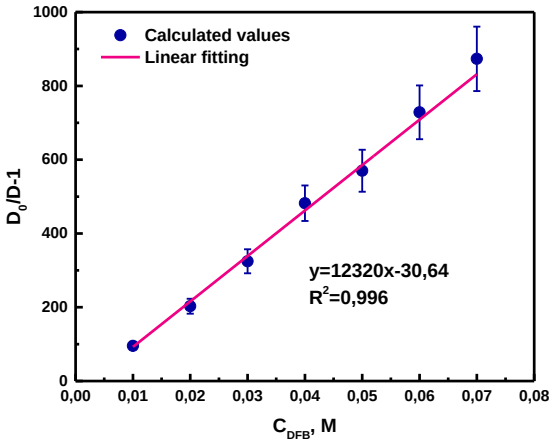

Figure 7 : Variations de [D_0/D-1] en fonction de la concentration totale de DFB (25°C, I=0,7 M, pC_H=1,5) et ajustement associé.

Le protocole d'étude de la complexation de U(IV), cation sensible à l'hydrolyse et à l'oxydation, a tout d'abord été développé avec deux acides hydroxamiques : AHA (acétohydroxamique) et BHA (benzohydroxamique). L'exploitation des spectres d'absorption UV-Visible a permis d'accéder aux constantes de stabilité des complexes $U(BHA)^{3+}$, $U(AHA)^{3+}$ et $U(AHA)_2^{2+}$ en milieu HCl 0,5 M à 25 °C. En raison de l'absence de données dans la littérature, les valeurs obtenues dans ce travail ont été comparées à celles relatives à Th et Pu(IV) : elles s'inscrivent parfaitement dans la droite de corrélation constante – inverse du rayon ionique. En revanche, dans le cas de la complexation avec la DFB, la très forte interaction avec U(IV) n'a pas permis d'obtenir des variations de spectre exploitables. Une alternative mettant en jeu une compétition avec un autre ligand comme le DTPA est à envisager.

L'ensemble des données thermodynamiques de complexation d'actinides (IV) déterminées dans ce travail est regroupé dans le **tableau 2** avec les données disponibles dans la littérature.

Tableau 2 : Constantes de formations de complexes Th et U avec la DFB (I = 0,7 M $NaClO_4$).

An(IV)	Ligand	logβ_{13}	logβ_{12}	Conditions	Méthode	Référence
^{227}Th	DFB[a]	40,9±0,1	38,2±0,1	25°C ; 0,7 M (Na,H)ClO_4	ELL	Ce travail
Th	DFB[a]	42,0±0,1	40,2±0,1	25°C ; 0,1M KCl	pot.	[2]
		logβ_{10}	logβ_{12}			
U	BHA[b]	11,0±0,1		25°C ; 0,5M HCl	sp.	Ce travail
U	BHA[c]	11,8±0,1		25°C ; 0,5M HCl	sp.	Ce travail

U	**AHA[d]**	**12,0±0,1**	**21,1±0,1**	**25°C ; 0,5M HCl**	**sp.**	**Ce travail**

$M+nL + mH \leftrightarrow M(L)_nH_m$ (β_{nm})

a. calculé avec pKa_1=8,54±0,01 ; pKa_2=9,06±0,01 ; pKa_3=9,70±0,02 ; pKa_4=10,89±0,06 [1]

b. calculé avec pKa(BHA)=8,07±0,06 [3]

c. calculé avec pKa(BHA)=8,83±0,01 [4]

d. calculé avec pKa(AHA)=9,15 [5]

Une étude structurale du complexe Th-DFB a été conduite par spectroscopie infrarouge en mode ATR. Le décalage de la bande de vibration de C=O de l'hydroxamate observé sur les spectres présentés **figure 8** confirment l'implication de ces groupements fonctionnels dans le complexe formé ; l'augmentation du pH peut être corrélé à la déprotonation progressive du ligand. Le décalage aux pH élevés permet alors d'observer le carbonyle de la fonction amide.

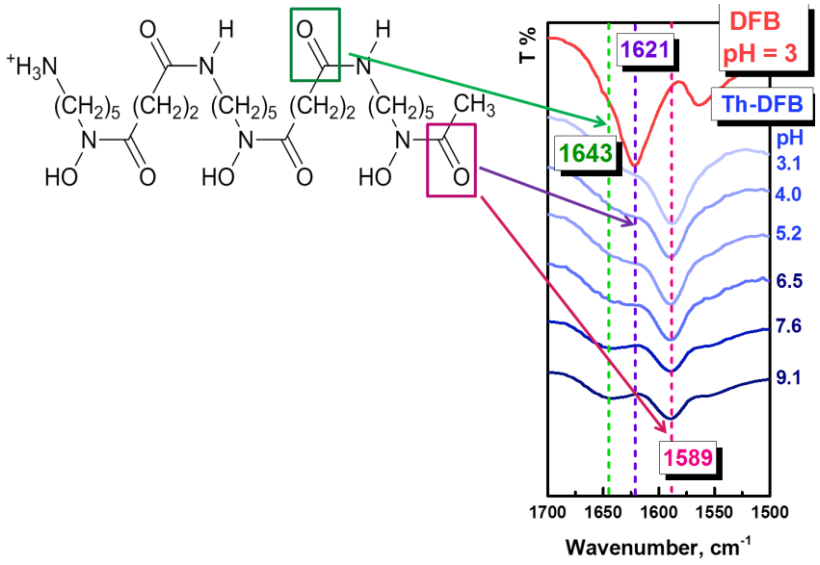

Figure 8 : Spectre IRTF-ATR du complexe Th-DFB en fonction du pH.

Des mesures par spectroscopie d'absorption des rayons X ont été réalisées sur la ligne MARS du synchrotron SOLEIL sur des échantillons Th-DFB et U(IV)-DFB (**figure 9**). L'ajustement des spectres EXAFS a été effectué en considérant la structure calculée de la **figure 10**. Une coordination de 8 des deux cations est assurée par 3 hydroxamates bidentates et 2 molécules d'eau, avec une distance moyenne métal-oxygène de 2,42 Å et 2,37 Å respectivement pour Th et U, variation en accord avec la diminution du rayon ionique.

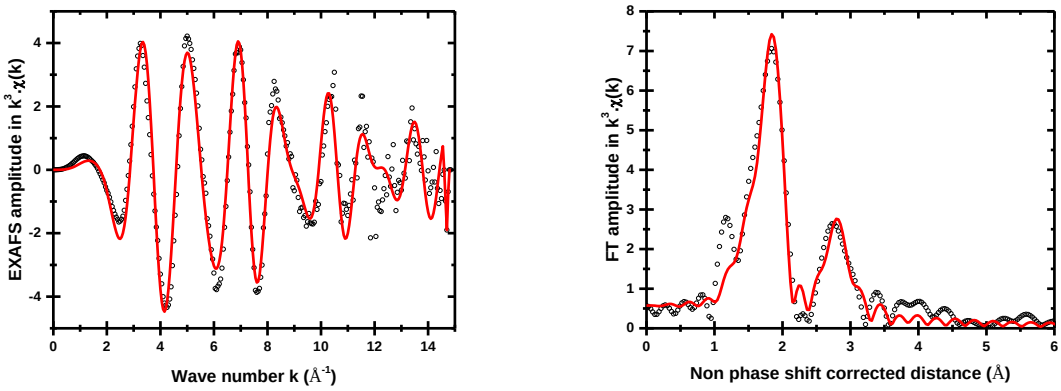

Figure 9 : Spectres EXAFS (à gauche) et transformées de Fourrier correspondantes (à droite) au seuil L_{III} de l'uranium de U(IV)-DFB à pH 5 (expérimental en noir, ajustement en rouge).

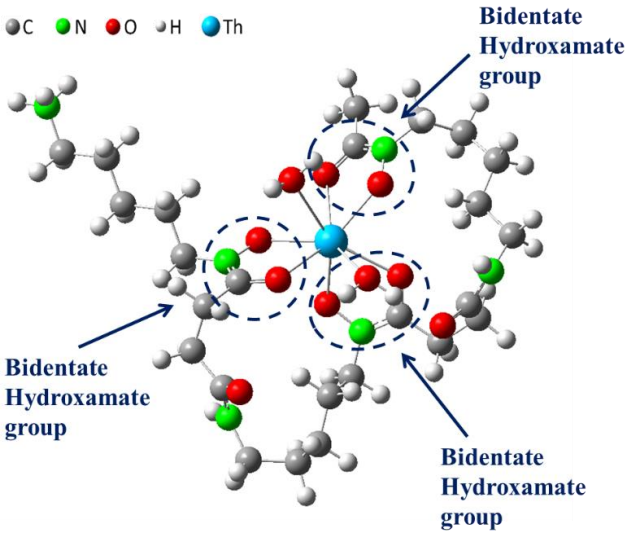

Figure 10 : Structure optimisée du complexe Th(HDFB) avec 3 hydroxamates bidentates obtenue par calculs DFT.

Références:

[1] Christenson, E. A. and Schijf, J. Stability of YREE complexes with the trihydroxamate siderophore desferrioxamine B at seawater ionic strength. Geochim. Cosmochim. Acta, 2011, **75**(22), 7047-7062.

[2] Whisenhunt, D. W., Neu, M. P., Hou, Z. G., Xu, J., Hoffman, D. C., and Raymond, K. N. Specific sequestering agents for the actinides .29. Stability of the thorium(IV) complexes of desferrioxamine B (DFO) and three octadentate catecholate or hydroxypyridinonate DFO derivatives: DFOMTA, DFOCAMC, and DFO-1,2-HOPO. Comparative stability of the plutonium(IV) DFOMTA complex. Inorg. Chem., 1996, **35** 4128-4136.

[3] Aksoy, M. S. Study of the interaction between chromium(III) and hydroxamic acids. J. Chem. Eng. Data, 2010, **55**(6), 2252-2256.

[4] Turkel, N. Stability of Metal Chelates of Some Hydroxamic Acid Ligands. J. Chem. Eng. Data, 2011, **56**(5), 2337-2342.

[5] Chung, D. Y., Choi, E. K., Lee, E. H., & Kim, K. W. Complexation of U(VI), Ce(III) and Nd(III) with acetohydroxamic acid in perchlorate aqueous solution. J. Radioanal. Nucl.Chem. 2011, **289**(2), 315-319.

Title: Complexation of actinides and analogues with hydroxamate ligands

Keywords: actinides, lanthanides, complexation, hydroxamate

Due to the increasing human activities in the civilian nuclear fields, the actual and potential release of radionuclides into the environment is a matter of concern. The mobility of radionuclides depends on several factors such as pH, ionic strength, oxidation state and the presence of organic ligands. In order to guarantee the safety of radioactive waste storage sites and to develop contaminated soil remediation processes, it is necessary to have fundamental data on actinides and natural organic ligands interactions.

This study focuses on the interaction between Th(IV), U(IV,VI), Cf(III) and Eu(III) and hydroxamates derivatives, desferrioxamine B, a bacterial siderophore with three hydroxamic functions. The stability constants of complexes are determined as function of acidity and ligand concentration, at fixed ionic strength and temperature, using several techniques and metal concentrations ranging from 10^{-10} to 10^{-3} M (liquid-liquid extraction coupled with γ-spectrometry, capillary electrophoresis with UV detection, UV-Vis absorption spectrophotometry).

The thermodynamic study is supplemented by a structural one using spectroscopic techniques such as Fourier transform infrared spectroscopy and X-ray absorption spectroscopy. Experimental measurements are compared with quantum chemistry calculations (DFT) in order to determine the coordination geometry of the metal ion and the interatomic distances.

Université Paris-Saclay
Espace Technologique / Immeuble Discovery
Route de l'Orme aux Merisiers RD 128 / 91190 Saint-Aubin, France

Titre: Complexation d'actinides et d'analogues par des ligands hydroxamates

Mots clés: actinides, lanthanides, complexation, hydroxamate

L'augmentation des activités humaines dans le domaine nucléaire civil comme militaire est à l'origine d'une dissémination effective ou potentielle de radionucléides dans l'environnement. Leur mobilité dépend de plusieurs facteurs tels que le pH, la force ionique, le degré d'oxydation et la présence de ligands organiques. Afin de garantir la sûreté de sites d'entreposage ou de stockage, de développer des procédés de remédiation de sols contaminés, il est nécessaire de disposer de données fondamentales sur les interactions entre actinides et ligands organiques susceptibles d'être présents dans l'environnement, vecteurs de migration ou de piégeage de ces radioéléments.

Dans ce contexte, l'étude s'est axée sur les interactions entre Th(IV), U(IV,VI), Cf(III) and Eu(III) et des dérivés hydroxamates, en particulier, la desferrioxamine B, un sidérophore bactérien comportant trois fonctions hydroxamiques. Les constantes de formation des complexes sont déterminées en fonction de l'acidité et de la concentration de ligand à force ionique et température fixées en mettant en jeu plusieurs techniques expérimentales et des concentrations en élément comprises entre 10^{-10} et 10^{-3} M (extraction liquide-liquide combinée à une détection par spectrométrie γ, électrophorèse capillaire avec détection UV, spectrophotométrie d'absorption UV-visible).

L'approche thermodynamique de cette étude est complétée par une étude structurale à l'aide de techniques spectroscopiques telles que la spectroscopie infrarouge à transformée de Fourier et de la spectroscopie d'absorption des rayons X. Ces mesures expérimentales sont alors confrontées à des calculs théoriques (DFT), afin de déterminer l'arrangement structural du métal et les distances interatomiques.

Université Paris-Saclay
Espace Technologique / Immeuble Discovery
Route de l'Orme aux Merisiers RD 128 / 91190 Saint-Aubin, France